Graz University of Technology

Institut für Baustatik –
Institute for Structural Analysis
Lessingstraße 25/II
8010 Graz, Austria

PhD Thesis

Modelling of Ground Support in Tunnelling using the BEM

by

Katharina Riederer

submitted on December 20th, 2009

Primary Advisor : Gernot Beer
Institute for Structural Analysis
Graz University of Technology, Austria

Second Examiner : Adrián Pablo Cisilino
Department of Mechanical Engineering
University of Mar del Plata, Buenos Aires, Argentina

Abstract

Numerical simulation is a growing and important tool in the field of tunnel construction; it can be very helpful, allowing the investigation of various alternatives in virtual reality rather than reality. Selecting the best option can result in significant cost savings, reduced construction time and in improved safety. Commonly used methods require a significant amount of computational costs especially for large 3D simulations. The effort for mesh generation as well as the calculation time increase considerably.

An attractive alternative for simulating tunnelling problems is the Boundary Element Method (BEM). In this method the discretised mesh is much smaller and simpler, thus the mesh generation is more user-friendly, the calculation time is shorter and the mesh is less error-prone. The effort to do 3D simulations is significantly reduced. However, the BEM is not as far developed as other methods at the moment. There are currently no commercial programs available that include all the features required for conventional tunnelling, for example the simulation of ground support and ground improvement techniques.

The aim of this work was the development and the implementation of methods to simulate ground support (rock bolts and pipe roofs) into the BEM program (BEFE++). Novel methods were developed to simulate these *inclusions* efficiently and realistically.

In these methods the inclusions are simulated by applying stresses or forces to the system. These stresses or forces are calculated within an iterative algorithm. Because of this, a huge number of inclusions (for example rock bolts) can be calculated efficiently and the iterative procedure can be easily combined with

a non-linear calculation (for example to simulate plastic material behaviour). Next to the simulation of rock bolts and pipe roofs these methods can be used to simulate geological inhomogeneities as well. In contrast to commonly used methods the mesh generation for such problems is very easy and independent from any domain discretisation. This means a considerable increase in user friendliness and accuracy especially for the simulation of rock bolts in comparison with other methods. The high stress variations in the near-field of the bolt can be simulated more accurately. With a relative small effort very accurate results are obtained.

Keywords: Boundary Element Method, body forces, internal cells, inclusions, inhomogeneities, tunnelling, ground support, rock bolts, anchors, pipe umbrella.

Kurzfassung

Um Tunnelbauprojekte hinsichtlich Sicherheit, Kosten und Qualität zu optimieren werden realitätsnahe numerische Simulationen sowohl in der Planungsphase als auch während der Ausführung eingesetzt. Derzeit verwendete Simulationsmethoden stoßen speziell bei der Berechnung von großen 3D Problemstellungen schnell an ihre Grenzen. Der Rechen- und Modellierungs- Aufwand steigt enorm an.

Eine attraktive Alternative dazu stellt die Randelemente Methode (REM) dar. Durch ein kleineres, einfaches und überschaubares Netz wird die Netzgenerierung benutzerfreundlicher, die Berechung weniger Fehleranfällig und der Rechenaufwand geringer als bei anderen Methoden. Das stellt speziell bei 3D Simulationen einen wesentlichen Vorteil dar. Allerdings ist die REM noch nicht auf dem gleichen Entwicklungsstand wie derzeit gängige Methoden. Es sind bis heute noch keine kommerziellen Randelemente Programme erhältlich die in der Lage sind alle nötigen Bestandteile eines konventionellen Tunnelvortriebs zu simulieren (wie z.B. den Einbau verschiedener Stützmittel usw.).

Ziel dieser Arbeit war die Entwicklung von Methoden zur Simulation von Stützmitteln (Felsanker und Rohrschirme) in das Randelemente Programm (BEFE++) und deren Implementierung . Es wurden völlig neue Methoden entwickelt um diese *Einschlüsse* effizient und realitätsnah zu simulieren. Dabei werden anstelle der Einschlüsse Spannungen oder Kräfte auf das System aufgebracht welche diese Einschlüsse simulieren. Diese Spannungen oder Kräfte werden mithilfe eines iterativen Algorithmus berechnet. Durch dieses iterative Verfahren kann eine große Anzahl von Einschlüssen (Felsankern, Rohrschirme) effizient berechnet werden und der Algorithmus kann einfach und effektiv mit

einer nichtlinearen Berechnung (z.B. bei plastischem Materialverhalten) kombiniert werden. Neben der Berechnung von Felsankern und Rohrschirmen kann diese Methode auch zur Simulation von geologischen Inhomogenitäten herangezogen werden. Die Generierung eines solchen Netzes ist denkbar einfach und unabhänging von einer Bereichs-diskretisierung. Dies stellt besonders bei der Simulation von Felsankern eine wesentliche Verbesserung gegenüber derzeit verwendeten Methoden dar. Die hohen Spannungsvariationen im Umfeld des Ankers können sehr genau wieder gegeben werden. Mit relativ geringem Rechenaufwand werden qualitativ hochwertige Ergebnisse erzielt.

Schlüsselwörter: Rand Elemente Methode, Volumskräfte, Zellen, Einschlüsse, Inhomogenitäten, Tunnel, Stützmittel, Felsanker, Rohrschirm.

Contents

Chapter 1

Introduction

1.1 Motivation

In the design of engineering structures, numerical simulation plays an increasingly important role. This has become very popular due to rapid advancements in computer technology and its availability to engineers. Numerical techniques have been developed for solving many kinds of engineering problems, also in the field of underground engineering structures.

For tunnelling problems, numerical techniques help the designer in dimensioning the opening, selecting the best alignment, the best excavation sequence, choosing and dimensioning the support structures, and to quantitatively assess its overall behaviour through parametric or sensitivity studies. Diverse information about geology, physics, construction techniques, economy, the environment and their interactions can be considered. Problems with arbitrary shape, with nonlinear material behaviour, consideration of ground support, self weight, external forces, in situ stresses, pre-stressing, etc. can be calculated. All this achievements have greatly enhanced the development of modern rock mechanics; see Jing and Hudson (2002), Gioda and Swoboda (1999), Pande et al. (1990). Simulations allow testing of various alternatives in virtual reality rather than reality; this results in significant cost savings, reduction of construction time and makes tunnelling safer.

A number of computational methods have been developed. However, it is clear that a very important step in numerical simulation is the early choice of the *best* numerical method in terms of scope, accuracy, efficiency and user-friendliness. The Finite Element Method (FEM) is perhaps the most widely applied numerical method in engineering fields. Today's FEM-programs have reached a very high development-stage; almost all important features involved in underground engineering problems are included. However, it has some disadvantages as well:

Domain based methods, like the FEM are techniques in which the discretisation has to be introduced in the entire domain. In tunnelling this means the discretisation of the whole surrounding rock mass into small elements. Thus, one can imagine that the system of equations and the effort for mesh generation become very huge; especially for three dimensional analyses. The required effort is the reason why unrealistic 2-D analyses are often carried out instead. However, the advancing process of a tunnel has an essentially 3D nature. 3D modelling is necessary for the simulation of effects ahead of the tunnel face, of the correct stress-strain distribution, the non-linear behaviour of the rock mass, and the influence of support measures. Furthermore, when simulating tunnels supported by rock bolts, the mesh around the bolts has to be extremely fine to handle the local stress concentrations. This problem leads either to an extremely large number of elements or to inaccurate results.

This leads to the statement that currently used numerical methods have major drawbacks with respect to user-friendliness and efficiency. An attractive alternative is the Boundary Element Method (BEM), where only the excavation surface has to be discretised and the effort to do 3D simulations is significantly reduced. However, the BEM is much less developed than the FEM and currently there are no commercial programs available that are able to include all relevant features for tunnelling problems in their calculation. This means especially the following features: calculation of sequential excavation, non-linear material behaviour, inhomogeneous ground conditions, support measurements (as shotcrete, rock bolts or pipe umbrella systems) and a user-friendly pre-processor.

The goal of the research activities of the Institute for Structural Analysis at the University of Technology in Graz is the development of the BE-program BEFE++ which is especially capable to simulate conventional tunnelling processes, including all important features, mentioned before. The calculation of sequential excavation processes was developed in Duenser (2001); non-linear material behaviour are discussed by Ribeiro (2006), Thoeni (2009), Prazeres (2009); and the simulation of shotcrete refer to Prazeres (2009).

This thesis deals with the efficient calculation of rock bolts, pipe umbrella systems and general inclusions such as geological inhomogeneities. They have one thing in common: they are all inclusions inside the domain. Rock bolts are very narrow inclusions, a pipe umbrella system and geological inhomogeneities are inclusions with general shape. A novel method was developed that allows to model rock bolts (and also anchors and geological inclusions) efficiently with the BEM. An iterative solution procedure is used for solving the problem. Because of this, the system of equations stays small, even with a very large number of rock bolts (or anchors or inclusions) and the algorithm can be efficiently combined with the iterative procedure for the non-linear material behaviour. Especially for large scale problems, for problems containing a lot of rock bolts and for problems considering non-linear material behaviour this method is of great advantage.

The new method is applicable to:

- Passive (or non-stressed) fully grouted rock bolts. Features are included to calculate bolt yielding and bond slip effects.
- Anchors or bolts which are bonded at the ends (by cement grout, resin, or fixed by a mechanical anchor) and have a free length in between. They can be passive or active (pre-stressed) and bolt yielding can be considered.
- Geological inhomogeneities with general shape (which can have non-linear material behaviour).
- The simulation of pipe roofs (to improve the rock mass behaviour and stabilise the excavated area). They are approximately simulated by a homogenized plane-shaped umbrella-zone.

Next the conventional tunnelling will be described briefly and then an introduction to computational modelling will be presented. At the end of this introductory chapter the structure for the next chapters of this work will be given.

1.2 Conventional Tunnelling

1.2.1 Historical Development

The history in tunnel engineering is referred in several works, for example Kovari (2003a,b), Romana (2009), Schubert (1997), Karakus and Fowell (2004). Below a short overview of the main developments are summarised:

Kovari (2003a) claims that the beginning of tunnel engineering was seen in the 1.1 km long Tronquoy Tunnel in France, built by Napoleon in 1803. Here, for the first time, a large area of excavation in difficult ground conditions was realised. Thus, this tunnel is regarded as the first to be built on engineering principles. Since that, up to the middle of the 19th century, the most important modes of "ground response" were defined and classified. One of the first publications on tunnelling was written in 1844, by the Englishman F.W. Simms, see Kovari (2003a). He already expressed the idea that in the case of deep tunnels "a small portion only gets into motion, the upper part acting as a key, by which the mass supports itself". He clearly states that "it is the mass in adjusting itself to equilibrium". An other early and important work on tunnelling was written in 1870 by Rziha (see Schubert (1997)).

Timberwork

At this early state tunnels were supported by timberwork, however this timbering had a lot of disadvantages (for example: timber structure involved up to 60 percent of the cross-section; over-excavation was necessary; difficult construction ...). The replacement of timbering was introduced gradually, by steel supports,

then shotcrete, followed by rock anchors and finally, the systematic combination of these support measured on a broad scale (at about 1950).

Steel Support

Steel support were used in mining since 1862 (see Kovari (2003a)). At a very early state (in 1872) also Rziha proposed to replace timberwork by steel supports (Schubert (1997)). By the end of the 19th century, the basic construction problems using steel supports had been solved and this support system began to replace timbering mainly in the United States. In European tunnels, steel supports were not economical at this time, because of the high material costs in comparison to the personnel costs; this relation was different than in the United States.

Shotcrete and Rock bolts

The development of shotcrete and rock anchors represents one of the greatest advancements in tunnelling history. The first use of these support elements began already very early in the field of mining, with the first use of rock anchors in 1913 and that of shotcrete in 1914(Kovari (2003a)).

The development of shotcrete technology started with the American taxidermist C.E. Akeley; he invented the "cement-gun". The patent for an "apparatus for mixing and applying plastic or adhesive materials", which was called a "cement gun" was obtained in 1911. During the 1910s, shotcrete was used in mines in the United States and in the early 1920s it came to Europe. The possibilities for the application of shotcrete were recognised and utilised very rapidly by the technical world (see Kovari (2003a), Karakus and Fowell (2004)).

The history of rock bolting began in 1913, with the submission of a patent by Stephan, Fröhlich and Klüpfel: "... boreholes of sufficient depth will be drilled into the rock in which rods, tubes or cables of a load-bearing material, for example steel, will be inserted and fixed at the end in a proper manner or

cemented along the whole length." The first World War delayed the issuing of the patent until 1918, see Kovari (2003b).

Sprayed concrete lining method / New Austrian Tunnelling Method

The combined use of rock bolting, reinforcing nets and sprayed concrete has been practice in mining in Ontario, Canada, since approximately 1930. Keeley published 1934 in Canada a work, describing a support concept for mining which involves the use of expansion-bolts together with sprayed concrete. The introduction of a shotcreting machine by the Swiss engineer G. Senn in 1950 marks a new area for the sprayed concrete lining method. Since that the sprayed concrete lining took on a greater role than had earlier been assumed, see Kovari (2003b).

From about this point the opinions drift apart and the polemic in the international tunnelling community is big. One party promotes the idea of the *New Austrian Tunnelling Method* as a self-contained new method developed by the Austrian Rabcewicz. The other party appeal against this Austrian claim and proposes the name *Sprayed Concrete Lining Method*.

- One view is that after the introduction of the shotcreting machine 1950, very soon it was realized all over the world that a combination of shotcrete and rock anchors in many cases provides the most efficient method (both structurally and economically). The new methods of support opened several novel excavation concepts; and they were summarised as the **Sprayed Concrete Lining Method**; in the 1960s this method was firmly established. Not until 1963 the Austrian engineer Rabcewicz renamed the method in "New Austrian Tunnelling Method" (NATM); however, in this point of view NATM is only a nickname for the sprayed concrete lining method, which was developed and practised in the international community much earlier. For more detailed information see Kovari (2003b).
- The other view is that Rabcewicz had the first ideas for a new method after his experience in the second World War, building underground bunkers

in the Russian front. He invented dual-lining supports (initial and final support) expressing the concept of allowing the rock to deform before the application of the final lining so that the loads on lining are reduced. In 1948 Rabcewicz submitted an Austrian patent about this method. 1956-1958 he risks the first time the application of shotcrete and anchors as stand-alone support system without other supports for the construction of the highway- and railway-tunnels in Caracas, Venezuela. 1962 he proposed the term **New Austrian Tunnelling Method (NATM)** for this concept. The first urban application in soft ground of the NATM was the subway tunnel in Frankfurt, Germany in 1969 by Müller. Detailed information about the developments of the NATM can be seen in Schubert (1997), Karakus and Fowell (2004), Romana (2009).

The conflict about the name NATM lead back to the question: Is the NATM a construction method or is it more than that is it a design philosophy?

1.2.2 Design Philosophy and Construction Method

Rabcewic explains the NATM in 1964 by emphasizing three key points: the first is the application of a thin-sprayed concrete lining, the second is closure of the ring as soon as possible and the third is systematic deformation measurement. However, this definition might not been able to explain neither what's *new* nor what's *Austrian* about this method and thus induced the above mentioned conflicts. Because of that a lot of new definitions evolved which tried to specify the NATM in more detail; they argue that NATM is a design philosophy rather than a construction method (a set of excavation and support techniques), see Karakus and Fowell (2004).

Design Philosophy

Müller, one of the advocators of NATM proposed 1978 that: "The NATM is, rather, a tunnelling concept with a set of principles... Thus in the autor's

opinion it should not even called a construction method, since this implies a method of driving a tunnel." He summarised the NATM by the following points (see Romana 2009, Karakus and Fowell 2004): use the rock mass for the support of the terrain charges; allow deformation in order to develop the rock mass strength around the tunnel and to minimize the support needs; deformations must be controlled; design is done during the excavation; basic instrumentation control is done by convergence measurements.

An other definition was given by the Austrian National Committee on Underground Construction of the International Tunnelling Association (ITA) in 1980, see Karakus and Fowell (2004): "The New Austrian Tunnelling Method (NATM) is based on a concept whereby the ground (rock or soil) surrounding an underground opening becomes a load bearing structural component through activation of a ring like body of supporting ground".

A more actual definition of the design philosophy NATM has been formulated by Brown in 1995 (see Romana 2009): "The terrain strength around the tunnel is mobilized to a maximum possible level; this is done allowing for a controlled deformation. The primary support is installed with strength-deformation characteristics adequate for the terrain and in a compatible time with the terrain deformability. Instrumentation is used to control the support deformation in order to change (if/when necessary) the initial design and the excavation sequence. Movements at surface and around the tunnel are controlled in urban environment."

Construction Method

However, the NATM or Sprayed Concrete Lining Method can also be seen as a construction method. In 2002 Romero pointed out: "Tunnel excavation and support are done in a sequential way. The sequence can be changed. Initial support by: shotcrete; bolts; steel sets. Secondary lining is (very often, but not always) concrete put in place with forms." Thus, NATM is being used as a construction method and the design philosophy is not necessarily applied, see Romana (2009). In soils for example, the deformations are bigger and more

difficult to control. In this case it is easy to apply NATM as a construction method; however, it is difficult to apply NATM as a design philosophy.

As described in Galler (2009) the basic principles of the construction method NATM can be summarised as the following: Typical support elements in NATM are shotcrete and rock anchors to allow controllable deformation of the rock mass. Steel ribs or lattice girders provide limited early support before the shotcrete hardens and ensure correct profile geometry. Face bolts, sealing shotcrete and pipe roofs are installed, if ground conditions require support at or ahead of the excavation face. The subdivision of the excavation cross-section in top heading, bench and invert depends on geological conditions as well as on logistical requirements to facilitate the use of standard plant and machinery in tunnelling. Side drift galleries are provided to limit the size of large excavation faces and the associated surface settlements.

Different procedures have to be chosen for different ground conditions, see Galler (2009).

Hard Rock Conditions

In deep rock tunnels, the shotcrete lining thickness does not has to be larger; the main support elements are long rock anchors (2.5m to 9m length). The shotcrete lining is slotted and yielding supports are installed to allow deformations without damaging the shotcrete. Once the stabilisation of the system is confirmed by monitoring, the slots in the lining are closed with shotcrete. The typical cross-section for a deep rock tunnel is horse-shoe shaped. The cross-section is typically subdivided into the top heading (the top half of the tunnel cross section); the bench (excavated a few hundred meters behind); and an invert arch (which is only installed if ring closure is required by poor rock conditions). A ramp between top heading and bench is maintained on one half side of the cross-section.

Soft Rock Conditions

Shallow tunnels in soft ground situated in an urban environment require a rigid support. The shotcrete lining is more rigid, the advance length is short, and a rapid closure as well as a subdivision of the cross-section in side and centre drifts is necessary. The typical cross-section is similar to the cross-section of a hard rock tunnel; however an invert arch is arranged in the standard case throughout. A temporary invert in the top heading is employed in some cases. Furthermore, elephant feet and the arrangement of a pipe canopy can become necessary. Face reinforcement with dowels and a supporting core is usually required. The secondary lining is reinforced and its thickness is adjusted to the substantial ground loads depending on the depth of overburden.

1.3 Computational Modelling

Since about the 60's of the last century, a number of computational methods have been developed for numerical simulation. They have become popular due to rapid advancements in computer technology and its availability to engineers. Before, rock structures were designed mainly based on rules of thumb, experience and a trial and error procedure. Analytical or "closed form" solutions are available for some simple situations, see Pande et al. (1990). However, in most cases they simplify the real problem drastically concerning material, geometry, supports...; see for example Feder and Arwanitakis (1976), Kovari (2003a), Schweiger (2008), Schubert (1997).

However, the excavation and construction process and the technological details have a strong influence on the stress/strain distribution in the rock mass and in its support system. The stress/strain distribution is strongly dependent of the excavation sequence when dealing with supported openings or with non-linear material behaviour. Another important aspect is the complex geometrical nature; this is not only related to the shape of the opening, but also to discontinuities in the rock mass, of non-homogeneous or non-isotropic layers,

etc. This represents the main drawback for the analytical solutions, or for the approximated "standard" methods, which in most cases cannot consider this aspects with sufficient approximation, see Gioda and Swoboda (1999).

Today a number of advanced numerical techniques exist which are able to simulated underground engineering problems very accurately. Numerical techniques can help the designer in dimensioning the opening, in determining the loads carried by support structures and for quantitatively assessing its overall behaviour through parametric or sensitivity studies, see Gioda and Swoboda (1999). It is possible to analyse problems with arbitrary shape, nonlinear material behaviour, considering ground support, self weight, external forces, in situ stresses, pre-stressing, etc, see Pande et al. (1990).

A categorisation into four principal modelling methods can be pointed out (see Jing and Hudson 2002):

- Design based on previous experience:
  pre-existing standard methods; precedent type analyses
- Design based on simplified models:
  analytical methods; rock mass classification
- Design based on numerical modelling which attempts to capture most relevant mechanisms:
  basic numerical methods (FEM, BEM, FDM, DEM)
- Design based on "all-encompassing modelling":
  extended numerical methods; integrated systems approaches

Indeed, computing techniques have become daily tools for formulating diverse information about geology, physics, construction techniques, economy, the environment and their interactions. This achievement has greatly enhanced the development of modern rock mechanics - from the traditional "empirical" art of rock deformability, strength estimation and support design; to the rationalism of modern mechanics, see Jing and Hudson (2002).

Whereas the most commonly applied numerical methods for rock mechanics problems are (see Jing and Hudson 2002):

- Continuum methods
  - Finite Element Method (FEM)
  - Finite Difference Method (FDM)
  - Boundary Element Method (BEM)
- Discrete methods
  - Discrete Element Method (DEM)
  - Discrete Fracture Network (DFN)
- Hybrid continuum/discrete methods

Special issues and difficulties in numerical modelling of underground engineering problems are (see Jing and Hudson 2002):

- Scale effects, homogenization and upscaling methods
- Numerical representation of engineering processes, such as excavation sequence, grouting and reinforcement
- Large-scale computational capacities
- Representation of rock mass properties and behaviour as an equivalent continuum
- Quantification of fracture shape, size ...

It is clear that a very important step in numerical simulation is the early "conceptualisation" of the problem in terms of the dominant processes and their mathematical presentation. Thus, the choice of the *best* numerical method in terms of scope, accuracy, efficiency and user-friendliness is very important. Below the mostly used numerical methods are described briefly to have a better comparison later on.

Finite Element Method

The FEM is perhaps the most widely applied numerical method in engineering fields. Since its origin in the early 1960s, much work has been done in both theoretical developments and applications, and it has been applied to a large

number of problems in widely different fields. Today's FE-programs have reached such a stage that almost all important features involved in underground engineering problems are solved. This has been because it was the first numerical method with enough flexibility for the treatment of material heterogeneity, non-linear deformability, complex boundary conditions, in situ stresses and gravity, see Jing and Hudson (2002), Venturini (1983).

The physical meaning of the calculation-steps is relatively transparent: The method essentially involves dividing the body in smaller "elements" of various shapes, connected at the nodes. The displacements at the nodes are treated as unknowns and are calculated, see Pande et al. (1990).

The advantages and disadvantages of the FEM can be summarised (see Schweiger 2008, Venturini 1983, Pande et al. 1990):

Advantages:

- almost no limitations with respect to modelling complex geometries;
- construction steps; advanced constitutive models; change material properties during calculation;
- special elements for modelling joint sets;
- interface elements for soil/structure interaction; extensively used -> significant experience available;
- system of equations is normally banded and symmetric for constitutive models with associated flow rule;
- each element can have different material properties.

Disadvantages:

- volume discretisation required (significant pre- and postprocessing effort for 3D analysis);
- long calculation times for 3D and high disk storage requirements;
- non-symmetric equation system for constitutive models with non-associated flow rule;

- modelling of post peak behaviour (softening material) requires special formulations and algorithms;
- not suitable for blocky structures (discontinua).

However, for simulating problems like narrow fractures or reinforcements inside large scale problems the FEM is handicapped by the requirement of very small element sizes in the nearfield of the narrow discontinuity. This overall shortcoming makes the FEM less efficient in dealing with fracture problems than its BEM counterparts, see Jing and Hudson (2002).

Boundary Element Method

This method consists of transforming the governing partial differential equation into an integral equation relating only boundary values. As a direct consequence, the dimension of the problem is reduced by one. Only the surface (the *boundary*) of the rock mass to be analysed needs to be discretised, i.e. divided into boundary elements. The domain does not need to be discretised, thus the data preparation is relatively simple. Smaller systems of equations are obtained as compared with those from domain type techniques (e.g. FEM or DEM), see Venturini (1983), Pande et al. (1990).

In the BEM a lot of development work has been done; but the BEM has not yet reached the development-stage as the FEM. However, applications for general stress and deformation analysis for underground excavations, fracturing processes, dynamic analysis, soil-structure interaction and groundwater flow have been developed. The BEM can range from simple techniques such as the so-called indirect methods to the more versatile direct formulation, see Venturini (1983).

Inclusion of source terms, such as body forces, heat sources etc. leads to domain integrals in the BEM. This problem also appears when considering initial stress/strain effects for example for non-linear material behaviour. Different techniques have been developed over the years for dealing with such domain

integrals; one of them is the division of the domain into a number of internal cells, see Jing and Hudson (2002).

In the field of rock mechanics, the most notable original development of the BEM application may be attributed to early works, see for example: Venturini (1983), Brebbia et al. (1984), Pande et al. (1990), for a more detailed literature review see Jing and Hudson (2002), Jing (2003), Gioda and Swoboda (1999).

BEM appears to be a very efficient method for homogeneous, linear elastic problems, particularly in three dimensions. For complex nonlinear material laws with a number of sets of materials, advantages of the method are considerable diminished. The matrices of equations arising in this method are not banded and symmetric as for FEM, but are fully populated. Thus, although the number of equations to be solved is considerably reduced, computation time does not reduce in the same proportion, see Pande et al. (1990).

A great enhancement in comparison to the FEM is the BEMs applicability for stress or strain analysis problems. The solutions inside the domain are continuous; stress and strain results inside the domain have the same accuracy as displacement results. However the BEM is not as efficient as the FEM in dealing with material heterogeneities. The BEM is also not as efficient as the FEM in simulating non-linear material behaviour, such as plasticity and damage evolution processes. The BEM is more suitable for solving problems of fracturing in homogeneous and linearly elastic bodies, see Jing and Hudson (2002).

The advantages and disadvantages of the BEM can be summarised (see Schweiger 2008, Venturini 1983):

Advantages:

- only surface discretisation, no volume discretisation required;
- reduced set of equations, smaller amount of data;
- no interpolation error inside the domain;
- better accuracy of stress/strain results;

- proper modelling of infinite domains;
- valuable representation for stress concentration problems.

Disadvantages:

- equation system is non-symmetric and fully populated;
- not well suited to nonlinear material behaviour;
- not well suited to inhomogeneous material;
- modelling of excavation sequence is more difficult.

Finite Difference Method

The Finite Difference Method (FDM) was the first numerical approach formulated on mathematical bases which has been applied in continuum mechanics stress analysis. The method started as a numerical technique after Southwell had presented his relaxation method (1946), although no computer automatisation was possible at that time, see Venturini (1983).

In the FDM the partial differential equations (PDE) are approximated by replacing the derivative expressions by linear combinations of function values at the neighbouring grid points. With this the PDE is replaced by a linear system using only nodal values. With proper formulations, such as static or dynamic relaxation techniques, no global system of equations in matrix form needs to be solved. It also provides a more straightforward simulation of nonlinear material behaviour, such as plasticity and damage. The conventional FDM with regular grid system is not flexible in dealing with complex boundary conditions, material heterogeneities and fractures. However, progress has been made with irregular meshes, such as triangular grid or Voronoi grid systems, which leads to Finite Volume techniques (FVM), see Jing and Hudson (2002).

One very attractive feature of FDM is that it can be very easy implemented. The quality of a FEM approximation is often higher than in the corresponding FDM approach, but this is extremely problem dependent, see Wikipedia.

The advantages and disadvantages of the FDM can be summarised by (see Schweiger 2008):

Advantages:

- complex constitutive models easier to implement;
- no equation system is required for explicit solution algorithms.

Disadvantages:

- volume discretisation required;
- slightly less versatile with respect to geometric discretisation;
- not the same range of higher order elements available;
- long calculation times in 3D;
- for linear or moderately nonlinear systems less efficient than FEM;
- method is based on Newton's law of motion thus no "converged" solution for static problems exist (artificial damping required; long calculation time; with different time steps it converges to different solutions).

Discrete Element Method

In this method the rock mass is treated as a discontinuum. The domain is assumed to consists of rigid or deformable blocks/particles and the contacts between them need to be identified and updated during the deformation/motion process. When loads are applied, the changes in contact forces are traced with time. In the earlier versions of the method rigid spherical balls or discs were used as elements. In the recent versions of the method, the elements can be of arbitrary shape and they can be deformable. The elements can split up based on the assumed fracture criterion, see Pande et al. (1990), Jing and Hudson (2002).

This method is based on the equation of motion using implicit and explicit formulations. The implicit DEM is represented mainly by the discontinuous deformation analysis (DDA) approach. It uses standard FEM meshes over

blocks and the contacts are treated using the penalty method. The implicit DDA has two advantages over the explicit DEM: larger time steps and closed-form integrations for the stiffness matrices of elements, see Jing and Hudson (2002). The DEM is one of the most rapidly developing areas of computational mechanics, and it has wide applications in rock engineering.

There are, however, several drawbacks. Firstly, the parameters required for the description of the material behaviour and additional parameters like damping are required to be chosen quite carefully. And the computation time required to solve even simple problems can be excessive, see Pande et al. (1990).

The advantages and disadvantages of the DEM can be summarised by (see Schweiger 2008):

Advantages:

- modelling of blocky structures (discontinua);
- for explicit solution algorithms no equation system required;
- suitable for studying micromechanical behaviour of granular materials.

Disadvantages:

- volume discretisation required;
- very long calculation times (for 3D);
- artificial damping required for static problems;
- influence of various input parameters (difficult to judge, i.e. joint stiffness may cause numerical problems, a lot of experience required).

Conclusion

The mostly used numerical methods were described and their main advantages and disadvantages have been specified. It was shown that the BEM is the only method who does not need the volume discretisation. Thus, this method has two big advantages compared to the other methods: only surface discretisation is required (more user-friendly mesh generation); and the system of equations is

smaller (less amount of data). Additional advantages are the better accuracy of stress/strain results and the accurate computability of stress concentration problems. Because of this, we wanted to invest further development work into this rather common method. Especially for the 3D tunnelling simulation we expect great enhancements in user-friendliness and efficiency compared to other methods.

The subject of this thesis is the simulation of rock bolts, pipe umbrella systems and geological inhomogeneities. A novel method was developed that allows to model these inclusions in combination with non-linear material behaviour efficiently with the BEM, see chapter 3.

Especially the simulation of rock bolts and anchors has key benefits compared to other methods. Whereas the FEM needs an extremely fine mesh around the bolts to handle the local stress concentrations, the capability of the BEM to deal with stress concentration problems is utilised and makes the BEM more efficient and more precisely for this kind of problems, see chapter 5 and chapter 6.

1.4 Structure of this work

The work consists of eight chapters. After this first introductory chapter, an overall description of the Boundary Element Method for elasto static continua is given in chapter two. In chapter three the basic idea of the solution procedure for calculating embedded inclusions of different kinds will be described. Different kinds of rock bolts can be calculated with this procedure as well as general inclusions like geological inhomogeneities or pipe umbrella systems. In the next chapters the special treatments for simulating different kinds of inclusions are described in detail: chapter four deals with general inclusions and pipe roofing systems; chapter fife with fully bonded rock bolts; and chapter six with discrete anchored bolts. Final some numerical examples will be presented in chapter seven.

Chapter 2

Boundary Element Method

2.1 Introduction

2.1.1 Numerical Simulation of Engineering Problems

To obtain engineering solutions for real problems following three steps have to be taken in general (see also Gaul et al. (2003)):

- A basic physical theory has to be chosen, which is suitable to the observed problem. Additional assumptions and simplifications are introduced (for example on the type of analysis, material, loading, etc). This leads us to the *physical model*. In this work elastostatic continua are outlined, the governing Partial Differential Equation (PDE) is formulated in section 2.2.
- In the next step the physical model has to be translated into a suitable *mathematical model*. For our problem the Boundary Integral Equation (BIE) is formulated at this point, which fulfils exactly the governing PDE; this is demonstrated in section 2.3. In addition the boundary and initial conditions and additional constraints have to be defined.
- After having the particular mathematical description of the problem (in our case the BIE), a numerical computational method is used to approximate the solution; this procedure is described in section 2.4

2.2 Physical Model

In this section the physical model for an elastostatic continuum will be described briefly, and with this the governing Partial Differential Equation (PDE) for elastostatics will be obtained. For this, three components are required: the kinematic relations; the kinetic relations (balance or conservation laws); and the constitutive equations; see also Gaul et al. (2003). The detailed description of the concepts of continuum mechanics is not subject of this work, it is very well explained in several standard textbooks.

Kinematics: "Kinematics (from Greek $\kappa\iota\nu\varepsilon\iota\nu$, kinein, to move) is the branch of classical mechanics that describes the motion of objects without consideration of the causes leading to the motion.", see Wikipedia.

The general non-linear kinematics of a continuous body is a rather complex subject and can be described in various ways which is treated exhaustively in many publications. Here a commonly used simplified relation is used; assuming small strains we obtain the symmetric linear strain tensor:

$$\varepsilon_{ij} = \frac{1}{2}\left(u_{i,j} + u_{j,i}\right) \tag{2.1}$$

ε_{ij} is the strain tensor and u_i is the displacement vector.

Kinetics: "In physics and engineering, kinetics is a term for the branch of classical mechanics that is concerned with the relationship between the motion of bodies and its causes, namely forces and torques.", see Wikipedia. In other words it deals with the external loading of a body and the resulting internal force field (balance law).

The Cauchy's equation of motion can be derived for a general dynamic problem:

$$\sigma_{ji,j} + b_i = \varrho \ddot{u}_i \tag{2.2}$$

where $\sigma_{ji,j}$ are the derivatives of the stress tensor; b_i are the body forces; ϱ is the mass density; and $\ddot{u}_i$ is the acceleration (the time derivative of the velocity $\dot{u}_i$). For elastostatic problems time effects are neglected, the

right side vanishes in equation 2.2 and we obtain:

$$\sigma_{ji,j} + b_i = 0 \tag{2.3}$$

Constitutive Equations: "In physics, a constitutive equation is a relation between two physical quantities (often described by tensors) that is specific to a material or substance, and approximates the response of that material to external forces", see Wikipedia. Here it describes the relation between the stress tensor σ_{ij} and the strain tensor ε_{kl}.

In the general nonlinear case the constitutive equation is obtained in differential form:

$$d\sigma_{ij} = C_{ijkl}\left(\varepsilon_{kl}\right) d\varepsilon_{kl} \tag{2.4}$$

$d\sigma_{ij}$ and $d\varepsilon_{kl}$ are the differential stress- and strain-rates, $C_{ijkl}\left(\varepsilon_{kl}\right)$ is the constitutive tensor depending on the strain state ε_{kl}. Considering linear elastic material behaviour we obtain the generalised Hooke's law:

$$\sigma_{ij} = C_{ijkl}\varepsilon_{kl} \tag{2.5}$$

Strictly speaking this is valid only for the case that $\sigma^0_{ij} = 0$; where σ^0_{ij} are stresses in the unstrained state (initial stresses). The general relation considering initial stresses is:

$$\sigma_{ij} = \sigma^0_{ij} + C_{ijkl}\varepsilon_{kl} \tag{2.6}$$

Combining these three concepts we achieve the field equation. Using equation 2.1, equation 2.2 and equation 2.5 and the symmetry of the stress tensor the governing Partial Differential Equation (PDE) for elastodynamic problems is obtained (the well known Navier's equation):

$$C_{ijkl}u_{k,lj} + b_i = \varrho\ddot{u}_i \tag{2.7}$$

In elastostatics we use equation 2.3 instead of equation 2.2 and it occurs:

$$C_{ijkl}u_{k,lj} + b_i = 0 \tag{2.8}$$

To solve the particular boundary-value problem additional information (boundary conditions) are needed. Boundary conditions can be classified as follows:

- Dirichlet boundary condition: prescribed the primary field variable (here the displacement vector u_i)
- Neumann boundary condition: prescribed the derivative of the primary field variable (here the traction vector t_i)
- Robin boundary condition: prescribed a function of the primary field variable and its derivative (here not used)

The governing PDE can be obtained for different types of physical phenomena in an analogical way; not only for elastodynamics and elastostatics but also for example for heat conduction, electrodynamics, thermoelasticity, acoustics and piezoelectricity. However, in this work the elastostatic problem is investigated.

2.3 Integral Formulation

In this section it is shown how to solve the physical problem (section 2.2) with the Boundary Integral Equation (BIE) for the elastostatic case. The derivation of the BIE can be done in different ways; one general method is the *Weighted Residual Approach* which can be applied to any kind of linear differential operator with constant coefficients (see for example Gaul et al. 2003, Brebbia et al. 1984). However, a more direct and engineering-like way is to derive the BIE by using *Betti's theorem* (see for example Beer and Watson 1994, Paris and Canas 1997, Gaul et al. 2003). In this work the second way using Betti's theorem is described since this is the easier comprehensible way.

2.3.1 Betti's Theorem

Two problems are considered: the actual configuration and the auxiliary configuration, see figure 2.1. It is assumed that both configurations are related to the same linear elastic material, see for example Paris and Canas (1997).

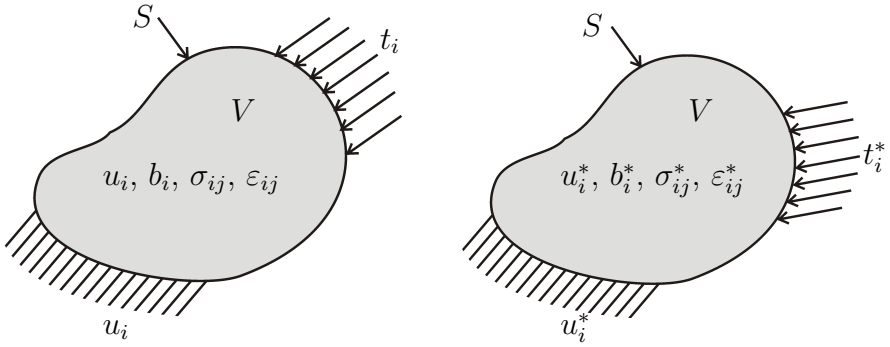

(a) Actual configuration (b) Auxiliary configuration

Figure 2.1: Configurations involved in Betti's theorem

Betti's First Theorem

The first theorem establishes the reciprocity of the *internal work* of these two problems:

$$\int_V \sigma_{ij}\varepsilon_{ij}^* dV = \int_V \sigma_{ij}^*\varepsilon_{ij} dV \tag{2.9}$$

Where $\sigma_{ij}, \sigma_{ij}^*$ and $\varepsilon_{ij}, \varepsilon_{ij}^*$ are the stresses and the strains in the two configurations; V is the volume. It states that the work of σ_{ij} on ε_{ij}^* is the same as the work of σ_{ij}^* on ε_{ij}. This can be demonstrated immediately using following assumptions:

$$\begin{aligned} \sigma_{ij} &= 2G\varepsilon_{ij} + \lambda\varepsilon_{kk}\delta_{ij} \\ \sigma_{ij}^* &= 2G\varepsilon_{ij}^* + \lambda\varepsilon_{kk}^*\delta_{ij} \end{aligned} \tag{2.10}$$

Substituting this into the first part of equation 2.9 we obtain:

$$\begin{aligned}\int_V \sigma_{ij}\varepsilon^*_{ij}dV &= \int_V \left(2G\varepsilon_{ij} + \lambda\varepsilon_{kk}\delta_{ij}\right)\varepsilon^*_{ij}dV \\ &= \int_V \left(2G\varepsilon_{ij}\varepsilon^*_{ij} + \lambda\varepsilon_{kl}\delta_{kl}\varepsilon^*_{ij}\delta_{ij}\right)dV \\ &= \int_V \left(2G\varepsilon^*_{ij} + \lambda\varepsilon^*_{kk}\delta_{ij}\right)\varepsilon_{ij}dV = \int_V \sigma^*_{ij}\varepsilon_{ij}dV\end{aligned} \tag{2.11}$$

Betti's Second Theorem

The second theorem establishes the reciprocity of the *external work* of the two problems:

$$\int_V b_i u^*_i dV + \int_S t_i u^*_i dS = \int_V b^*_i u_i dV + \int_S t^*_i u_i dS \tag{2.12}$$

The external loads consist of the boundary loads t_i, t^*_i (tractions on the boundary S) and the domain loads b_i, b^*_i (body forces in the domain V); u_i, u^*_i are the displacements. The tractions are defined to be boundary stresses:

$$t_i = \sigma_{ij}n_j \qquad t^*_i = \sigma^*_{ij}n_j \tag{2.13}$$

where n_i is a unit vector in the direction normal to the the boundary S.

To achieve Betti's second theorem different ways are possible, two of them are described here:

- One easy and short way to reach equation 2.12 is to apply the *Virtual Work Theorem* and substitute this into equation 2.9 (see Paris and Canas 1997).

$$\int_V \sigma_{ij}\varepsilon^*_{ij}dV = \int_V b_i u^*_i dV + \int_S t_i u^*_i dS \tag{2.14}$$

$$\int_V \sigma^*_{ij}\varepsilon_{ij}dV = \int_V b^*_i u_i dV + \int_S t^*_i u_i dS \tag{2.15}$$

- An other way which leads to the same equation 2.12 is the following (see for example Brebbia et al. 1984, Gaul et al. 2003): first we use the kinematic equation 2.1 and assume the symmetry of stress- and strain- tensor which leads to $\varepsilon_{ij} = u_{i,j}$. Substituting this into equation 2.9, integrating by parts both sides and applying the theorem of Gauss we obtain:

$$\int_V \sigma_{ij,j} u_i^* dV + \int_S \sigma_{ij} u_i^* n_j dS = \int_V \sigma_{ij,j}^* u_i dV + \int_S \sigma_{ij}^* u_i n_j dS \tag{2.16}$$

  Substituting Cauchy's equation 2.3 and the relations of equation 2.13 into the above equation 2.16, it follows identically the same relation as in equation 2.12.

For Betti's second theorem to be true, u_i and u_i^* have to be twice continuously differentiable. In the derivation of the BIE this condition is essential.

2.3.2 Somigliana's Identity

Betti's second theorem (equation 2.12) can be modified further by assuming that the body force components in the reciprocal field b_i^* corresponds to unit point loads applied at the load points $P \in V$, see figure 2.2 (see for example Brebbia et al. 1984). The unit point load can be described by the Dirac delta function $\delta(P,Q)$ and a unit vector in the direction of the load n_i:

$$b_i^* = \delta(P,Q)\, n_i \tag{2.17}$$

The Dirac delta function has following properties:

$$\begin{aligned} &\delta(P,Q) = \infty && \text{if } P = Q \\ &\delta(P,Q) = 0 && \text{if } P \neq Q \\ &\int_V g(Q)\, \delta(P,Q)\, dV(Q) = g(P) \end{aligned} \tag{2.18}$$

where g is any function.

With this, the first integral of the right-side of equation 2.12 can be rewritten:

$$\int_V b_i^* u_i dV = u_i n_i \tag{2.19}$$

Thus, u_i^* is defined to be the particular solution for a point load in an infinite domain, it represents the displacement response due to the point load b_i^*. u_i^* is the so-called *fundamental solution*, which is described later in more detail in section 2.3.3. At this point it is assumed that the fundamental solution u_i^* has been found.

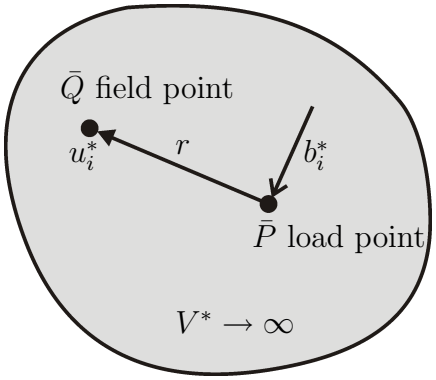

Figure 2.2: Unit point load b_i^* in the domain V^*

By applying the point load b_i^* in all three coordinate directions, all three components of the displacement vector are obtained. This leads to three different fundamental solutions u_i^* which can be combined to the fundamental solution tensor U_{ij}.

$$u_i^*(Q) = U_{ij}(P, Q)\, n_j(P) \tag{2.20}$$

The displacement u_i^* at point Q results from the unit point load at P acting in the direction n_j.

Substituting the generalised Hooks law (equation 2.5) and the kinematic equation 2.1 into the definition for the tractions (equation 2.13) and assuming the symmetry of the strain tensor, the traction t_i^* can be derived directly from the

primary field variable u_i^*:

$$t_i^* = \sigma_{ij}^* n_j = C_{ijkl}\varepsilon_{kl}^* n_j = C_{ijkl} u_{k,l}^* n_j \tag{2.21}$$

Thus, the fundamental solution tensor for the traction response T_{ij} due to unit point loads b_i^* in all three coordinate directions can be calculated similar to equation 2.20:

$$t_i^*(Q) = T_{ij}(P,Q)\, n_j(P) \tag{2.22}$$

Substituting equation 2.19, equation 2.20 and equation 2.22 into Betti's second theorem (equation 2.12) and reduce n_j it arises:

$$\begin{aligned} u_i\left(\bar{P}\right) = &\int_S U_{ij}\left(\bar{P},Q\right) t_i(Q)\, dS(Q) - \int_S T_{ij}\left(\bar{P},Q\right) u_i(Q)\, dS(Q) \\ &+ \int_V U_{ij}\left(\bar{P},\bar{Q}\right) b_i\left(\bar{Q}\right) dV\left(\bar{Q}\right) \end{aligned} \tag{2.23}$$

Equation 2.23 is known as *Somigliana's identity* for displacements; it is also called *representation formula*. Equation 2.23 allows us to calculate unknown displacements $u_i\left(\bar{P}\right)$ inside the domain, when the boundary variables $t_i(Q)$ and $u_i(Q)$ and the body forces $b_i\left(\bar{Q}\right)$ are known. Henceforward, the points with the over bar character are defined to be inside the domain $\bar{P}, \bar{Q} \in V$ and the points without an over bar are defined to be at the boundary $Q, P \in S$.

2.3.3 Fundamental Solutions

For elastostatics, the fundamental solution is the displacement distribution in a material, due to a concentrated point force acting on an infinite elastic domain. In other words, it is a function that satisfies the governing PDE (Navier's equation 2.8), by applying a unit point load as body force (see equation 2.17):

$$C_{ijkl} u_{k,lj}^* + \delta(P,Q)\, n_i = 0 \tag{2.24}$$

assuming isotropic material behaviour, equation 2.24 can be written as:

$$Gu^*_{i,jj} + \frac{G}{1-2\nu} u^*_{j,ij} + \delta(P,Q)\, n_i = 0 \tag{2.25}$$

where G is the shear modulus and ν is the Poisson's ratio. This is a set of three coupled PDE with very difficult solutions. However, it is possible to transform the equation 2.25 into a set of uncoupled equations by introducing the *Galerkin vector* (a three dimensional vector considering potential functions). This set of uncoupled equations can be solved (for a detailed description see for example Brebbia et al. 1984, Paris and Canas 1997, Gaul et al. 2003) and the fundamental solution is obtained. Using the expressions for the fundamental displacement tensor U_{ij} (equation 2.20) the solution of equation 2.25 is given by:

$$U_{ij}(P,Q) = \frac{1}{16\pi(1-\nu)Gr}\left\{(3-4\nu)\,\delta_{ij} + r_{,i}r_{,j}\right\} \quad \text{... 3D} \tag{2.26}$$

$$U_{ij}(P,Q) = \frac{-1}{8\pi(1-\nu)G}\left\{(3-4\nu)\ln(r)\,\delta_{ij} + r_{,i}r_{,j}\right\} \quad \text{... plane strain} \tag{2.27}$$

U_{ij} is Kelvin's fundamental solution for 3D and 2D (plain strain). $r = r(P,Q)$ represents the distance between the load point P and the field point Q, see figure 2.2.

$$\begin{aligned} r &= |\boldsymbol{Q} - \boldsymbol{P}| = (r_i r_i)^{\frac{1}{2}} \\ r_i &= Q_i - P_i \\ r_{,i} &= \frac{\partial r}{\partial} = \frac{r_i}{r} \end{aligned} \tag{2.28}$$

Once the fundamental solution for displacements are known the equations of the elasticity theory can be applied to determine the fundamental solution for tractions T_{ij}. Using equation 2.21 and equation 2.22 we obtain:

$$\begin{aligned} T_{ij}(P,Q) = & \frac{-1}{4\alpha\pi(1-\nu)r^{\alpha}} \\ & \left\{\left[(1-2\nu)\,\delta_{ij} + \beta r_{,i}r_{,j}\right]\frac{\partial r}{\partial n} - (1-2\nu)\left(r_{,i}n_j - r_{,j}n_i\right)\right\} \end{aligned} \tag{2.29}$$

$\alpha = 2; \beta = 3$ for 3D and $\alpha = 1; \beta = 2$ for plane strain. The fundamental solution tensors for strains and stresses are defined by:

$$\begin{aligned} \varepsilon^*_{jk} &= E_{ijk} n_i \\ \sigma^*_{jk} &= R_{ijk} n_i \end{aligned} \tag{2.30}$$

They are determined by using the kinematic relations (equation 2.1) and the generalised Hooke's law (equation 2.5), see also Gao and Davies (2002), Beer et al. (2008):

$$\begin{aligned} E_{jki}(P,Q) = &\frac{-1}{8\alpha\pi(1-\nu)Gr^\alpha} \\ &\{(1-2\nu)(r_{,k}\delta_{ij} + r_{,j}\delta_{ik}) - r_{,i}\delta_{jk} + \beta r_{,i} r_{,j} r_{,k}\} \end{aligned} \tag{2.31}$$

$$\begin{aligned} R_{jki}(P,Q) = &\frac{-1}{4\alpha\pi(1-\nu)r^\alpha} \\ &\{(1-2\nu)(r_{,k}\delta_{ij} + r_{,j}\delta_{ki} - r_{,i}\delta_{jk}) + \beta r_{,i} r_{,j} r_{,k}\} \end{aligned} \tag{2.32}$$

The plane strain expressions are valid for plane stress too, by replacing ν with $\bar{\nu} = \nu/(1+\nu)$. In addition to these fundamental solutions which are valid for an infinite domain, fundamental solutions can be adopted to half-space problems.

Generally, Fundamental solutions are known for homogeneous materials, whether isotropic or not, and so the common BIE is applicable to the analysis of homogeneous domains only. By various mathematical techniques, fundamental solutions of a wide range of PDE have been derived.

2.3.4 Boundary Integral Equation

As noted before in section 2.3.2, Somigliana's identity (equation 2.23) returns the values of displacements in the interior of the domain when the boundary solutions u_i and t_i and the body forces b_i are known. However at the beginning only one set of boundary conditions are known, either u_i or t_i, the other set is unknown and Somigliana's identity can not be solved. To obtain an equation that

contains only the boundary data and the body forces, we have to move the load point from the domain $\bar{P} \in V$ to the boundary $P \in S$. The resulting equation is called Boundary Integral Equation (BIE), which describes the field problem exclusively in terms of boundary variables (and the known body forces).

The process of moving the load point to the boundary is not trivial because singularities arise at the point $P = Q$. For this the boundary is augmented by a small spherical extension (radius ε) in the load point, see figure 2.3. And than a limiting process has to be carried out, where the spherical extension tends to zero $\varepsilon \to 0$, taking this limit the modified boundary approaches the original boundary:

$$S = \lim_{\varepsilon \to 0} S - S_\varepsilon + \bar{S}_\varepsilon \tag{2.33}$$

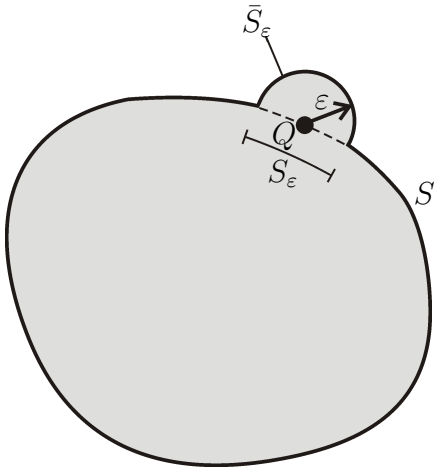

Figure 2.3: Spherical boundary extension around the load point Q

Applying this modified boundary and the limiting process to equation 2.23 we

obtain:

$$\begin{aligned} u_i(P) = &\lim_{\varepsilon\to 0}\int\limits_{S-S_\varepsilon} U_{ij}(P,Q)\, t_j(Q)\, dS(Q) + \lim_{\varepsilon\to 0}\int\limits_{\bar{S}_\varepsilon} U_{ij}(P,Q)\, t_j(Q)\, dS(Q) \\ &- \lim_{\varepsilon\to 0}\int\limits_{S-S_\varepsilon} T_{ij}(P,Q)\, u_j(Q)\, dS(Q) - \lim_{\varepsilon\to 0}\int\limits_{\bar{S}_\varepsilon} T_{ij}(P,Q)\, u_j(Q)\, dS(Q) \\ &+ \int\limits_V U_{ij}\left(P,\bar{Q}\right) b_j\left(\bar{Q}\right) dV\left(\bar{Q}\right) \end{aligned} \tag{2.34}$$

Integration over U_{ij}

The integral over the fundamental solution U_{ij} in equation 2.34 leads to a *weakly singular* or *improper* integral, see section 2.5.1. The weakly singular integral exists independently of how the limit ε tends to zero. In the 2D case the fundamental solution has the order $U_{ij} = \mathcal{O}(\ln(r))$ and in the 3D case it has the order $U_{ij} = \mathcal{O}(1/r)$, see section 2.3.3. By introducing cylindrical coordinates in the 2D case ($dS = rdrd\Theta$) or polar coordinates in the 3D case ($dS = r^2 \sin(\Theta_1)\, d\Theta_1 d\Theta_2$) the singularity is cancelled out.

The integral over the boundary extension $\bar{S}_\varepsilon$ vanishes.

$$\lim_{\varepsilon\to 0}\int\limits_{\bar{S}_\varepsilon} U_{ij}(P,Q)\, t_j(Q)\, dS(Q) = 0 \tag{2.35}$$

The integral over $S - S_\varepsilon$ can be calculated by taking the limit $\varepsilon \to 0$, it leads to a finite solution:

$$\lim_{\varepsilon\to 0}\int\limits_{S-S_\varepsilon} U_{ij}(P,Q)\, t_j(Q)\, dS(Q) = \int\limits_S U_{ij}(P,Q)\, t_j(Q)\, dS(Q) \tag{2.36}$$

Integration over T_{ij}

The integration over the fundamental solution T_{ij} in equation 2.34 leads to a *strongly singular* integral. However, in this case the strongly singular integral exists as *Cauchy principal value*. In other words it exists for a certain form of the limit ε, if certain symmetry-conditions are fulfilled the infinite part adds to zero, see section 2.5.2.

The integral over the boundary extension $\bar{S}_\varepsilon$ can be written as:

$$\lim_{\varepsilon \to 0} \int_{\bar{S}_\varepsilon} T_{ij}(P,Q)\, u_j(Q)\, dS(Q) = \lim_{\varepsilon \to 0} \int_{\bar{S}_\varepsilon} T_{ij}(P,Q)\, [u_j(Q) - u_j(P)]\, dS(Q) + \lim_{\varepsilon \to 0} u_j(P) \int_{\bar{S}_\varepsilon} T_{ij}(P,Q)\, dS(Q) \tag{2.37}$$

The first integral on the right side in equation 2.37 disappears because in the limit $(P = Q)$ the part $[u_j(Q) - u_j(P)]$ vanishes. In the second term on the right side $u_j(P)$ might be taken out of the integral because it is independent of the integral variable Q.

The integral over $S - S_\varepsilon$ exists too, and it is written as follows:

$$\lim_{\varepsilon \to 0} \int_{S - S_\varepsilon} T_{ij}(P,Q)\, u_j(Q)\, dS(Q) = \oint_S T_{ij}(P,Q)\, u_j(Q)\, dS(Q) \tag{2.38}$$

where $\oint$ denotes the Cauchy principal value integral.

Boundary Integral Equation

Substituting this (equation 2.35, equation 2.36, equation 2.37 and equation 2.38) into equation 2.34 we obtain finally the Boundary Integral Equation (BIE):

$$c_{ij}(P)\,u_j(P) = \int_S U_{ij}(P,Q)\,t_j(Q)\,dS(Q) - \oint_S T_{ij}(P,Q)\,u_j(Q)\,dS(Q) + \int_V U_{ij}\left(P,\bar{Q}\right) b_j\left(\bar{Q}\right) dV\left(\bar{Q}\right) \tag{2.39}$$

where $c_{ij}(P)$ contains the remaining part of the integral in equation 2.37 and is called *free term*:

$$c_{ij}(P) = \delta_{ij} + \lim_{\varepsilon \to 0} \int_{\bar{S}_\varepsilon} T_{ij}(P,Q)\,dS(Q) \tag{2.40}$$

If the boundary at point P is smooth, the free term is $c_{ij}(P) = \delta_{ij}/2$.

Equation 2.39 provides the relation between boundary displacements, boundary tractions and body forces. The BIE is the starting point for the numerical solution.

2.3.5 Body Forces

In many practical applications nonzero body forces are present; therefore a procedure is presented for computing its influence into the analysis. It has been shown that if body forces are considered, domain integrals have to be computed (see equation 2.40), see for example Gao and Davies (2002), Beer et al. (2008).

Solving the Domain Integral

In some particular cases, if the body force is constant or a harmonic function (i.e. it satisfies $b_{,ii} = 0$) the domain integral can be transformed to a boundary

integral, and thus a domain discretisation can be avoided, see Gaul et al. (2003), Brebbia et al. (1984)). This is used for example to analyse gravitational loads (assuming a constant mass density and a constant gravitational field); for problems considering a centrifugal load; or for problems considering thermal loadings; see Brebbia et al. (1984). However, in several cases this transformation to the boundary is not possible; this is the case when body forces are neither constant nor harmonic functions or if they are acting on certain areas only. Here a cell-integration technique is used for this kind of problems, in which the domains where the body forces are acting are discretised by a certain number of cells and numerical integration is carried out over these cells. While the cells have the appearance of a Finite Element mesh, it is essentially different because there are no unknowns in the domain and the cells are only used to carry out the integration (e.g. Gaussian quadrature).

Different Kinds of Body Forces

In addition to the applied forces b_j in equation 2.40, it is also possible to apply initial stresses $\sigma_{0\,ij}$ and initial strains $\varepsilon_{0\,ij}$ inside the domain (see figure 2.4). Adding this additional *external loads* to the actual configuration and apply the virtual work theorem (see section 2.3.1, equation 2.14) we obtain Betti's second theorem (see equation 2.12) in the following form:

$$\int_V b_i u_i^* dV + \int_V \sigma_{0\,ij} \varepsilon_{ij}^* dV + \int_V \varepsilon_{0\,ij} \sigma_{ij}^* dV + \int_S t_i u_i^* dS = \int_V b_i^* u_i dV + \int_S t_i^* u_i dS \tag{2.41}$$

With this and by using the fundamental solutions tensors for stresses (equation 2.32) and for strains (equation 2.31), Somigliana's identity (see equa-

tion 2.23) can be written:

$$u_i\left(\bar{P}\right) = \int_S U_{ij}\left(\bar{P},Q\right) t_j\left(Q\right) dS\left(Q\right) - \int_S T_{ij}\left(\bar{P},Q\right) u_j\left(Q\right) dS\left(Q\right) + f_i\left(\bar{P}\right) \tag{2.42}$$

with

$$\begin{aligned} f_i\left(\bar{P}\right) = & \int_V U_{ij}\left(\bar{P},\bar{Q}\right) b_j\left(\bar{Q}\right) dV\left(\bar{Q}\right) \\ & + \int_V E_{ijk}\left(\bar{P},\bar{Q}\right) \sigma_{0\,jk}\left(\bar{Q}\right) dV\left(\bar{Q}\right) \\ & + \int_V R_{ijk}\left(\bar{P},\bar{Q}\right) \varepsilon_{0\,jk}\left(\bar{Q}\right) dV\left(\bar{Q}\right) \end{aligned} \tag{2.43}$$

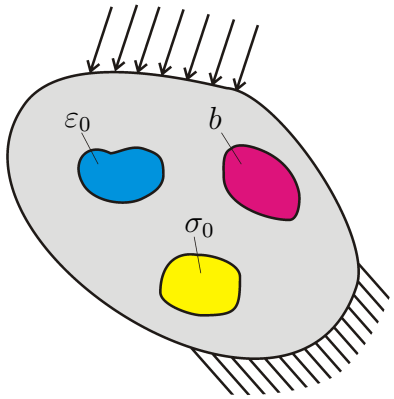

Figure 2.4: Problem considering forces $\boldsymbol{b}$, initial stresses $\boldsymbol{\sigma_0}$, initial strains $\boldsymbol{\varepsilon_0}$

In order to simplify the presentation, the volume integrals considering the *body forces* (forces b_j, initial stresses $\sigma_{0\,jk}$ and initial strains $\varepsilon_{0\,jk}$) are represented by the body force vector f_i. Applying the limiting process of section 2.3.4 ($\bar{P} \rightarrow P$),

the BIE is obtained:

$$c_{ij}(P)\,u_j(P) = \int_S U_{ij}(P,Q)\,t_j(Q)\,dS(Q) - \int_S T_{ij}(P,Q)\,u_j(Q)\,dS(Q) + f_i(P,) \tag{2.44}$$

Point Forces and Line Loads

In some problems a concentrated force has to be considered, for example to simulate a pre-stressed anchor (see chapter 6). When using domain discretisation methods like Finite Elements or Finite Differences such problems are difficult to incorporate: a very fine mesh around the concentrated force would be necessary to handle the stress distributions correctly. In contrast, the Boundary Element Method is excellently suitable to solve problems with concentrated sources since the fundamental solutions are already exact solutions of the governing equations for a point source (see Gaul et al., 2003). Assuming a concentrated force of the magnitudes b_i^p at the point $\bar{Q}$ inside the domain V (see figure 2.5), the body force vector f_i can be written as

$$f_i(P) = U_{ij}\left(P,\bar{Q}\right) b_i^p\left(\bar{Q}\right) \tag{2.45}$$

In this case no volume integral occurs.

An other kind of problems are forces acting along a line inside the domain (see figure 2.5), this can be used for example to simulate fully bonded rock bolts (see chapter 5). Assuming a line with the length L and applying a line load b_i^l on it, the body force vector f_i can be written as

$$f_i(P) = \int_L U_{ij}\left(P,\bar{Q}\right) b_i^l\left(\bar{Q}\right) dL\left(\bar{Q}\right) \tag{2.46}$$

In this case the volume integral is replaced by the integral over the line-length.

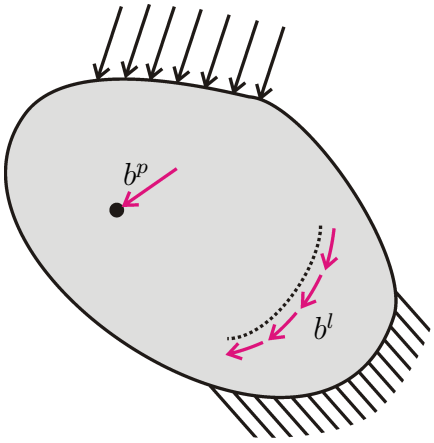

Figure 2.5: Problem considering a concentrated point forces $\boldsymbol{b^p}$ and a line-loading $\boldsymbol{b^l}$

2.3.6 Internal Results

Once the BIE (equation 2.39) is solved all boundary quantities have been found (u_i, t_i on S). After that, displacements, strains or stresses can be calculated at any point inside the domain.

Displacements at Internal Points

At this stage u_i and t_i are known over the whole boundary S and the displacements at the internal points $\bar{P}$ can be calculated directly by using Somigliana's Identity (see equation 2.42):

$$u_i\left(\bar{P}\right) = \int_S U_{ij}\left(\bar{P},Q\right) t_i\left(Q\right) dS\left(Q\right) - \int_S T_{ij}\left(\bar{P},Q\right) u_i\left(Q\right) dS\left(Q\right) + f_i\left(\bar{P}\right) \tag{2.47}$$

After the displacements are known the strains and stresses could be obtained by deriving the displacements according to a certain interpolation, as it is done

in the Finite Element Method. Thus strains and stresses would have a lower level of accuracy. In the Boundary Element Method it is possible to calculate them directly with the integral representation of strains and stresses. With this the same level of precision as for the displacements is achieved.

Strains at Internal Points

The strains can be expressed as a function of displacements (equation 2.1):

$$\varepsilon_{ij} = \frac{1}{2}\left(u_{i,j} + u_{j,i}\right) \tag{2.48}$$

Assuming the symmetry of the strain tensor, and substituting u_i given in equation 2.47 into equation 2.48 we obtain:

$$\begin{aligned}\varepsilon_{ij}\left(\bar{P}\right) = u_{i,j}\left(\bar{P}\right) = \frac{\partial u_i\left(\bar{P}\right)}{\partial x_j\left(\bar{P}\right)} = \\ \int_S \underbrace{\frac{\partial U_{ik}\left(\bar{P},Q\right)}{\partial x_j\left(\bar{P}\right)}}_{D^{\varepsilon}_{kij}} t_k\left(Q\right) dS\left(Q\right) - \int_S \underbrace{\frac{\partial T_{ik}\left(\bar{P},Q\right)}{\partial x_j\left(\bar{P}\right)}}_{S^{\varepsilon}_{kij}} u_k\left(Q\right) dS\left(Q\right) + f^{\varepsilon}_{ij}\left(\bar{P}\right)\end{aligned} \tag{2.49}$$

The differentiation of the displacements yields the strains. Both of the differentials in equation 2.49 can be evaluated without difficulty. The representation in compact form is:

$$\begin{aligned}\varepsilon_{ij}\left(\bar{P}\right) = \int_S D^{\varepsilon}_{kij}\left(\bar{P},Q\right) t_k\left(Q\right) dS\left(Q\right) - \int_S S^{\varepsilon}_{kij}\left(\bar{P},Q\right) u_k\left(Q\right) dS\left(Q\right) \\ + f^{\varepsilon}_{ij}\left(\bar{P}\right)\end{aligned} \tag{2.50}$$

where:

$$D^{\varepsilon}_{kij} = \frac{1}{8\alpha\pi\left(1-\nu\right)Gr^{\alpha}}\left[\left(1-2\nu\right)\left(\delta_{ik}r_{,j} + \delta_{jk}r_{,i}\right) - \delta_{ij}r_{,k} + \beta r_{,i}r_{,j}r_{,k}\right] \tag{2.51}$$

$$S^{\varepsilon}_{kij} = \frac{1}{4\alpha\pi\left(1-\nu\right)r^{\beta}}\left[\beta r_{,m}n_m\left[\nu\left(\delta_{ik}r_{,j}+\delta_{jk}r_{,i}\right)+\delta_{ij}r_{,k}-\gamma r_{,i}r_{,j}r_{,k}\right]\right.$$
$$\left.+\left(1-2\nu\right)\left(\delta_{ik}n_j-\delta_{ij}n_k+\delta_{jk}n_i+\beta r_{,i}r_{,j}n_k\right)+\beta\nu\left(n_j r_{,i}r_{,k}+n_i r_{,j}r_{,k}\right)\right] \tag{2.52}$$

With $\alpha = 1$, $\beta = 2$ for 2D (plain strain) and $\alpha = 2$, $\beta = 3$ for 3D, see for example Beer et al. (2008). Under consideration of the different kinds of body forces (forces, initial stresses and initial strains; see equation 2.43) the body force vector for the strain integral equation f^{ε}_{ij} can be derived:

$$\begin{aligned} f^{\varepsilon}_{ij}\left(\bar{P}\right) = \int_V \underbrace{\frac{\partial U_{ik}\left(\bar{P},\bar{Q}\right)}{\partial x_j\left(\bar{P}\right)}}_{D^{\varepsilon}_{kij}} b_k\left(\bar{Q}\right) dV\left(\bar{Q}\right) \\ + \frac{\partial}{\partial x_j\left(\bar{P}\right)}\int_V E_{kli}\left(\bar{P},\bar{Q}\right)\sigma_{0\,kl}\left(\bar{Q}\right) dV\left(\bar{Q}\right) \\ + \frac{\partial}{\partial x_j\left(\bar{P}\right)}\int_V R_{kli}\left(\bar{P},\bar{Q}\right)\varepsilon_{0\,kl}\left(\bar{Q}\right) dV\left(\bar{Q}\right) \end{aligned} \tag{2.53}$$

It can be seen that the differential in the first integral of equation 2.53 is equal to the D^{ε}_{kij} in equation 2.49. However, the last two terms include derivations over strongly singular integrals and thus needs further investigations, see also Telles (1983), Brebbia et al. (1984). Here the procedure is shown to solve the first of these two terms; the second one can be done in a similar way.

First a sphere with the radius ε located in the load point $\bar{P}$ is removed from volume V, the remaining volume is called V_{ε}, see figure 2.6. By taking the limit $\varepsilon \to 0$ the modified volume approaches the original volume:

$$V = \lim_{\varepsilon\to 0} V_{\varepsilon} \tag{2.54}$$

Applying this modified volume and the limiting process to the second term on the right side of equation 2.53 we obtain:

$$\frac{\partial}{\partial x_j}\int_V E_{kli}\sigma_{0\,kl}dV = \lim_{\varepsilon\to 0}\frac{\partial}{\partial x_j}\int_{V_{\varepsilon}} \partial E_{kli}\sigma_{0\,kl}dV \tag{2.55}$$

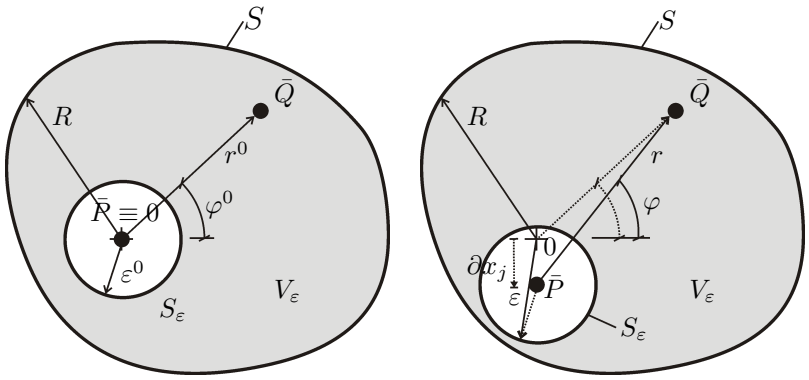

(a) Cylindrical coordinate system based on $P \equiv 0$

(b) Moving the singular point by a small increment ∂x_j

Figure 2.6: Introducing a modified volume V_ε

Cylindrical coordinates $(r,\, \varphi)$ are introduced for the 2D case and polar coordinates for the 3D case; here the 2D case is presented. Expressing the tensor E_{kli} with cylindrical coordinates we obtain:

$$E_{kli} = \frac{1}{r} g_{kli}\left(\varphi\right) \tag{2.56}$$

Where $g_{kli}\left(\varphi\right)$ is a function depending on φ. When the load point is located at the origin of the cylindrical coordinate system $\bar{P} \equiv 0$ it holds $r = r^o$ and $\varphi = \varphi^0$, see figure 2.6(a); but if $\bar{P}$ moves with a small increment ∂x_j, $r = r\left(r^o \varphi^0\right)$ and $\varphi = \varphi\left(r^o \varphi^0\right)$ becomes different, see figure 2.6(b).

Substituting equation 2.56 into equation 2.55 and transforming the coordinates $(dV = r^o dr^o d\varphi^0)$, it occurs:

$$\int_0^{2\pi} \lim_{\varepsilon \to 0} \left(\frac{\partial}{\partial x_j} \int_{\varepsilon^0}^{R} \frac{g_{kli}\left(\varphi\left(r^o \varphi^0\right)\right)}{r\left(r^o \varphi^0\right)} \sigma_{0\,kl} r^o dr^o \right) d\varphi^o \tag{2.57}$$

wich allows the application of Leibnitz formula; Leibnitz formula is defined as:

$$\frac{d}{d\alpha} \int_{\varphi_1(\alpha)}^{\varphi_2(\alpha)} F\left(x, \alpha\right) dx = \int_{\varphi_1(\alpha)}^{\varphi_2(\alpha)} \frac{\partial F}{\partial \alpha} dx - F\left(\varphi_1, \alpha\right) \frac{d\varphi_1}{d\alpha} + F\left(\varphi_2, \alpha\right) \frac{d\varphi_2}{d\alpha} \tag{2.58}$$

Applying this to the term between the brackets of equation 2.57 we obtain:

$$\begin{aligned}&\frac{\partial}{\partial x_j}\int\limits_{\varepsilon^0}^{R}\frac{g_{kli}\left(\varphi\right)}{r}\sigma_{0\,kl}r^o dr^o = \\ &\int\limits_{\varepsilon^0}^{R}\frac{\partial}{\partial x_j}\frac{g_{kli}\left(\varphi\right)}{r}\sigma_{0\,kl}r^o dr^o - \frac{g_{kli}\left(\varphi\right)}{r}\sigma_{0\,kl}\varepsilon^0\frac{\partial\varepsilon^0}{\partial x_j} + \frac{g_{kli}\left(\varphi\right)}{r}\sigma_{0\,kl}R\frac{\partial R}{\partial x_j}\end{aligned} \tag{2.59}$$

The last term in equation 2.59 vanishes, because R is independent of x_j and thus $\partial R/\partial x_j = 0$. For a detailed proof see Telles (1983), Brebbia et al. (1984). Substituting this bag into the brackets from equation 2.57 and taking into consideration that $P \equiv 0$ and $r = \varepsilon$ it arise:

$$\int\limits_{0}^{2\pi}\lim_{\varepsilon\to 0}\left(\int\limits_{\varepsilon^0}^{R}\frac{\partial}{\partial x_j}\frac{g_{kli}\left(\varphi\right)}{r}\sigma_{0\,kl}r^o dr^o - \frac{g_{kli}\left(\varphi\right)}{r}\sigma_{0\,kl}r\frac{\partial r}{\partial x_j}\right)d\varphi^o \tag{2.60}$$

After that, one can transform equation 2.60 back to rectangular coordinates (with $r = r^0$ and $dS = r^0 d\varphi^o$ and using equation 2.56):

$$\frac{\partial}{\partial x_j}\int\limits_{V}E_{kli}\sigma_{0\,kl}dV = \int\limits_{V}\underbrace{\frac{\partial E_{kli}}{\partial x_j}}_{W^{\varepsilon}_{ijkl}}\sigma_{0\,kl}dV \underbrace{- \int\limits_{S_\varepsilon}E_{kli}r_{,j}dS\,\sigma_{0\,kl}}_{F^{\varepsilon}_{ijkl}} \tag{2.61}$$

in which the first integral is interpreted as Cauchy principal value; the last term F^{ε}_{ijkl} is called *free term.*

The term for applying initial strains $\varepsilon_{0\,kl}$ (the last term of equation 2.53) can be calculated similar as described above. At the end we obtain:

$$\frac{\partial}{\partial x_j}\int\limits_{V}R_{kli}\varepsilon_{0\,kl}dV = \int\limits_{V}\underbrace{\frac{\partial R_{kli}}{\partial x_j}}_{V^{\varepsilon}_{ijkl}}\varepsilon_{0\,kl}dV \underbrace{- \int\limits_{S_\varepsilon}R_{kli}r_{,j}dS\,\varepsilon_{0\,kl}}_{H^{\varepsilon}_{ijkl}} \tag{2.62}$$

The whole integral equation for strains can be written in compact form:

$$\varepsilon_{ij} = \int_S D^{\varepsilon}_{kij} t_k dS - \int_S S^{\varepsilon}_{kij} u_k dS + f^{\varepsilon}_{ij} \tag{2.63}$$

and

$$\begin{aligned} f^{\varepsilon}_{ij} = \int_V D^{\varepsilon}_{kij} b_k dV + \int_V W^{\varepsilon}_{ijkl} \sigma_{0\,kl} dV + F^{\varepsilon}_{ijkl} \sigma_{0\,kl} \\ + \int_V V^{\varepsilon}_{ijkl} \varepsilon_{0\,kl} dV + H^{\varepsilon}_{ijkl} \varepsilon_{0\,kl} \end{aligned} \tag{2.64}$$

With

$$\begin{aligned} W^{\varepsilon}_{ijkl} = \frac{1}{8\alpha\pi G\,(1-\nu)\,r^{\alpha+1}} \big[& (1-2\nu)\,(\delta_{ik}\delta_{jl} + \delta_{jk}\delta_{il}) - \delta_{ij}\delta_{kl} \\ & + \beta\nu\,(\delta_{il} r_{,j} r_{,k} + \delta_{jk} r_{,i} r_{,l} + \delta_{ik} r_{,j} r_{,l} + \delta_{jl} r_{,i} r_{,k}) \\ & + \beta\,(\delta_{kl} r_{,i} r_{,j} + \delta_{ij} r_{,k} r_{,l} - \gamma r_{,i} r_{,j} r_{,k} r_{,l}) \big] \end{aligned} \tag{2.65}$$

$$F^{\varepsilon}_{ijkl} = \frac{-1}{2\eta G\,(1-\nu)} \left[\delta_{jk}\delta_{il} - C_1\,(\delta_{ik}\delta_{jl} + \delta_{ij}\delta_{kl}) \right] \tag{2.66}$$

$$\begin{aligned} V^{\varepsilon}_{ijkl} = \frac{1}{4\alpha\pi\,(1-\nu)\,r^{\alpha+1}} \big[& (1-2\nu)\,(\delta_{ik}\delta_{jl} + \delta_{jk}\delta_{il} - \delta_{ij}\delta_{kl}) \\ & + \beta\nu\,(\delta_{il} r_{,j} r_{,k} + \delta_{jk} r_{,i} r_{,l} + \delta_{ik} r_{,j} r_{,l} + \delta_{jl} r_{,i} r_{,k}) \\ & + \beta\,((1-2\nu)\,\delta_{kl} r_{,i} r_{,j} + \delta_{ij} r_{,k} r_{,l} - \gamma r_{,i} r_{,j} r_{,k} r_{,l}) \big] \end{aligned} \tag{2.67}$$

$$H^{\varepsilon}_{ijkl} = \frac{-1}{\eta\,(1-\nu)} \left[C_1\,(\delta_{jk}\delta_{il} + \delta_{ik}\delta_{jl}) - C_2 \delta_{ij}\delta_{kl} \right] \tag{2.68}$$

With $\alpha = 1$, $\beta = 2$, $\gamma = 4$, $\eta = 8$, $C_1 = 3 - 4\nu$, $C_2 = 1$ for 2D (plain strain) and $\alpha = 2$, $\beta = 3$, $\gamma = 5$, $\eta = 15$, $C_1 = 4 - 5\nu$, $C_2 = 1 - 5\nu$ for 3D, see Beer et al. (2008).

Stresses at Internal Points

The stress integral equation can be derived from the strain integral equation by using following relation:

$$\sigma_{ij} = C_{ijkl}\varepsilon_{kl} \tag{2.69}$$

Substituting equation 2.63 into equation 2.69 we obtain directly the stress integral equation. In compact form it can be written as:

$$\sigma_{ij} = \int_S D^{\sigma}_{kij} t_k dS - \int_S S^{\sigma}_{kij} u_k dS + f^{\sigma}_{ij} \tag{2.70}$$

and

$$\begin{aligned} f^{\sigma}_{ij} = \int_V D^{\sigma}_{kij} b_k dV + \int_V W^{\sigma}_{ijkl}\sigma_{0\,kl} dV + F^{\sigma}_{ijkl}\sigma_{0\,kl} \\ + \int_V V^{\sigma}_{ijkl}\varepsilon_{0\,kl} dV + H^{\sigma}_{ijkl}\varepsilon_{0\,kl} \end{aligned} \tag{2.71}$$

With

$$D^{\sigma}_{ijk} = \frac{1}{4\alpha\pi\,(1-\nu)\,r^{\alpha}} \left[(1-2\nu)\,(\delta_{ik}r_{,j} + \delta_{jk}r_{,i} - \delta_{ij}r_{,k}) + \beta r_{,i}r_{,j}r_{,k}\right] \tag{2.72}$$

$$\begin{aligned} S^{\sigma}_{ijk} = {} & \frac{G}{2\alpha\pi\,(1-\nu)\,r^{\beta}} \\ & \big[\beta r_{,m}n_m\left[(1-2\nu)\,\delta_{ij}r_{,k} + \nu\,(\delta_{ik}r_{,j} + \delta_{jk}r_{,i}) - \gamma r_{,i}r_{,j}r_{,k}\right] \\ & + \beta\nu\,(n_i r_{,j}r_{,k} + n_j r_{,i}r_{,k}) \\ & + (1-2\nu)\,(\beta r_{,i}r_{,j}n_k + \delta_{ik}n_j + \delta_{jk}n_i +) - (1-4\nu)\,\delta_{ij}n_k\big] \end{aligned} \tag{2.73}$$

$$\begin{aligned} W^{\sigma}_{ijkl} = {} & \frac{1}{4\alpha\pi\,(1-\nu)\,r^{\alpha+1}}\big[(1-2\nu)\,(\delta_{ik}\delta_{jl} + \delta_{jk}\delta_{il} - \delta_{ij}\delta_{kl} + \beta\delta_{ij}r_{,k}r_{,l}) \\ & + \beta\nu\,(\delta_{il}r_{,j}r_{,k} + \delta_{jk}r_{,i}r_{,l} + \delta_{ik}r_{,j}r_{,l} + \delta_{jl}r_{,i}r_{,k}) \\ & + \beta\,(\delta_{kl}r_{,i}r_{,j} - \gamma r_{,i}r_{,j}r_{,k}r_{,l})\big] \end{aligned} \tag{2.74}$$

$$F^{\sigma}_{ijkl} = \frac{-1}{\alpha\eta\,(1-\nu)}\left[C_3\,(\delta_{jk}\delta_{il} + \delta_{ik}\delta_{jl}) + C_4\delta_{ij}\delta_{kl}\right] \tag{2.75}$$

$$V^{\sigma}_{ijkl} = \frac{g}{2\alpha\pi\,(1-\nu)\,r^{\alpha+1}}\big[(1-2\nu)\,(\delta_{ik}\delta_{jl}+\delta_{jk}\delta_{il}) - (1-2\alpha\nu)\,\delta_{ij}\delta_{kl} + \beta\nu\,(\delta_{il}r_{,j}r_{,k}+\delta_{jk}r_{,i}r_{,l}+\delta_{ik}r_{,j}r_{,l}+\delta_{jl}r_{,i}r_{,k}) + \beta\,((1-2\nu)\,\delta_{kl}r_{,i}r_{,j}+C_5\delta_{ij}r_{,k}r_{,l}-\gamma r_{,i}r_{,j}r_{,k}r_{,l})\big] \tag{2.76}$$

$$H^{\sigma}_{ijkl} = \frac{G}{\kappa\,(1-\nu)}\left[C_3\,(\delta_{ik}\delta_{jl}+\delta_{jk}\delta_{il})+C_6\delta_{ij}\delta_{kl}\right] \tag{2.77}$$

With $\alpha = 1$, $\beta = 2$, $\gamma = 4$, $\eta = 8$, $C_1 = 3-4\nu$, $C_2 = 1$ for 2D (plain strain) and $\alpha = 2$, $\beta = 3$, $\gamma = 5$, $\eta = 15$, $C_1 = 4-5\nu$, $C_2 = 1-5\nu$ for 3D, see Beer et al. (2008).

2.4 Numerical Implementation

To solve the BIE equation 2.44 numerically, some approximations have to be introduced. On the one hand the geometry of the problem has to be approximated numerically, on the other hand also the distribution of physical quantities (e.g. boundary displacements and boundary tractions) has to be approximated numerically. Both, the geometry and the physical quantities on the boundary are approximated by using boundary elements. Applying point collocation on the element nodes a system of equations can be obtained. In order to simplify the notation, form now on matrix notation will be used instead of indicial notation.

2.4.1 Discretisation of the Boundary Geometry

The boundary S of the domain is discretised with boundary elements S^e, see figure 2.7(a).

$$S \approx \sum_{e=1}^{E} S^e \tag{2.78}$$

where E is the number of boundary elements. For the 2D case we use 1D boundary elements with two nodes for linear interpolation over the element or with three nodes for quadratic interpolation over the element.

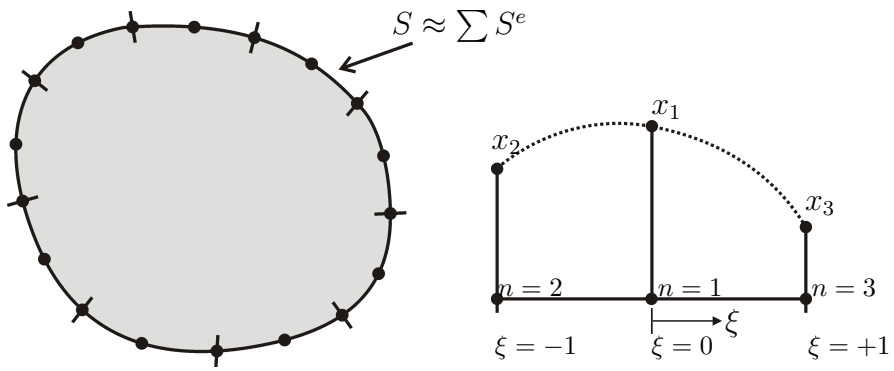

(a) Discretisation of the boundary S

(b) Quadratic Boundary element

Figure 2.7: Boundary discretisation in 2D with quadratic elements

Each boundary element is transformed into a local intrinsic coordinate system (with the intrinsic coordinate ξ), see figure 2.7(b). The coordinate vector $\boldsymbol{x^e}(\xi)$ of any point ξ at the element e can be interpolated by using the interpolation functions $\Phi_n(\xi)$ and the nodal coordinate vectors of the element $\boldsymbol{x^e}_n$:

$$\boldsymbol{x^e}(\xi) = \sum_{n=1}^{N^e} \Phi_n(\xi)\, \boldsymbol{x^e}_n \tag{2.79}$$

When using 1D quadratic elements we have three nodes at one element ($N^e = 3$) The interpolation functions are defined to have a unit value at the node n and a zero value at the other nodes, see figure 2.8:

$$\begin{aligned} \Phi_1 &= \frac{1}{2}\left(-\xi + \xi^2\right) \\ \Phi_2 &= \frac{1}{2}\left(\xi + \xi^2\right) \\ \Phi_3 &= 1 - \xi^2 \end{aligned} \tag{2.80}$$

For the 3D case 2D boundary elements are used, they can have for example four nodes $N^e = 4$ (linear interpolation) or eight nodes $N^e = 8$ (quadratic interpolation). The intrinsic coordinates are ξ and η, see figure 2.9.

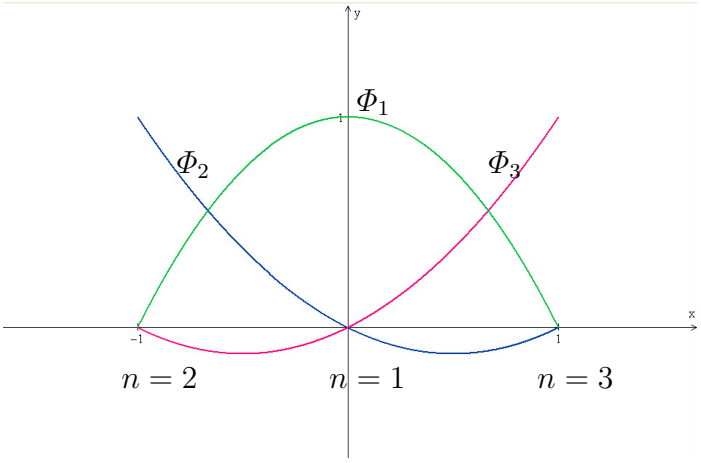

Figure 2.8: Quadratic shape functions for a 1D element

The interpolation functions for a quadratic quadrilateral element are:

$$\begin{aligned}
\Phi_1 &= \frac{1}{4}(1-\xi)(1-\eta)(-\xi-\eta-1) & \Phi_5 &= \frac{1}{2}\left(1-\xi^2\right)(1-\eta) \\
\Phi_2 &= \frac{1}{4}(1+\xi)(1-\eta)(\xi-\eta-1) & \Phi_6 &= \frac{1}{2}\left(1-\eta^2\right)(1+\xi) \\
\Phi_3 &= \frac{1}{4}(1+\xi)(1+\eta)(\xi\eta-1) & \Phi_7 &= \frac{1}{2}\left(1-\xi^2\right)(1+\eta) \\
\Phi_4 &= \frac{1}{4}(1-\xi)(1+\eta)(-\xi+\eta-1) & \Phi_8 &= \frac{1}{2}\left(1-\eta^2\right)(1-\xi)
\end{aligned} \tag{2.81}$$

and the coordinates for the node at the element $\boldsymbol{x^e}(\xi,\eta)$ can be interpolated as in equation 2.79:

$$\boldsymbol{x^e}(\xi,\eta) = \sum_{n=1}^{N^e} \Phi_n(\xi,\eta)\,\boldsymbol{x^e}_n \tag{2.82}$$

For more details and linear interpolation functions see for example Beer and Watson (1994); for the interpolation of triangular elements see for example Gaul et al. (2003).

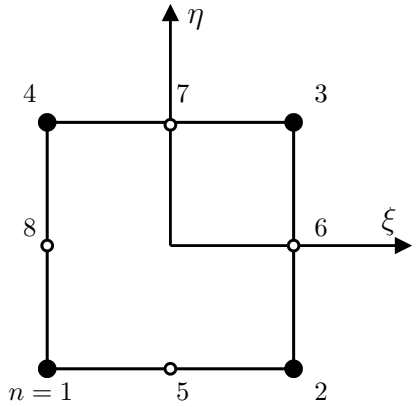

Figure 2.9: Quadratic quadrilateral element, intrinsic coordinates ξ and η and local nodes $n = 1...8$

2.4.2 Approximation of Physical Quantities

In addition to the discretisation of the boundary geometry, the displacement- and traction- vectors $\boldsymbol{u}$ and $\boldsymbol{t}$ at the boundary have to be approximated too:

$$\boldsymbol{u}^{\boldsymbol{e}} = \sum_{n=1}^{N^e} \Phi_n \boldsymbol{u}^{\boldsymbol{e}}{}_n \tag{2.83}$$

$$\boldsymbol{t}^{\boldsymbol{e}} = \sum_{n=1}^{N^e} \Phi_n \boldsymbol{t}^{\boldsymbol{e}}{}_n \tag{2.84}$$

where $\boldsymbol{u}^{\boldsymbol{e}}{}_n$ and $\boldsymbol{t}^{\boldsymbol{e}}{}_n$ are the displacement- and traction- vectors at node n of element e. And the same interpolation functions Φ_n as for the geometry in section 2.4.1 can be used. The fact that the traction interpolation function is of the same order as the displacement interpolation presents an advantage over the Finite Element Method, where stresses and tractions are calculated by differentiation of the displacement interpolation functions and thus results in loss accuracy.

The BIE involves the three coordinates of the traction vector $\boldsymbol{t}$ at the boundary nodes; however, the stress tensor has six independent components and three of them cannot be calculated directly with the BIE; however, the boundary

stresses cannot be calculated with the integral equation for stresses as well, because the kernel function S^{σ}_{ijk} is hyper singular (see also section 2.4.5). The most popular and easiest way to compute boundary stresses is the *traction recovery* (or *stress recovery*) method, see for example Gao and Davies (2002), Brebbia et al. (1984).

2.4.3 Discretisation inside the Domain

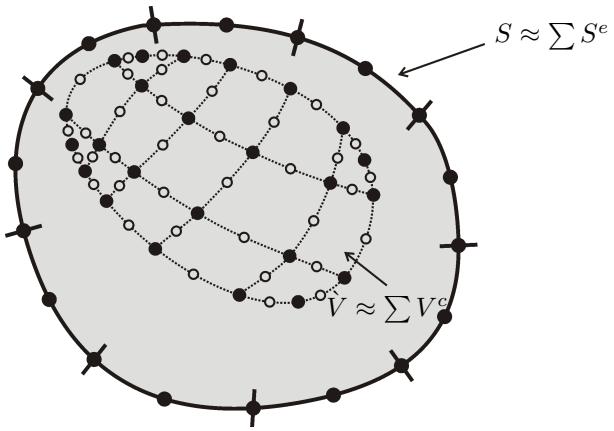

Figure 2.10: Domain discretised with integration cells V^c

As described before, the boundary geometry and the boundary quantities are approximated by using boundary elements. However, for a problem containing body forces (forces, initial stresses or initial strains) domain integrals have to be computed, see section 2.3.5. One way to calculate the domain integral is the *cell integration technique* in which the volume $\grave{V}$ on which the body forces are acting is subdivided into a certain number C of cells, see figure 2.10:

$$\grave{V} \approx \sum_{c=1}^{C} V^c \tag{2.85}$$

The geometry and the distribution of the body forces are defined by the nodal

cell values and the interpolation functions.

$$\boldsymbol{x^c} = \sum_{n=1}^{N^c} \Phi_n \boldsymbol{x^c}_n \tag{2.86}$$

$$\boldsymbol{b^c} = \sum_{n=1}^{N^c} \Phi_n \boldsymbol{b^c}_n; \qquad \boldsymbol{\sigma^{0\,c}} = \sum_{n=1}^{N^c} \Phi_n \boldsymbol{\sigma^{0\,c}}_n; \qquad \boldsymbol{\varepsilon^{0\,c}} = \sum_{n=1}^{N^c} \Phi_n \boldsymbol{\varepsilon^{0\,c}}_n \tag{2.87}$$

N^c is the number of cell-nodes. For 2D problems 2D cells are used (equal to the 2D boundary elements described before) and for 3D problems 3D cells (brick cells) are used, for example linear brick cells (with eight nodes $N^c = 8$) or quadratic brick cells (with 20 nodes $N^c = 20$). For the 3D case three intrinsic coordinates are introduced (ξ, η and ζ), see figure 2.11.

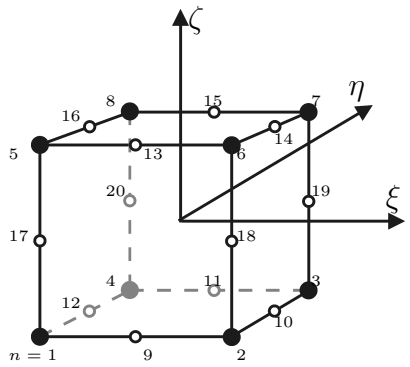

Figure 2.11: Quadratic brick cells, intrinsic coordinates ξ, η, ζ and local nodes $n = 1...20$

The interpolation functions for quadratic brick cells are:

$$\Phi_\alpha = \frac{(1+\xi_\alpha\xi)\,(1+\eta_\alpha\eta)\,(1+\zeta_\alpha\zeta)\,(\xi_\alpha\xi+\eta_\alpha\eta+\zeta_\alpha\zeta-2)}{8} \qquad \text{for } \alpha = 1\cdots 8 \tag{2.88}$$

$$\Phi_\alpha = \frac{(1+\xi_\alpha\xi)\,(1+\eta_\alpha\eta)\,(1+\zeta_\alpha\zeta)\,\{1+(\xi_\alpha^2-1)\,\xi^2+(\eta_\alpha^2-1)\,\eta^2+(\zeta_\alpha^2-1)\,\zeta^2\}}{8} \qquad \text{for } \alpha = 9\cdots 20 \tag{2.89}$$

2.4.4 Matrix Assembly / System of equations

Applying the boundary discretisation (equation 2.78) to the BIE equation 2.44 and expressing it in matrix notation we obtain the equation system for the load point (subscript l):

$$\boldsymbol{c}_l \boldsymbol{u}_l = \sum_{e=1}^{E} \int_{S^e} \boldsymbol{U}_l \boldsymbol{t}^e dS - \sum_{e=1}^{E} \int_{S^e} \boldsymbol{T}_l \boldsymbol{u}^e dS + \boldsymbol{f} \tag{2.90}$$

Substituting the displacement- and traction- approximation of equation 2.83 and equation 2.84 into equation 2.90:

$$\boldsymbol{c}_l \boldsymbol{u}_l = \sum_{e=1}^{E} \sum_{n=1}^{N^e} \underbrace{\int_{S^e} \boldsymbol{U}_l \Phi_n dS}_{\boldsymbol{\Delta U}^e_{l\,n}} \boldsymbol{t}^e_n - \sum_{e=1}^{E} \sum_{n=1}^{N^e} \underbrace{\int_{S^e} \boldsymbol{T}_l \Phi_n dS}_{\boldsymbol{\Delta T}^e_{l\,n}} \boldsymbol{u}^e_n + \boldsymbol{f}_l \tag{2.91}$$

Where $\boldsymbol{\Delta U}^e_{l\,n}$ and $\boldsymbol{\Delta T}^e_{l\,n}$ are introduce to replace the integrands of the products of the fundamental solution with the shape functions. Replacing the double summation over the elements E and the element nodes N^e by the summation over all nodes N, it remain:

$$\boldsymbol{c}_l \boldsymbol{u}_l = \sum_{n=1}^{N} \boldsymbol{\Delta U}_{l\,n} \boldsymbol{t}_n - \sum_{n=1}^{N} \boldsymbol{\Delta T}_{l\,n} \boldsymbol{u}_n + \boldsymbol{f}_l \tag{2.92}$$

In section 2.4.5 it is described how to solve the integrals $\boldsymbol{\Delta U}_{l\,n}$ and $\boldsymbol{\Delta T}_{l\,n}$ numerically. To setup the entire system of equations for all N unknowns, the load point (subscript l) is placed at all global discretisation nodes N. The whole system of equations is:

$$\boldsymbol{c}\boldsymbol{u} = \boldsymbol{\Delta U}\boldsymbol{t} - \boldsymbol{\Delta T}\boldsymbol{u} + \boldsymbol{f} \tag{2.93}$$

Where $\boldsymbol{u}$, $\boldsymbol{t}$ and $\boldsymbol{f}$ are defined to be the global vectors containing the complete set of N nodal vectors $\boldsymbol{u}_l$, $\boldsymbol{t}_l$ and $\boldsymbol{f}_l$. $\boldsymbol{\Delta T}$, $\boldsymbol{\Delta U}$ are assembled matrices. By defining the matrix $\boldsymbol{\Delta \hat{T}}$ in such a way that the free term $\boldsymbol{c}$ is already included,

we obtain:

$$\boldsymbol{\Delta \hat{T} u} = \boldsymbol{\Delta U t} + \boldsymbol{f} \tag{2.94}$$

The boundary conditions are imposed by changing columns between the matrices $\boldsymbol{\Delta \hat{T}}$ and $\boldsymbol{\Delta U}$ and the following system of equations is obtained:

$$\boldsymbol{A\,x} = \boldsymbol{b} + \boldsymbol{f} \tag{2.95}$$

where $\boldsymbol{x}$ contains the unknown boundary values, either tractions $\boldsymbol{t}$ or displacements $\boldsymbol{u}$; $\boldsymbol{A}$ is a matrix containing a mixture of $\boldsymbol{\Delta \hat{T}}$ and $\boldsymbol{\Delta U}$, related to $\boldsymbol{x}$; $\boldsymbol{b}$ contains the contributions due to the known boundary values; and $\boldsymbol{f}$ is a vector containing the contributions due to the body forces. Assuming a problem containing all three types of body forces (forces $\boldsymbol{b}$, initial stresses $\boldsymbol{\sigma_0}$ and initial strains $\boldsymbol{\varepsilon_0}$), the body force vector given in equation 2.43 can be written in the form:

$$\boldsymbol{f} = \boldsymbol{\Delta U b} + \boldsymbol{\Delta E \sigma_0} + \boldsymbol{\Delta R \varepsilon_0} \tag{2.96}$$

$\boldsymbol{\Delta U}$, $\boldsymbol{\Delta E}$ and $\boldsymbol{\Delta R}$ are the assembled matrices including the integrals of the products of the fundamental solutions with the shape functions over the cell-volumes. $\boldsymbol{b}$, $\boldsymbol{\sigma_0}$ and $\boldsymbol{\varepsilon_0}$ are the global vectors containing the complete set of all M nodal body force vectors. M is due to the number of cells C and the number of nodes per cell N^c ($M = CN^c$).

The systems of equations for calculating results at interal points (load point is inside the domain, subscript i) can be expressed in an analogous manner (see also equation 2.47,equation 2.63 and equation 2.70):

$$\boldsymbol{u}_i = \boldsymbol{\Delta U}_i\,\boldsymbol{t} - \boldsymbol{\Delta T}_i\,\boldsymbol{u} + \boldsymbol{f}_i \tag{2.97}$$

$$\boldsymbol{\varepsilon}_i = \boldsymbol{\Delta D^{\varepsilon}}_i\,\boldsymbol{t} - \boldsymbol{\Delta S^{\varepsilon}}_i\,\boldsymbol{u} + \boldsymbol{f^{\varepsilon}} \tag{2.98}$$

$$\boldsymbol{\sigma}_i = \boldsymbol{\Delta D^{\sigma}}_i\,\boldsymbol{t} - \boldsymbol{\Delta S^{\sigma}}_i\,\boldsymbol{u} + \boldsymbol{f^{\sigma}} \tag{2.99}$$

Where the body force vector $\boldsymbol{f}_i$ for the displacement results is described in equation 2.96 and the body force vectors for the strains and for the stresses $\boldsymbol{f^{\varepsilon}}$

and $\boldsymbol{f^{\sigma}}$ are defined as follows:

$$\boldsymbol{f^{\epsilon}}_i = \boldsymbol{\Delta D^{\epsilon}}_i \boldsymbol{b} + \boldsymbol{\Delta W^{\epsilon}}_i \boldsymbol{\sigma_0} + \boldsymbol{F^{\epsilon}} \boldsymbol{\sigma_0} + \boldsymbol{\Delta V^{\epsilon}}_i \boldsymbol{\varepsilon_0} + \boldsymbol{H^{\epsilon}} \boldsymbol{\varepsilon_0} \tag{2.100}$$

$$\boldsymbol{f^{\sigma}}_i = \boldsymbol{\Delta D^{\sigma}}_i \boldsymbol{b} + \boldsymbol{\Delta W^{\sigma}}_i \boldsymbol{\sigma_0} + \boldsymbol{F^{\sigma}} \boldsymbol{\sigma_0} + \boldsymbol{\Delta V^{\sigma}}_i \boldsymbol{\varepsilon_0} + \boldsymbol{H^{\sigma}} \boldsymbol{\varepsilon_0} \tag{2.101}$$

2.4.5 Numerical Integration

The last thing to do before we are able to operate with the system of equations in section 2.4.4 is to carry out the integrals over the boundary elements S^e and over the volume cells V^c. All these integrals consist of the product of the fundamental solution $(\cdot)(P,Q)$ and the interpolation functions $\phi(Q)$:

$$I_n^e(P) = \int_{S^e} (\cdot)(P,Q)\, \phi_n(Q)\, dS(Q) \tag{2.102}$$

$$I_n^c(P) = \int_{V^c} (\cdot)(P,Q)\, \phi_n(Q)\, dV(Q) \tag{2.103}$$

Equation 2.102 shows an integral over a boundary element (like in equation 2.91) and equation 2.103 shows an integral over a cell. Analytical integration is rarely used because even when it is possible to calculate the final expression, it can be very complicated and its evaluation can have high cost from the computational point of view (see Paris and Canas 1997). Several numerical procedures (e.g. trapezoidal rule, Simpson's rule) are described in literature to approximate an integral like this. However, the *Gauss quadrature formula* shows the best accuracy for a given number of points, thus these technique is commonly used in the BEM.

Depending on the distance of the load point P to the element $S^e(Q)$ over which the integration is carried out, we have to distinguish between *regular integrals*, *singular integrals* and ideally also *nearly singular integrals*, see for example Gaul et al. (2003).

Regular Integration

The load point P is far away from the element S^e or the cell V^c, respectively. For this the *standard Gauss quadrature* (also called *Gauss-Legendre quadrature*) is used. The original integral can be calculated in the form:

$$\int_{x_1}^{x_2} f(x)\, dx = \sum_{j=1}^{M} w_j f(x_j) \tag{2.104}$$

We can find a set of M weights w and abscissas x (also called *Gauss points*) such that the approximation is exact if $f(x)$ is a polynomial of the order R ($M = 2R - 1$). Once the order M is chosen, the Gauss points and the weights can be calculated, for a detailed description see Press et al. (2002). Regarding a 1D element with the intrinsic coordinates ($-1 \leq \xi \leq 1$) the weights w_j and Gauss points ξ_j for $M = 1, 2, 3$ are:

M	ξ_j	w_j
1	0.	2.
2	+0.57735, -0.57735	1., 1.
3	+0.77459, 0., -0.77459	0.55555, 0.88888, 0.55555

Table 2.1: Gauss points ξ and weights w for Gauss quadrature

Applying this to the integral equation 2.102 it occurs:

$$I_n^e(P) \approx \sum_{j=1}^{M} (\cdot)(P, \xi_j)\, \phi_n(\xi_j)\, J(\xi_j)\, w_j \tag{2.105}$$

where $J(\xi_j)$ is the *Jacobian* which transforms the coordinates x_j to the intrinsic coordinates ξ_j:

$$dS(x, y) = \sqrt{\left(\frac{dx}{d\xi}\right)^2 + \left(\frac{dy}{d\xi}\right)^2} = J d\xi \quad \text{... 2D boundary element} \tag{2.106}$$

$$dS\left(x,y,z\right)=\frac{\partial\left(x,y,z\right)}{\partial\left(\xi,\eta\right)}=Jd\xi d\eta \quad \text{... 3D boundary element} \tag{2.107}$$

The integration over the volume cells (equation 2.103) can be done analogous:

$$dV\left(x,y\right)=\frac{\partial\left(x,y\right)}{\partial\left(\xi,\eta\right)}=Jd\xi d\eta \qquad \text{... 2D cell} \tag{2.108}$$

$$dV\left(x,y,z\right)=\frac{\partial\left(x,y,z\right)}{\partial\left(\xi,\eta,\zeta\right)}=Jd\xi d\eta d\zeta \qquad \text{... 3D cell} \tag{2.109}$$

Nearly Singular Integration

The load point P is close to the element S^e or the cell V^c, respectively. In this case, the integrand is still regular and the standard Gauss quadrature formula can be used. However, a high number of Gauss points x_j is needed for an accurate approximation of the pronounced peak for $r\left(P,Q\right)\ll$. A better way to obtain a better accuracy is the *subdivision method*. If the point is too close to the element to be integrated, the element is divided into smaller sub-elements, see Ribeiro (2006).

Singular Integration

When the load point P lies on the element S^e or on the cell V^c, respectively the integrand becomes singular for $r=0$ $(P=Q)$. Depending on the type of fundamental solutions different types of singularities occur:

	1D Integration	2D Integration	3D Integration
weakly singular	$\ln r$	$\frac{1}{r}$	$\frac{1}{r^2}$
strongly singular	$\frac{1}{r}$	$\frac{1}{r^2}$	$\frac{1}{r^3}$
hyper singular	$\frac{1}{r^2}$	$\frac{1}{r^3}$	

Table 2.2: Different types of singularities

Thus the integrands in the BIE include weak and strong singularities at $P = Q$:

$$\boldsymbol{cu}\left(P\right) = \underbrace{\boldsymbol{\Delta U}\left(P,Q\right)}_{\text{weak}}\boldsymbol{t}\left(Q\right) - \underbrace{\boldsymbol{\Delta \hat{T}}\left(P,Q\right)}_{\text{strong}}\boldsymbol{u}\left(Q\right) + \boldsymbol{f}\left(P\right) \tag{2.110}$$

and the body force terms consists of weakly singular volume integrals only in the case that $P = \bar{Q}$:

$$\boldsymbol{f}\left(P\right) = \underbrace{\boldsymbol{\Delta U}\left(P,\bar{Q}\right)}_{\text{weak}}\boldsymbol{b}\left(\bar{Q}\right) + \underbrace{\boldsymbol{\Delta E}\left(P,\bar{Q}\right)}_{\text{weak}}\boldsymbol{\sigma_0}\left(\bar{Q}\right) + \underbrace{\boldsymbol{\Delta R}\left(P,\bar{Q}\right)}_{\text{weak}}\boldsymbol{\varepsilon_0}\left(\bar{Q}\right) \tag{2.111}$$

However, the integral equations for computing stresses or strains consist of strongly and hyper singular integrals for $\bar{P} = Q$:

$$\boldsymbol{\varepsilon},\boldsymbol{\sigma}\left(\bar{P}\right) = \underbrace{\boldsymbol{\Delta D}^{\boldsymbol{\varepsilon},\boldsymbol{\sigma}}\left(\bar{P},Q\right)}_{\text{strong}}\boldsymbol{t} - \underbrace{\boldsymbol{\Delta S}^{\boldsymbol{\varepsilon},\boldsymbol{\sigma}}\left(\bar{P},Q\right)}_{\text{hyper}}\boldsymbol{u} + \boldsymbol{f}^{\boldsymbol{\varepsilon},\boldsymbol{\sigma}}\left(\bar{P}\right) \tag{2.112}$$

To avoid hyper singular integrals, the integral equation 2.112 is used to calculate stresses and strains at internal points only. For the boundary we use the stress recovery technique. Thus we obtain regular boundary integrals only:

$$\boldsymbol{\varepsilon},\boldsymbol{\sigma}\left(\bar{P}\right) = \underbrace{\boldsymbol{\Delta D}^{\boldsymbol{\varepsilon},\boldsymbol{\sigma}}\left(\bar{P},Q\right)}_{\text{regular}}\boldsymbol{t} - \underbrace{\boldsymbol{\Delta S}^{\boldsymbol{\varepsilon},\boldsymbol{\sigma}}\left(\bar{P},Q\right)}_{\text{regular}}\boldsymbol{u} + \boldsymbol{f}^{\boldsymbol{\varepsilon},\boldsymbol{\sigma}}\left(\bar{P}\right) \tag{2.113}$$

and the volume integrals for the body forces contain strongly singularities at $\bar{P} = \bar{Q}$:

$$\begin{aligned}\boldsymbol{f}^{\boldsymbol{\varepsilon},\boldsymbol{\sigma}}\left(\bar{P}\right) = &\underbrace{\boldsymbol{\Delta D}^{\boldsymbol{\varepsilon},\boldsymbol{\sigma}}\left(\bar{P},\bar{Q}\right)}_{\text{weak}}\boldsymbol{b}\left(\bar{Q}\right)\\ &+ \underbrace{\boldsymbol{\Delta W}^{\boldsymbol{\varepsilon},\boldsymbol{\sigma}}\left(\bar{P},\bar{Q}\right)}_{\text{strong}}\boldsymbol{\sigma_0}\left(\bar{Q}\right) + \boldsymbol{F}^{\boldsymbol{\varepsilon},\boldsymbol{\sigma}}\boldsymbol{\sigma_0}\left(\bar{Q}\right)\\ &+ \underbrace{\boldsymbol{\Delta V}^{\boldsymbol{\varepsilon},\boldsymbol{\sigma}}\left(\bar{P},\bar{Q}\right)}_{\text{strong}}\boldsymbol{\varepsilon_0}\left(\bar{Q}\right) + \boldsymbol{H}^{\boldsymbol{\varepsilon},\boldsymbol{\sigma}}\boldsymbol{\varepsilon_0}\left(\bar{Q}\right)\end{aligned} \tag{2.114}$$

The different types of singularities are described in more detail in section 2.5. However, here a short overview is given, how to integrate them numerically

inside the BE-program:

Weak Singularity The integral exists and can be calculated analytically (see section 2.5.1). The numerical evaluation using the standard Gauss-Legendre quadrature (section 2.4.5) is inaccurate since the behaviour in the neighbourhood of the singularity can not be approximated very good with polynomial functions. For the 1D boundary integration a special Gauss formula the *Gauss-Laguerre formula* is used, see Beer et al. (2008), Press et al. (2002).

For 2D and 3D integrations some regularising transformations have to be considered in which the Jacobian J vanishes at the singularity (e.g. Lachat-Watson transformation). Quadrilateral elements or cells (2D integration) have to be subdivided into two triangles. Brick cells (3D integration) have to be subdivided into pyramid shaped sub-cells. With this subdivisions new coordinates are introduced and the Jacobian vanishes in the singular point. For detailed description see for example Ribeiro (2006), Beer et al. (2008).

Strong Singularity The strongly singular integrals appearing in the BEM exist in the sense of Cauchy principal values, see section 2.5.2. In the BEM they often can be evaluated indirectly using the traction-free rigid body motion; so that the evaluation of the strongly singular integrals can be avoided. However, in some cases we have to evaluate the strongly singular integrals explicitly, see Gaul et al. (2003). Therefore different methods can be used based on analytical or semi-analytical integration. Here the Guiggiani approach (Guiggiani and Casalini (1987), Guiggiani and Gigante (1990)) is used. This method is based on the idea of regularising the singularity by subtraction. First we simplify the problem by introducing a function $g(0)$:

$$\oint_a^b \frac{g(x)}{x} dx = \underbrace{\int ab \frac{g(x) - g(0)}{x} dx}_{regular} + \oint_a^b \frac{g(0)}{x} dx \tag{2.115}$$

The first integral on the right side is regular and can be evaluated using standard Gauss quadrature. The second integral remains strongly singular but its solution is known:

$$\int_a^b \frac{g(0)}{x} dx = g(0) \ln |\frac{b}{a}| \tag{2.116}$$

This procedure can be used for 2D and 3D integrations as well.

As for the weak singular integration, the quadrilaterals or bricks are subdivided into triangular or pyramid shaped sub-elements, respectively. For example the 2D integration for the strongly singular term $\boldsymbol{\Delta T}$ given by equation 2.91 is expressed in local polar coordinates (φ, r) based at the singular load point P:

$$\begin{aligned} \Delta T_{ij} = & \sum_{e=1}^{N} \lim_{\varepsilon \to 0} \int_{S^e - S^\varepsilon} T_{ij} \Phi_n dS = \\ & \sum_{e=1}^{N} \lim_{\varepsilon \to 0} \int_{\varphi=\frac{3}{4}\pi}^{\pi} \int_{r_0(\varepsilon,\varphi)}^{r_1(\varphi)} f_{ij}(r,\varphi)\, r dr d\varphi \end{aligned} \tag{2.117}$$

where S^e is the boundary of the element and S^ε is the boundary of the vanishing neighbourhood around the singularity. Then the distance vector r_i is approximated by developing a Taylor series for the field point Q near the load point. Thus the integrand in the vicinity of the load point approximate by:

$$\breve{f}_{ij}(r,\varphi) = \frac{1}{r^2} \breve{f}^*_{ij}(\varphi) \tag{2.118}$$

The integrand has been separated into a regular part $\breve{f}^*_{ij}(\varphi)$ which is only a function of φ and a singular part $\frac{1}{r^2}$. Similar to the 1D integration

function $\breve{f}_{ij}(r,\varphi)$ is subtracted and added:

$$\begin{aligned}\Delta T_{ij} = &\sum_{e=1}^{N} \int_{\varphi=\frac{3}{4}\pi}^{\pi} \int_{0}^{r_1(\varphi)} \left(f_{ij}(r,\varphi) - \frac{\breve{f}^*_{ij}(\varphi)}{r^2} \right) r dr d\varphi \\ &+ \sum_{e=1}^{N} \lim_{\varepsilon \to 0} \int_{\varphi=\frac{3}{4}\pi}^{\pi} \int_{r_0(\varepsilon,\varphi)}^{r_1(\varphi)} f_{ij}(r,\varphi) \frac{\breve{f}^*_{ij}(\varphi)}{r} dr d\varphi \end{aligned} \tag{2.119}$$

where the first integral is regular and can be evaluated using standard Gauss quadrature. The second integral can be carried out analytically over r, see Gaul et al. (2003), Ribeiro (2006).

Hyper Singularity As it was shown in equation 2.112 hyper singular integrals occur when we want to calculate stresses or strains at the boundary. To avoid this kind of singularity the stresses and strains at the boundary are not calculated directly by using the integral equations, however stresses and strains can be computed by using special techniques. The most popular and easiest way is the *traction recovery* (or *stress recovery*, *strain recovery*) method, see for example Gao and Davies (2002), Brebbia et al. (1984).

For a general description of weakly and strongly singular integrals see section 2.5.

To apply special kinds of body forces, such as line loads or concentrated point forces as it is described in section 2.3.5, the singularities have to be considered in special ways. However, this will be described later in more detail in chapter 5 and chapter 6 where line loads and point forces are used to model different kinds of rock bolts.

2.5 Singular Integrals

For detailed descriptions of singular integrals see for example the mathematics books Gakkov (1966), Mikhilin and Prössdorf (1987); for a more engineering description related to the BEM see for example Paris and Canas (1997), Gaul et al. (2003). In this section short overview over weak and strong singularities is given.

2.5.1 Weak Singularity

The definition of the weakly singular integral can be given in a visual way (see Gaul et al. 2003): the integrand is infinite at a point c of the integration range $a \leq c \leq b$ but its integral is finite and continuous at c. See for example the integrand $f(x)$:

$$f(x) = \ln(|x|) \qquad I(x) = \int f(x)\,dx = x\ln(|x|) - x \tag{2.120}$$

The integral $I(x)$ is continuous, see figure 2.12

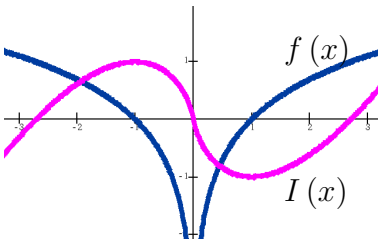

Figure 2.12: Weak singularity: integrand $f(x)$ and integral $I(x)$

In mathematics this kind of integral is called *improper integral*. The integral is carried out by removing the neighbourhood of the singular point c and integrating over the remaining part and passing to the limit:

$$\lim_{\varepsilon_1 \to 0;\, \varepsilon_2 \to 0} \left[\int_a^{c-\varepsilon_1} f(x)\,dx + \int_{c+\varepsilon_2}^{b} f(x)\,dx \right] \tag{2.121}$$

For the improper integral this limit exists. In this definition it is important that the neighbourhood cut out is entirely arbitrary ($\varepsilon_1 \neq \varepsilon_2$); see for example Gakkov (1966), Paris and Canas (1997).

2.5.2 Strong Singularity

We have a stong singularity if the integrand is infinite at a point c and its integral is infinite too. See for example (figure 2.13):

$$f(x) = \frac{1}{x} \qquad I(x) = \int f(x)\, dx = \ln(|x|) \tag{2.122}$$

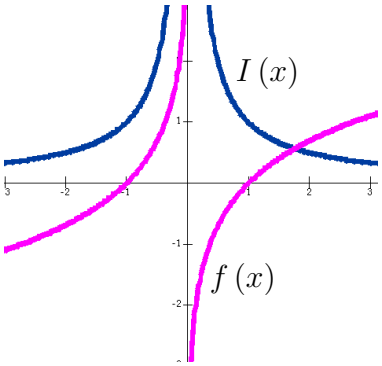

Figure 2.13: Strong singularity: integrand $f(x)$ and integral $I(x)$

This kind of integrals can not be solved as an improper integral:

$$\int_a^b \frac{1}{x} dx = \lim_{\varepsilon_1 \to 0;\, \varepsilon_2 \to 0} \left[\int_a^{-\varepsilon_1} \frac{1}{x} dx + \int_{+\varepsilon_2}^b \frac{1}{x} dx \right] = \ln\left(\frac{|b|}{|a|}\right) + \lim_{\varepsilon_1 \to 0;\, \varepsilon_2 \to 0} \ln\left(\frac{\varepsilon_1}{\varepsilon_2}\right) \tag{2.123}$$

It is evident that the limit of the last expression depends on the manner in which ε_1 and ε_2 tend to zero. However, it can be given a meaning if a dependence between ε_1 and ε_2 is established; i.e. $\varepsilon_1 = \varepsilon_2 = \varepsilon$. In this example this gives a

finite value the integral is said to exist in the sense of a *Cauchy principal value*, see also Gakkov (1966), Paris and Canas (1997):

$$\int_a^b \frac{1}{x} dx = \lim_{\varepsilon \to 0} \left[\int_a^{-\varepsilon} \frac{1}{x} dx + \int_{+\varepsilon}^b \frac{1}{x} dx \right] = \ln \left(\frac{|b|}{|a|} \right) \tag{2.124}$$

However, some strongly singular integrands do not converge in the sense of Cauchy principal value (they do not lead to a finite value); these integrals are called *divergent integrals*, see Paris and Canas (1997). For example:

$$\begin{aligned} \int_a^b \frac{1}{|x|} = \int_a^b \frac{1}{r} \lim_{\varepsilon \to 0} \left[\int_a^{-\varepsilon} \frac{1}{r} dx + \int_{+\varepsilon}^b \frac{1}{r} dx \right] = \\ \lim_{\varepsilon \to 0} \left[-\ln|-\varepsilon| + \ln|a| + \ln|b| - \ln|\varepsilon| \right] = \infty \end{aligned} \tag{2.125}$$

If the integrand were multiplied by a certain function $u(x)$ the integral could exist in the sense of Cauchy principal value.

2.6 Conclusion

The principles of the BEM were shown in this chapter. It was stated that the classical boundary integral equation can deal only with homogeneous, elastic media. In standard BE-approaches different regions have to be defined for simulating problems containing inclusions with different materials.

In this work a novel method is presented to simulate different materials with only one single BE region. Therefore the possibilities to apply body forces (initial forces, initial stresses or initial strains), presented in this chapter, will be used. In this chapter it was shown how to apply body forces on volumes, line loads along lines and concentrated forces on points. In the next chapters it will be presented how to use these possibilities for the new method to simulate different kinds of inclusions: general inclusions or narrow inclusions like continuous anchored rock bolts as well as discrete anchored rock bolts.

Chapter 3

Solution Procedure for Embedded Inclusions

3.1 Introduction

The analysis of solids including embedded inclusions is a very common problem in engineering, for example a rock mass with stiff or soft layers which are often found in underground engineering problems. An other example are solids which are reinforced by thin inclusions (as rock bolts in tunnelling) or other ground improvement methods like pipe roofing, where a stiff umbrella-shaped zone is created inside the grond.

As described in chapter 2 the classical boundary integral equation (BIE) can deal with homogeneous and linear elastic materials only, since fundamental solutions are known for homogeneous materials. The boundary element method (BEM) is already proved suitable for solving homogenous and linear elastic problems. For problems where the material properties of the solid changes for example in the case of embedded inclusions or if nonlinear material behaviour appear, special treatments have to be introduced:

BEM-FEM Coupling: The combination of BEM and FEM is the most commonly used technique to treat these cases. The inclusions are modelled with

finite elements and combined (coupled) with the boundary elements, see figure 3.1(a). Also if some areas inside the solid become plastic this technique can be used by discretising these plastic zones with finite elements and the rest with boundary elements. The philosophy of this technique is to have the best of each method, Zienkiewicz was the first who presented the "marriage a la mode - The best of both worlds" in his classical paper presented in Zienkiewicz et al. (1977). Up to now this method is well-established and an extensive number of research has been done on this subject, see for example Beer and Watson (1994), Brebbia et al. (1984), Hagen (2005), Pereira (2008).

BEM-BEM Coupling: Another alternative technique is the BEM sub-region technique. Where zones with different materials are considered by boundary element sub-regions which are connected to each other, see figure 3.1(b). Each region can be assigned different elastic material properties. However, the BEM regions can not behave in a nonlinear manner, they have to be linear elastic. One early work presenting an elastic body divided into sub-regions was written by Lachat and Watson (1976), further works dealing with this problem are for example Beer (2001), Duenser (2001), Leite and Venturini (2005).

Body force approach: A completely different technique to deal with different material properties with the BEM is the approach which will be called here "body force approach" (this can be either an *initial stress* or an *initial strain* or an *initial force* approach as well). In this method the whole solid is discretised by one single region and the effects of the zones with different material properties are simulated by applying body forces of any kind (initial stresses, initial strains or initial forces), see figure 3.1(c).

In the literature this method is commonly used to simulate nonlinear material behaviour. The development of simulating nonlinear material behaviour with the BEM started in the early 1970s. Since that many approaches have been proposed, see for example Telles (1983), Gao and Davies (2002), Cisilino and Aliabadi (1998), Ribeiro et al. (2008).

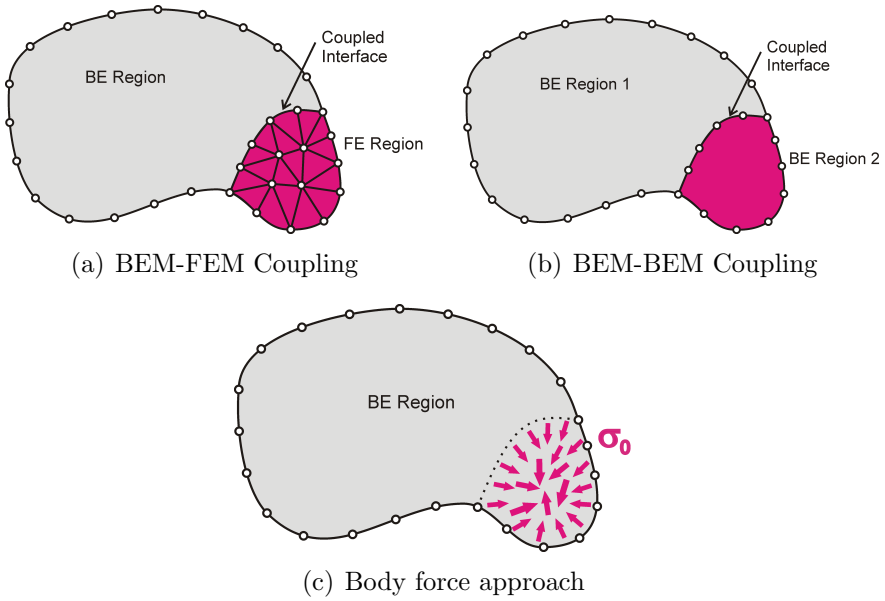

(a) BEM-FEM Coupling (b) BEM-BEM Coupling

(c) Body force approach

Figure 3.1: Methods to simulate inhomogeneous domains

In this work a body force approach is proposed, not only for simulating plastic zones in an homogeneous media as described in various papers, but also for simulating embedded inclusions. This inclusions can be softer or stiffer than the surrounding material and they can also plastify, see also Riederer and Beer (2009).

3.2 Body Force Approach

The idea in this approach is to introduce only one single region and apply initial loadings or "body forces" (initial stresses, initial strains or initial forces) to simulate the effect of the different materials, see figure 3.2.

For simulating nonlinear material behaviour like plasticity or visco-plasticity this method is well known, commonly an initial stress formulation or an initial strain formulation is used. The varying material properties in the plastic zones are simulated by initial stresses or initial strains, the magnitudes and the distribution of these initial loadings are calculated in an iterative procedure.

In this work embedded inclusions are proposed to be simulated in a similar way. The system of equations considering some kind of body forces is given as (see chapter 2):

$$\boldsymbol{A}\boldsymbol{x} = \boldsymbol{b} + \boldsymbol{f} \tag{3.1}$$

Where is $\boldsymbol{x}$ a vector with the unknown boundary quantities (displacements and tractions), $\boldsymbol{b}$ is a vector with the contributions due to the known boundary values, and $\boldsymbol{f}$ is a vector containing the contributions due to the body forces (e.g. initial stresses $\boldsymbol{\sigma_0}$).

The system of equations (3.1) can be solved directly to obtain the unknown boundary values $\boldsymbol{x}$ if the body forces and thus the vector $\boldsymbol{f}$ is known. For the simulation of inclusions the body forces are unknown at the beginning and thus the system of equations (3.1) is under-determined and can not be solved directly.

However, a second condition can be formulated which relates the body forces to internal results. For example: the relation of the initial stress loadings $\boldsymbol{\sigma_0}$ and stress results $\boldsymbol{\sigma}$ is given by using the constitutive matrices of the domain and the inclusion material. With this second condition another set of equations are introduced which leads to a determined problem which can be solved.

This problem can be either solved directly or iteratively. In the next two sections both approaches are described and at the end their advantages and disadvantages will be discussed.

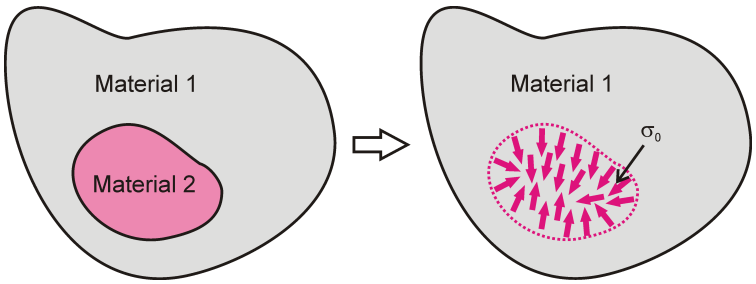

Figure 3.2: Simulation of embedded inclusions with initial stresses

3.2.1 Direct Solution Procedure

A direct solvable system of equations can be derived by using the BIE, the integral equation for computing internal results and a second condition for the relation of body forces and internal results. In general this problem could be arranged in several variations; body forces can be either, initial stresses, initial strains or initial forces and also the internal results can vary form stresses, strains or displacements. Here an initial stress approach in combination with stress results at internal nodes is used for explanation, but every other assortment could be used in a similar way.

First the system of equations (see equation 2.95) considering initial stress loading ($\boldsymbol{f} = \boldsymbol{\Delta E}\boldsymbol{\sigma}_0$) is rewritten:

$$\boldsymbol{A}\boldsymbol{x} - \boldsymbol{\Delta E}\boldsymbol{\sigma}_0 = \boldsymbol{b} \tag{3.2}$$

For a better view over the system of equations equation 3.2 will be presented in a way in which the sizes of the vectors and matrices are indicated:

$$[\boldsymbol{A}]_{ee}\{\boldsymbol{x}\}_e - [\boldsymbol{\Delta E}]_{ec}\{\boldsymbol{\sigma}_0\}_c = \{\boldsymbol{b}\}_e \tag{3.3}$$

The subscript e represents the total number of degree of freedoms at the boundary nodes and c is the total number of stress components at the cell nodes.

The system of integral equations for computing stresses at internal points is (see also equation 2.99):

$$[\boldsymbol{A}^{\sigma}]_{ce}\{\boldsymbol{x}\}_e - \left[\boldsymbol{\Delta W}^F\right]_{cc}\{\boldsymbol{\sigma}_0\}_c = \{\boldsymbol{\sigma}\}_c + \{\boldsymbol{b}^{\sigma}\}_c \tag{3.4}$$

Whereas $\boldsymbol{\Delta W}^F = \boldsymbol{\Delta W} + \boldsymbol{F}$ includes the integrated fundamental solution and the jump term. $\boldsymbol{A}^{\sigma}$ is a matrix containing sub-matrices $\boldsymbol{\Delta D}$ and $\boldsymbol{\Delta S}$ related to the unknown boundary conditions $\boldsymbol{x}$; and $\boldsymbol{b}^{\sigma}$ are the contributions due to the known boundary values.

Writing both equation 3.3 and equation 3.4 together, it arise a equation system of the form:

$$\begin{bmatrix} [\boldsymbol{A}]_{ee} & [\boldsymbol{\Delta E}]_{ec} \\ [\boldsymbol{A}^{\sigma}]_{ce} & \left[\boldsymbol{\Delta W}^{F}\right]_{cc} \end{bmatrix} \begin{bmatrix} \{\boldsymbol{x}\}_{e} \\ -\{\boldsymbol{\sigma}_0\}_{c} \end{bmatrix} = \begin{bmatrix} \{\boldsymbol{b}\}_{e} \\ \{\boldsymbol{\sigma}\}_{c} + \{\boldsymbol{b}^{\sigma}\}_{c} \end{bmatrix} \tag{3.5}$$

Now another condition has to be found which relates the initial stresses $\boldsymbol{\sigma}_0$ to the internal results $\boldsymbol{\sigma}$. Therefore following relations are introduced per node:

$$\boldsymbol{\sigma}^{Incl} = \boldsymbol{\sigma} \tag{3.6}$$

$$\boldsymbol{\sigma}^{Rock} = \boldsymbol{\sigma} + \boldsymbol{\sigma}_0 \tag{3.7}$$

$\boldsymbol{\sigma}^{Incl}$ are the stresses in the inclusion and $\boldsymbol{\sigma}^{Rock}$ are stresses which would appear in the solid if there where no inclusion. By introducing the compatibility condition of the strains ($\boldsymbol{\varepsilon} = \boldsymbol{\varepsilon}^{Incl} = \boldsymbol{\varepsilon}^{Rock}$) and by using Hooke's law we obtain:

$$\boldsymbol{\varepsilon} = \boldsymbol{C}^{Incl\ -1}\boldsymbol{\sigma}^{Incl} = \boldsymbol{C}^{Rock\ -1}\boldsymbol{\sigma}^{Rock} \tag{3.8}$$

Where $\boldsymbol{C}^{Incl}$ and $\boldsymbol{C}^{Rock}$ are the constitutive matrices of the inclusion and the solid material, respectively. With this it occurs:

$$\boldsymbol{\sigma}^{Rock} = \boldsymbol{C}^{Rock}\boldsymbol{C}^{Incl\ -1}\boldsymbol{\sigma}^{Incl} \tag{3.9}$$

Substituting equation 3.9 into equation 3.7 and using also the relation in equation 3.6 it occurs:

$$\boldsymbol{C}^{Rock}\boldsymbol{C}^{Incl\ -1}\boldsymbol{\sigma} = \boldsymbol{\sigma} + \boldsymbol{\sigma}_0 \tag{3.10}$$

This can be arranged for the whole system (for all cell nodes) and the matrix $\boldsymbol{C1}_{cc}$ is obtained, which gives finally the relation between initial stresses $\boldsymbol{\sigma}_0$ and internal results $\boldsymbol{\sigma}$:

$$\{\boldsymbol{\sigma}_0\}_{c} = \underbrace{\left(\left[\boldsymbol{C}^{Rock}\right]_{cc}\left[\boldsymbol{C}^{Incl}\right]_{cc}^{-1} - [\boldsymbol{I}]_{cc}\right)}_{[\boldsymbol{C1}]_{cc}}\{\boldsymbol{\sigma}\}_{c} \tag{3.11}$$

$[\boldsymbol{I}]_{cc}$ contains assembled identity matrices.

Substituting this additional relation in equation 3.11 into equation 3.5 a directly solvable system of equations is obtained:

$$\begin{bmatrix} [\boldsymbol{A}]_{ee} & -([\boldsymbol{\Delta E}]_{ec}[\boldsymbol{C1}]_{cc}) \\ [\boldsymbol{A}^{\sigma}]_{ce} & -\left(\left[\boldsymbol{\Delta W}^{F}\right]_{cc}[\boldsymbol{C1}_{cc}] - [\boldsymbol{I}_{cc}]\right) \end{bmatrix} \begin{pmatrix} \{\boldsymbol{x}\}_e \\ \{\boldsymbol{\sigma}\}_c \end{pmatrix} = \begin{pmatrix} \{\boldsymbol{b}\}_e \\ \{\boldsymbol{b}^{\sigma}\}_c \end{pmatrix} \tag{3.12}$$

Where the vector on the right hand side includes the contributions due to the known boundary conditions $\boldsymbol{b}$ and $\boldsymbol{b}^{\sigma}$; and the vector on the left hand side contains the unknown boundary conditions $\boldsymbol{x}$ and the unknown stresses at the cell nodes $\boldsymbol{\sigma}$.

3.2.2 Iterative Solution Procedure

Now an alternative solution procedure will be presented, where the unknown body force term $\boldsymbol{f}$ is calculated iteratively. The system of equations (3.1) is rewritten here:

$$\boldsymbol{Ax} = \boldsymbol{b} + \boldsymbol{f} \tag{3.13}$$

In contrast to the direct solvable system of equations 3.12 no additional unknowns arise in the system of equations (3.13) because of the inclusions; the system itself remains small.

This procedure looks very similar to the iterative procedure used for the nonlinear material behaviour and thus can easily combined with it. The advantage of this combination is that both, the solid and the inclusion are able to behave in a nonlinear manner without producing much additional effort in contrast to the direct solution procedure of section 3.2.1.

As for the direct solution, also here the problem could be arranged in several variations of body forces (initial stresses, initial strains or forces) and in several variations of internal results (stresses, strains or displacements). Below the procedure will be described in a general way, where different kinds of body force

loadings can be used and also different kinds of internal results (internal results are overall indicated by $\boldsymbol{r}$).

The iteration procedure starts with an initial analysis (subscript $j = 0$), in which the solid is assumed to be homogeneous without any inclusion, thus the body forces are zerro ($\boldsymbol{\Delta f}_{j=0} = 0$).

$$\boldsymbol{A}\ \boldsymbol{\Delta x}_{j=0} = \boldsymbol{b} \tag{3.14}$$

After solving 3.14, the results $\boldsymbol{\Delta r}_j$ at all cell nodes can be obtained. The total boundary results and internal results are initialised at this stage:

$$\begin{aligned} \boldsymbol{x}_{j=0} &= \boldsymbol{\Delta x}_{j=0} \\ \boldsymbol{r}_{j=0} &= \boldsymbol{\Delta r}_{j=0} \end{aligned} \tag{3.15}$$

After this homogeneous initial analysis the iteration procedure starts:

(i) The index for the iteration step is incremented $j = j + 1$.

(ii) Because of the different materials of the inclusion and the solid, the stresses are different in both. The results which are calculated before $\boldsymbol{i}_{j-1}$ may be incorrect. The error produced in the last analysis can be calculated and expressed in terms of residual loadings (e.g. residual initial stresses); with this the residual vector $\boldsymbol{\Delta f}_j$ is calculated.

(iii) The convergence is checked by comparing the vector-norm of the residuum $\parallel \boldsymbol{\Delta f}_j \parallel$ with a given tolerance:

$$\parallel \boldsymbol{\Delta f}_j \parallel \leq\ tol \tag{3.16}$$

After the first iteration step ($j > 1$) the tolerance is defined by a percentage of the of the fist residuum $tol = \parallel \boldsymbol{\Delta f}_1 \parallel \epsilon$. Whereas $\epsilon = 0.01$ is in most cases accurate enough. If the convergence criterion is fulfilled, the iteration procedure ends here, otherwise it continues with the next step (iv).

(iv) The previous calculated residuum is applied to the system of equations as new right hand side $\boldsymbol{\Delta f}_j$:

$$\boldsymbol{A}\,\boldsymbol{\Delta x}_j = \boldsymbol{\Delta f}_j \tag{3.17}$$

(v) After solving 3.17, the results $\boldsymbol{\Delta r}_j$ are calculated at all cell nodes.

(vi) The boundary results and the internal results will be updated:

$$\begin{aligned} \boldsymbol{x}_j &= \boldsymbol{x}_{j-1} + \boldsymbol{\Delta x}_j \\ \boldsymbol{r}_j &= \boldsymbol{r}_{j-1} + \boldsymbol{\Delta r}_j \end{aligned} \tag{3.18}$$

(vii) The iteration procedure continues with step (i).

The iterations proceed until convergence is reached in step (iii). The final system of equations can be written as the sum of the incremental systems:

$$\boldsymbol{A}\,\boldsymbol{x}_j = \boldsymbol{b} + \boldsymbol{f}_j \tag{3.19}$$

where $\boldsymbol{f}_j = \sum \boldsymbol{\Delta f}_j$ is the sum of all incremental residual vectors.

In the next chapters (chapter 4, chapter 5, chapter 6) the simulation of different types of inclusions will be described. For each kind of inclusion the procedure varies a bit: different kinds of cells, of body forces and of internal result types are used; also the computation of the residuum is done in different ways. However, the same iteration loop can be used for all this different kinds of inclusions and they can be calculated at the same time. For this reason *cellgroups* are introduced, which combine all cells with the same characteristics (as inclusion type, material properties and so on).

In addition nonlinear behaviour (like plasticity) may occur even for the solid or for the inclusion. The iterative procedure for simulation nonlinear material behaviour is very similar to the iterative procedure used for calculating the inclusions. The same iteration loop is used for both. For doing this, all plasticity cells have to be summarized by one cellgroup too. Considering plasticity in the

BEM is described in various publications, as for example in Telles (1983), Gao and Davies (2002), Cisilino and Aliabadi (1998), Ribeiro et al. (2008).

Using the concept of the cellgroups, the different methods can be combined into one iteration loop. For each cellgroup (index CG) the internal results $\boldsymbol{r}^{CG}$ and the applied body forces can be different; and the residuum can be calculated in diverse ways. The total residual vector is obtained by the sum over all cellgroup residual vectors ($\boldsymbol{\Delta f}_j = \sum \boldsymbol{\Delta f}_j^{CG}$). The final system of equations is:

$$\boldsymbol{A}\,\boldsymbol{x}_j = \boldsymbol{b} + \sum_{CG} \boldsymbol{f}_j^{CG} \tag{3.20}$$

The itrative solution procedure using as many cellgroups as desired, is presented in figure 3.3.

Iterative Procedure and Coupling

For the simulation of tunnelling problems the coupling of different regions is in most cases indispensable. For example the simulation of the excavation process in tunnelling, where the solid around the tunnel is defined by an infinite BE-region and the solid inside the tunnel surface is subdivided in several finite BE-regions. The excavation process is simulated, by deactivating the finite regions step by step, see Duenser (2001). Another example for coupled problems in tunnelling is the simulation of shotcrete along the tunnel surface. The thin shotcrete shell can be simulated efficiently with shell elements, see Prazeres (2009); however this FE's has to be coupled to the BE-region.

Thus, the iteration procedure described above has to be extended to coupled problems. The procedure is shown in figure 3.4, the index SYS denotes the whole system with all regions.

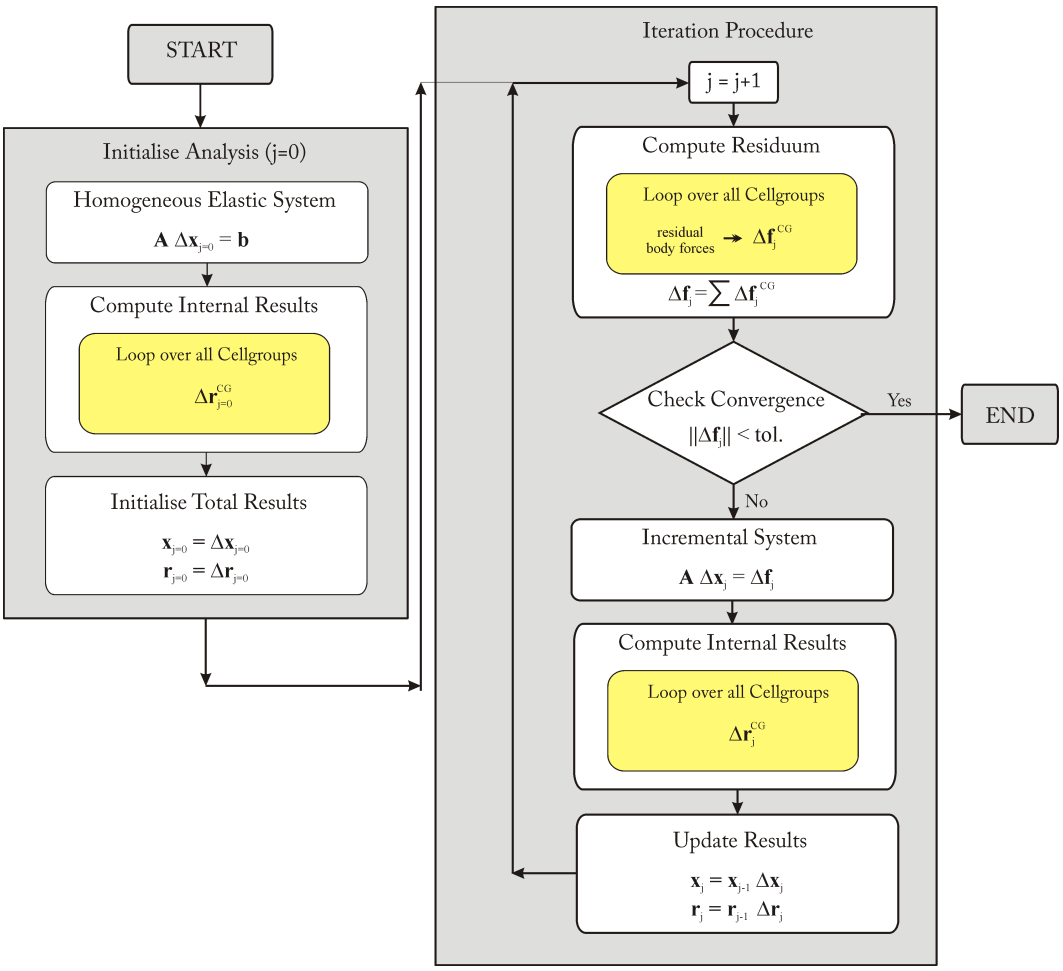

Figure 3.3: Flow chart of the iterative algorithm

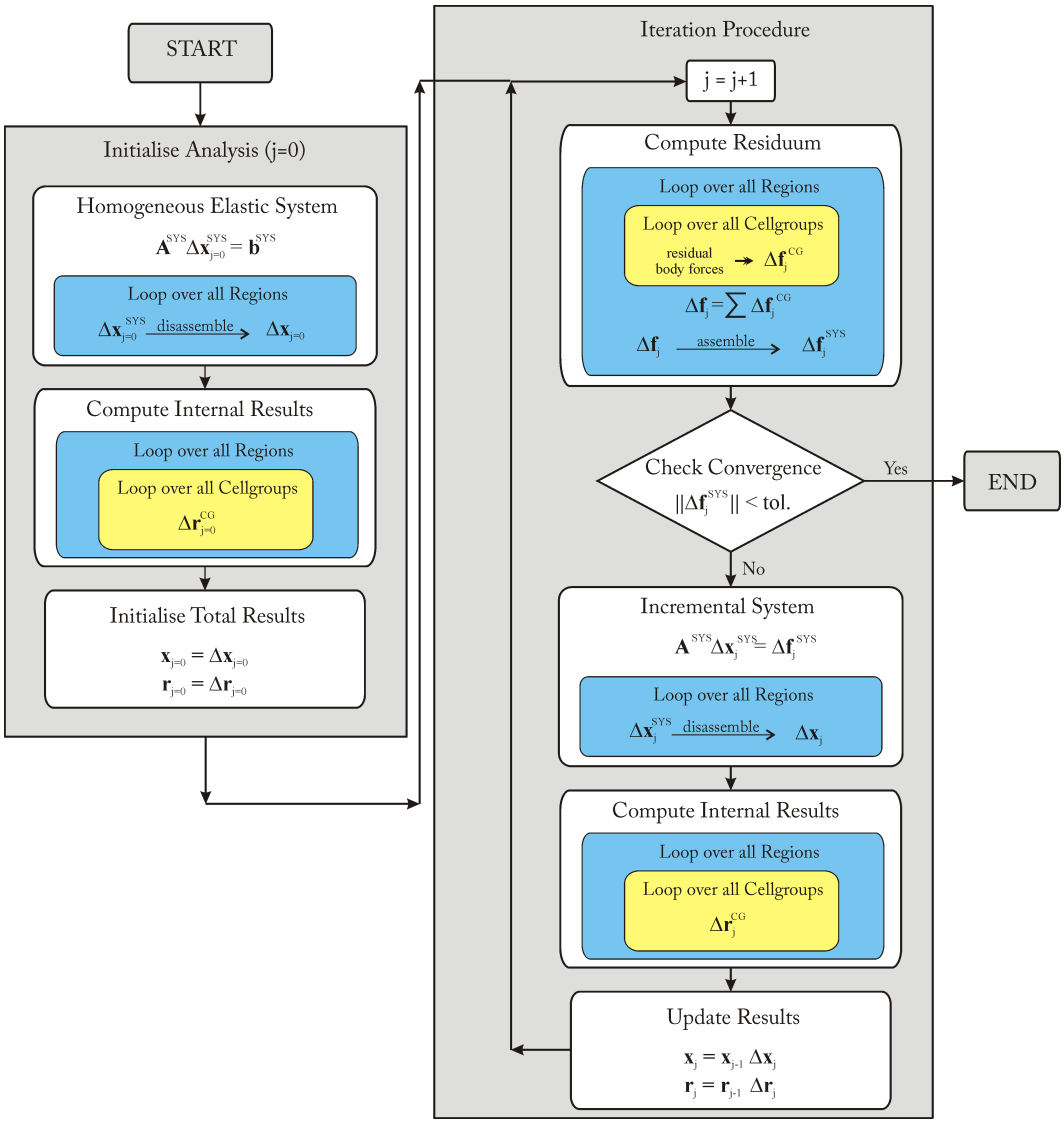

Figure 3.4: Flow chart of the iterative algorithm for coupled problems

3.3 Conclusion

In this work the iterative solution procedure section 3.2.2 is proposed. For problems where only linear elastic material behaviour is required, it would be possible to solve the problem directly (see section 3.2.1), in all other cases where nonlinear material behaviour occurs an iterative solution procedure has to be used for the material nonlinearity. In most tunnelling problems nonlinear material behaviour has to be considered; thus an iterative procedure and the discretisation of the domain with internal cells are necessary anyway. Because of this the iterative solution procedure is proposed in this work. The iterative procedure for calculating the inclusions can be efficiently combined with the iterative procedure for the nonlinear material behaviour and thus produces almost no additional expense in comparison to a system without inclusions.

In the next sections it is shown how the residual vectors are calculated for the different kinds of inclusions (fully grouted rock bolts, discrete anchored bolts or anchors and geological inhomogeneities or pipe umbrellas). Figure 3.5 shows a BE mesh of a tunnel including different cell-groups for plasticity, geological inclusions, pipe umbrella and rock bolts

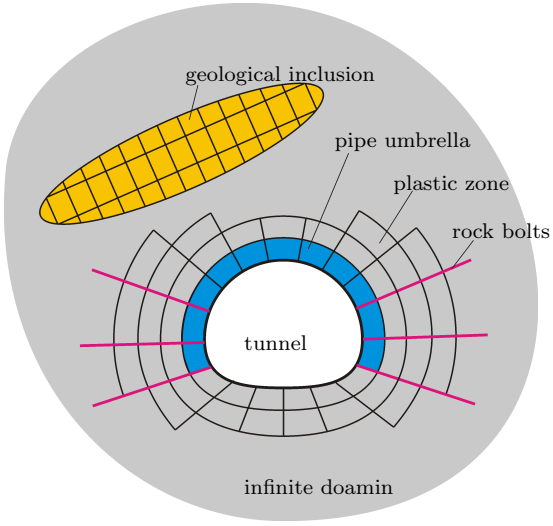

Figure 3.5: BE discretisation including different cells

Chapter 4

General Inhomogeneities and Pipe Umbrellas

4.1 General

Usually the ground will not be homogeneous and the simulation program should be able to consider this. In tunnelling problems different types of inclusions occur; on the one hand inclusions arise from the geology like fault zones and soft or stiff layers; on the other hand inclusions are placed in to support the excavated tunnel, for example rock bolt, anchors, pipe umbrella systems ...

As described in chapter 2 the classical BIE can deal with homogeneous, linear-elastic domains only. However, in chapter 3 a possibility was presented to simulate inclusions by applying *body forces* (e.g. initial stresses) calculated within an iterative procedure. In this chapter the approach for simulating geological inclusions and pipe umbrella systems will be presented.

4.1.1 General Inhomogeneities

The calculation of inclusions with arbitrary shape, like geological inhomogeneities, can be done within the iterative procedure described in chapter 3. The inclusions are modelled by ordinary volume-cells, see figure 4.1.

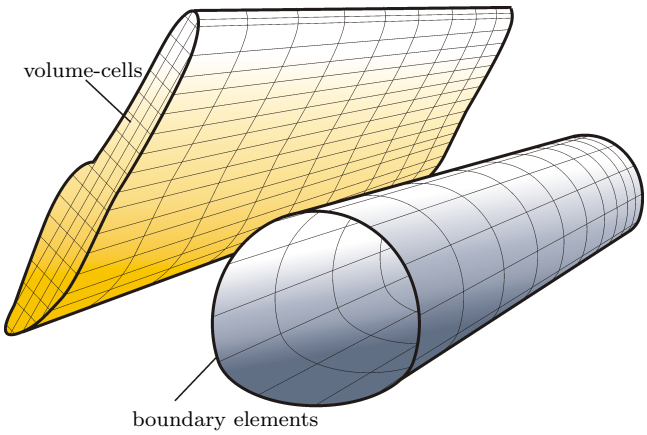

Figure 4.1: Geological inclusion discretised with cells

4.1.2 Pipe Umbrellas

Technique

To improve the behaviour of the ground and for the stabilisation of the excavated area, especially the working face, a grouted pipe-roofing technique can be used. In this technique a series of pipes are installed and after that grout is injected through the pipes. Thereby the properties of the ground between the pipes are changed and the pipes are connected to a kind of umbrella around the area to be excavated, see figure 4.2.

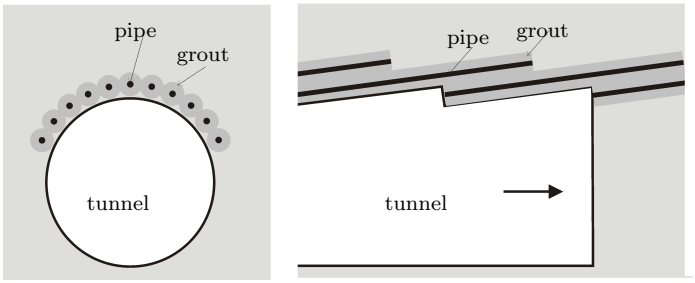

Figure 4.2: Grouted pipe roofing technique

Numerical Simulation

Such a pipe-roofing technique described before is a geometrically and mechanically complex problem. In this work it is proposed to approximately simulate this problem by a homogenized zone. Consequently, the same volume-cells and the same algorithm as for the general inhomogeneities can be used; one single layer of ordinary volume-cells is used for discretisation, see figure 4.3.

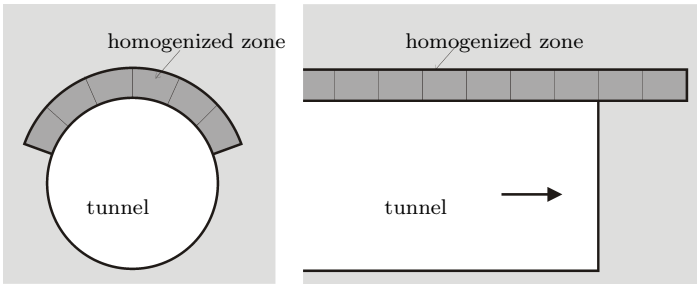

Figure 4.3: Approximated modelling of pipe roofs

4.2 BE-approach

The general procedure described in section 3.2.2 is adapted to model geological inhomogeneities. For this, the following special configurations are used:

- General volume-cells are used for discretisation: in 2D problems we have quadratic quadrilateral cells, in 3D problems quadratic brick cells (see section 2.4.3).
- Initial stresses $\boldsymbol{\sigma_0}$ are applied as loading in the volume-cells.
- Internal strain results $\boldsymbol{\Delta\varepsilon}_j$ are use for computing the residuum in the j-th iteration step, see section 4.2.2.
- The residual-vector is computed as described in section 4.2.3.

4.2.1 Iterative Procedure

The iterative procedure is used, as described in section 3.2.2.

First the homogeneous elastic problem is solved:

$$\boldsymbol{A}\,\boldsymbol{\Delta x}_{j=0} = \boldsymbol{b} \tag{4.1}$$

After that the strain results $\boldsymbol{\Delta\varepsilon}_{j=0}$ are calculated at all cell nodes. The total boundary results and internal results are initialised:

$$\begin{aligned} \boldsymbol{x}_{j=0} &= \boldsymbol{\Delta x}_{j=0} \\ \boldsymbol{\varepsilon}_{j=0} &= \boldsymbol{\Delta\varepsilon}_{j=0} \end{aligned} \tag{4.2}$$

Then the iteration starts and following steps have to be done:

(i) The index for the iteration step is incremented $j = j + 1$.

(ii) The residual vector $\boldsymbol{\Delta f}_j$ is calculated, see section 4.2.3.

(iii) The convergence is checked by comparing the vector-norm of the residuum $\| \boldsymbol{\Delta f}_j \|$ with a given tolerance:

$$\| \boldsymbol{\Delta f}_j \| \leq tol \tag{4.3}$$

After the first iteration step ($j > 1$) the tolerance is defined by a percentage of the fist residuum $tol = \| \boldsymbol{\Delta f}_1 \| \epsilon$. If the convergence criterion is fulfilled, the iteration procedure ends here, otherwise it continues with the next step (iv).

(iv) The residual vector is applied to the system of equations as new *right hand side*:

$$\boldsymbol{A}\, \boldsymbol{\Delta x}_j = \boldsymbol{\Delta f}_j \tag{4.4}$$

(v) The strain results $\boldsymbol{\Delta \varepsilon}_j$ are calculated at all cell nodes.

(vi) The boundary results and the strain results are updated:

$$\begin{aligned} \boldsymbol{x}_j &= \boldsymbol{x}_{j-1} + \boldsymbol{\Delta x}_j \\ \boldsymbol{\varepsilon}_j &= \boldsymbol{\varepsilon}_{j-1} + \boldsymbol{\Delta \varepsilon}_j \end{aligned} \tag{4.5}$$

(vii) The iteration procedure continues with step (i).

4.2.2 Computation of the Strains

Internal strain results ($\boldsymbol{\Delta \varepsilon}_j$) are needed for the computation of the residuum. Between two materials (like the ground and the inclusion) a jump arises in the stress-field. Because of this discontinuity the strains cannot be calculated directly by using the integral equation (see equation 2.63). For points inside one material (even if they are very near to the border) the integral equation 2.63 gives the correct results; but not for points located directly on the border. We have two options to compute strains at these nodes:

- For nodes located on the border to an other material, the strains are extrapolated from strain results of points inside the material.

- The other option is to calculate displacements at all cell nodes by using the integral equation 2.47. This can be done without problems, because the displacements do not have a jump at the border between two materials. Afterwards the strains are calculated for each cell by the derivation of the displacements (via the interpolation function of the cell).

In this work the second option (derivation of the displacements) is used for calculating the strains. Thus, this option is described in more detail:

The displacements over the cell are approximated using the interpolation functions Φ_n and the nodal displacements $\boldsymbol{u^c}_n$, see section 2.4.3:

$$\boldsymbol{u^c} = \sum_{n=1}^{N^c} \Phi_n \boldsymbol{u^c}_n \tag{4.6}$$

The strains for a one dimensional problem can be expressed by the derivative of the interpolation functions:

$$\varepsilon = \frac{\partial u^c}{\partial x} = \sum_{n=1}^{N^c} \frac{\partial \Phi_n}{\partial x} u^c_n \tag{4.7}$$

For the general 2D or 3D case this can be written in matrix form:

$$\boldsymbol{\varepsilon} = \sum_{n=1}^{N^c} \boldsymbol{B^c}_n \boldsymbol{u^c}_n \tag{4.8}$$

Where $\boldsymbol{B^c}_n$ is a matrix containing the derivation of the interpolation functions:

$$\boldsymbol{B^c}_n = \begin{bmatrix} \frac{\partial \Phi_n}{\partial x} & 0 \\ 0 & \frac{\partial \Phi_n}{\partial y} \\ \frac{\partial \Phi_n}{\partial y} & \frac{\partial \Phi_n}{\partial x} \end{bmatrix} \qquad \text{for 2D} \tag{4.9}$$

$$\boldsymbol{B^c}_n = \begin{bmatrix} \frac{\partial \Phi_n}{\partial x} & 0 & 0 \\ 0 & \frac{\partial \Phi_n}{\partial y} & 0 \\ 0 & 0 & \frac{\partial \Phi_n}{\partial z} \\ \frac{\partial \Phi_n}{\partial y} & \frac{\partial \Phi_n}{\partial x} & 0 \\ 0 & \frac{\partial \Phi_n}{\partial z} & \frac{\partial \Phi_n}{\partial y} \\ \frac{\partial \Phi_n}{\partial z} & 0 & \frac{\partial \Phi_n}{\partial x} \end{bmatrix} \qquad \text{for 3D} \tag{4.10}$$

4.2.3 Computation of the Residuum

The residual initial stresses $\boldsymbol{\Delta\sigma_{0}}_j$ for one iteration step j are calculated by using the strain results $\boldsymbol{\Delta\varepsilon}_j$ and the generalised Hooke's law for the two different materials. In order to get a better convergence, different methods are used for the cases when the inclusion material is softer than the rock mass or when it is stiffer.

After the residual initial stresses $\boldsymbol{\Delta\sigma_{0}}_j$ are calculated at all cell nodes, the residual vector $\boldsymbol{\Delta f}_j$ can be computed (see equation 2.43):

$$\boldsymbol{\Delta f}_j = \int_V \boldsymbol{E\Delta\sigma_{0}}_j dV \tag{4.11}$$

Soft Inclusions

If the inclusion material is soft compared to the rock mass (for example soft layers), the residual initial stresses are computed by:

$$\boldsymbol{\Delta\sigma_{0}}_j = \left(\boldsymbol{C^{Rock}} - \boldsymbol{C^{Incl}}\right) \boldsymbol{\Delta\varepsilon}_{j-1} \tag{4.12}$$

$\boldsymbol{C^{Rock}}$ and $\boldsymbol{C^{Incl}}$ are the constitutive matrices of the rock-material and the inclusion-material, respectively. Equation 4.12 is appropriate to calculate soft inclusions; because the strains $\boldsymbol{\Delta\varepsilon}_{j-1}$ are related to the rock mass (which is stiffer than the inclusion), see figure 4.4.

Hard Inclusions

If the inclusion is harder than the surrounding solid (as it is the case for pipe umbrellas) the residual stress computed with equation 4.12 would be very high and the iteration would not converge in many cases. For this, the residual stresses are computed in an alternative way:

$$\boldsymbol{\Delta\sigma_{0}}_{j} = \left(\boldsymbol{C^{Rock}} - \boldsymbol{C^{Incl}}\right) \boldsymbol{\Delta\varepsilon^{Incl}}_{j-1} \tag{4.13}$$

$\boldsymbol{\Delta\varepsilon}_{j-1}^{Incl}$ means that the strains are related to the inclusion material:

$$\begin{aligned} \boldsymbol{\Delta\varepsilon^{Incl}}_{j-1} &= \boldsymbol{C^{Incl}}^{-1} \boldsymbol{\Delta\sigma^{Incl}}_{j-1} \\ &= \boldsymbol{C^{Incl}}^{-1} \left(\boldsymbol{\Delta\sigma^{Rock}}_{j-1} - \boldsymbol{\Delta\sigma_{0}}_{j-1}\right) \\ &= \boldsymbol{C^{Incl}}^{-1} \left(\boldsymbol{C^{Rock}} \boldsymbol{\Delta\varepsilon}_{j-1} - \boldsymbol{\Delta\sigma_{0}}_{j-1})\right) \end{aligned} \tag{4.14}$$

The difference of both variants are schematically shown in figure 4.4. In order to get convergence in the iteration procedure, the strains are related to the harder material in each case, thus the residual initial stresses are not too high.

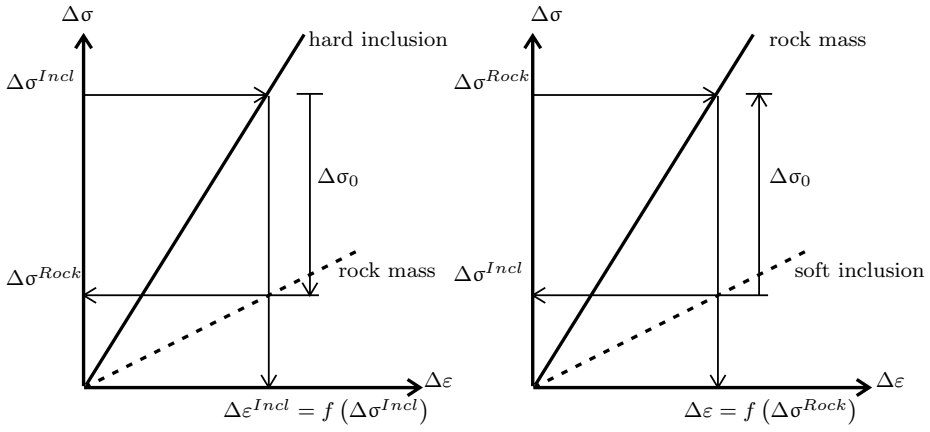

Figure 4.4: Schematic diagram for computing the residuum for soft and hard inclusions

Inclusion with Nonlinear Material

For a problem where the inclusion material behaves nonlinear (e.g. it plastifies) the residual initial stress consists of two parts: the elastic part $\boldsymbol{\sigma_0^e}$ and the plastic part $\boldsymbol{\sigma_0^p}$, see figure 4.5:

$$\boldsymbol{\sigma_0} = \boldsymbol{\sigma_0^e} + \boldsymbol{\sigma_0^p} \tag{4.15}$$

The elastic part is computed as described before; with this the situation of an elastic inclusion is obtained (see equation 4.16). The plastic part is computed starting from the elastic inclusion state $\boldsymbol{\sigma^{Incl\ e}}$, see equation 4.17; the plastic part can be calculated as described in various publications, see for example Telles (1983), Gao and Davies (2002), Ribeiro et al. (2008).

$$\boldsymbol{\sigma^{Incl\ e}} = \boldsymbol{\sigma^{Rock}} + \boldsymbol{\sigma_0^e} \tag{4.16}$$

$$\boldsymbol{\sigma^{Incl}} = \boldsymbol{\sigma^{Incl\ e}} + \boldsymbol{\sigma_0^p} = \boldsymbol{\sigma^{Rock}} + \boldsymbol{\sigma_0} \tag{4.17}$$

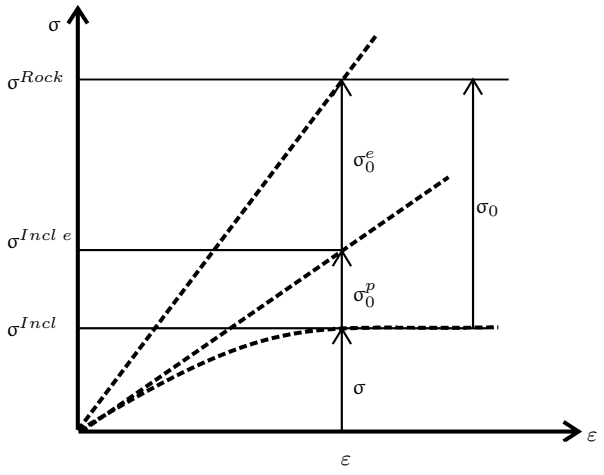

Figure 4.5: Schematic figure of the stress states for inclusions with nonlinear material behaviour

4.2.4 Evaluation of the Integral

In order to achieve the residual vector $\boldsymbol{\Delta f}_j$ an integration over the volume-cells has to be carried out, see equation 4.11. This is done in the standard way as described in section 2.4.5.

4.3 Verification Examples

Some very simple examples are presented to verify the described method. Soft, elastic or plastic inclusions have been tested in 2D and 3D examples. A soft inclusion in combination with multiple regions has been tested as well; and also a stiff inclusion and changing material properties within different calculation steps has been tested.

4.3.1 Example 1: Soft inclusion in plane strain

The first example shows a block with a soft inclusion in plane strain. The dimension of the block is 2m x 2m; the Young's modulus is E=5000MN/m^2; and the Poisson's ratio is ν=0.3. The block is fixed at the bottom and on the top of the block a constant pressure is applied p=1MN/m^2.

Three calculations were carried out: the first without an inclusion; the second with an elastic inclusion and the third with an inclusion with nonlinear material behaviour. The soft inclusion has a square shape, placed in the centre of the block; its dimension is 1m x 1m. The elastic material properties for the inclusion in the second and the third calculation are: Young's modulus E=2500MN/m^2; Poisson's ratio ν=0.3. For the third calculation the Drucker Prager yield criterion is used with an associated flow rule; the cohesion is c=0.1MN/m^2 and the friction angle is Φ=30°.

The results are compared with reference solutions calculated with the same BE-program but with multiple regions (BEM MR); where the inclusion is defined as an own region. The third calculation is also compared with results from a FE-analysis. The results are presented in figure 4.6 and figure 4.7.

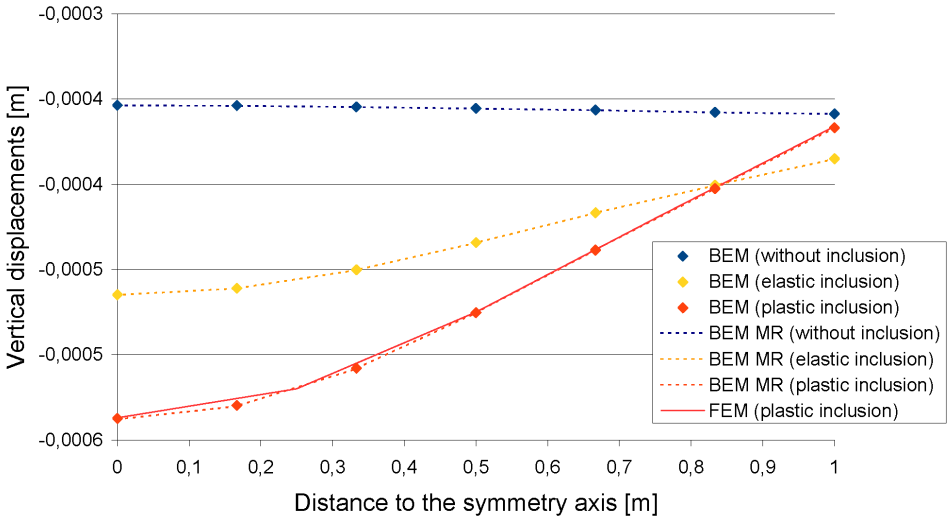

Figure 4.6: Example 1: vertical displacements on the top of the block

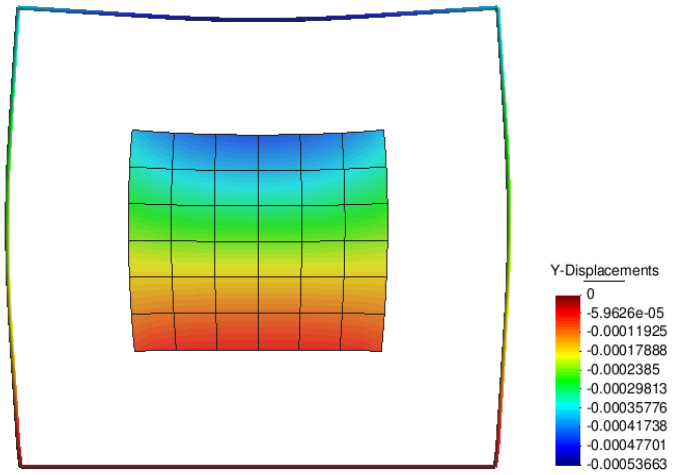

Figure 4.7: Example 1: deformed mesh and contours of vertical displacements

4.3.2 Example 2: Soft inclusion in 3D

This example shows a 3D block with a soft inclusion. The dimension of the block is 10m x 10m x 10m; the Young's modulus is E=5000MN/m^2; and the Poisson's ratio is ν=0.0. The block is fixed at the bottom and a constant pressure is applied at the top of the block p=50MN/m^2.

Three calculations were carried out: the first without an inclusion and the second with an soft elastic inclusion and the third with a plastic inclusion. The inclusion is placed in the centre of the block and has the dimensions 4m x 4m x 4m. The elastic material properties of the inclusion are: Young's modulus is E=2000MN/m^2; Poisson's ratio is ν=0.3. And for the third calculation the Drucker Prager yield criterion is used with an associated flow rule; the cohesion is c=5.0MN/m^2; the friction angle is Φ=30°.

The deformed mesh with the contours of the vertical displacements are shown in figure 4.8. The results are compared with those calculated with the FEM, see figure 4.9 and figure 4.10.

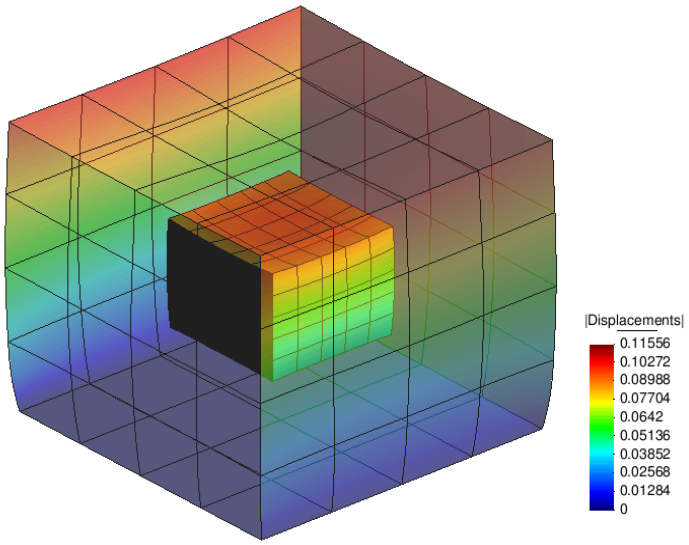

Figure 4.8: Example 2: deformed mesh and contours of vertical displacements

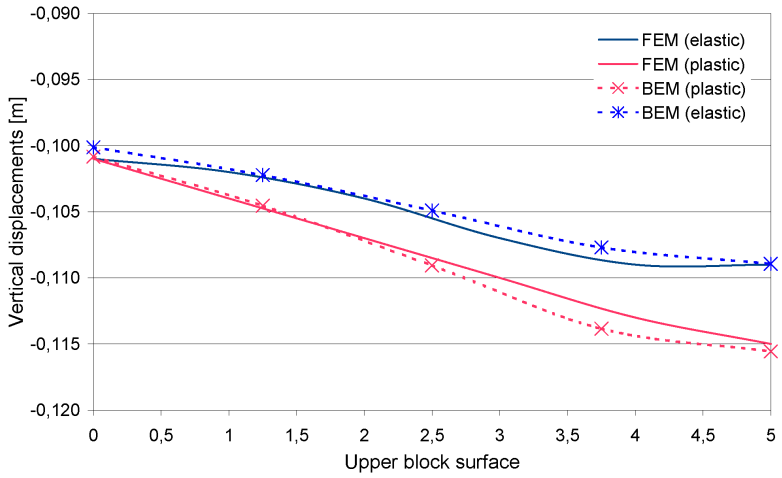

Figure 4.9: Example 2: vertical displacements along the top of the block

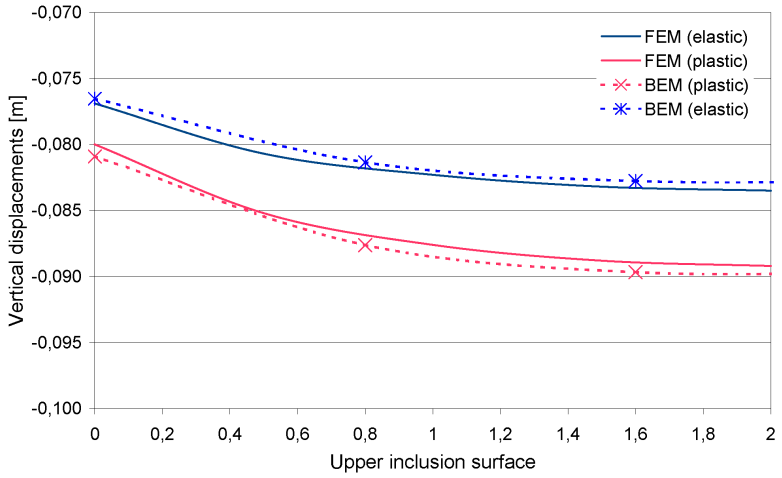

Figure 4.10: Example 2: vertical displacements along the top of the inclusion

4.3.3 Example 3: Soft inclusion and multiple regions

The third example shows again a block with a soft inclusion in plane strain conditions, but it exhibits the compatibility of this algorithm with multiple region problems. Two variational calculations have been carried out to calculate the same problem. The first is with a single region; and the second with two regions where the splitting is directly in between the inclusion. Both calculations show good agreement for the displacement results but also for the stress results, see figure 4.11 and figure 4.12.

The dimension of the block is 2.167m x 2m; the Young's modulus is E=5000MN/m^2; and the Poisson's ratio is ν=0.0. The block is fixed at the bottom and on the top of the block a constant pressure is applied p=1MN/m^2. The inclusion has a dimension of 1m x 1m; the Young's modulus is E=500MN/m^2; and the Poisson's ratio ν=0.0.

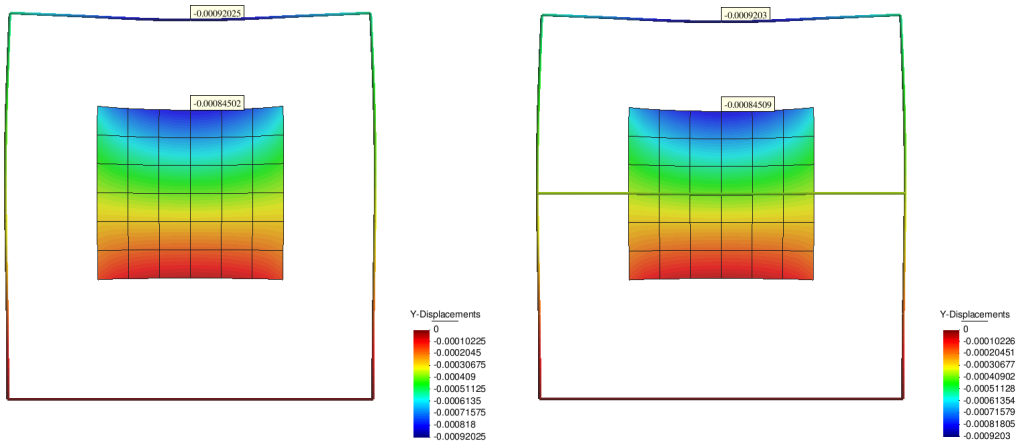

(a) Single region (b) Two regions

Figure 4.11: Example 3: deformed shape and displacement contours

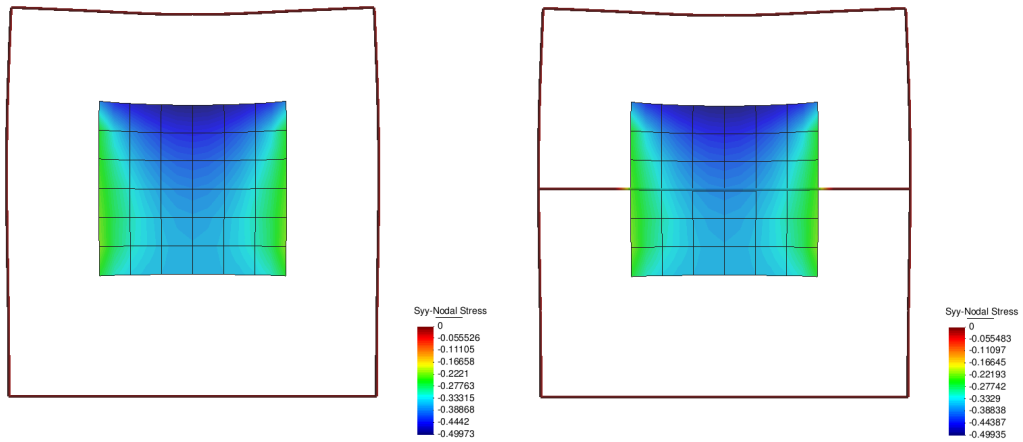

(a) Single region (b) Two regions

Figure 4.12: Example 3: deformed shape and contours of vertical stresses

4.3.4 Example 4: Cantilever with stiff inclusion in second analysis step

The last example is testing a stiff inclusion (modelled by one layer of cells) wich is under bending load. This shows the applicability of this method to model pipe umbrellas within a strongly reduced example. In a first step a homogeneous cantilever beam is loaded over the entire length with a constant pressure; after that in a second step, an additional loading is applied and the material in the upper part of the cantilever is changing to be stiffer then before. This stiffer part is modelled by one layer of inclusion cells, see figure 4.13. The results are compared with those calculated by the FEM, see figure 4.14.

The cantilever is 10m long and 2m high; it is fixed at the left side and loaded with a constant pressure along the whole length (in the first step the pressure is p=$5MN/m^2$ and in the second step an additional pressure of p=$5MN/m^2$ is applied). The Young's modulus of the cantilever is E=$10000MN/m^2$ and the Poisson's ratio is ν=0.3. In the second step a stiffer zone in the upper part of the cantilever is introduced, it has a high of 0.5m and the Young's modulus is E=$50000MN/m^2$ and the Poisson's ratio is ν=0.3.

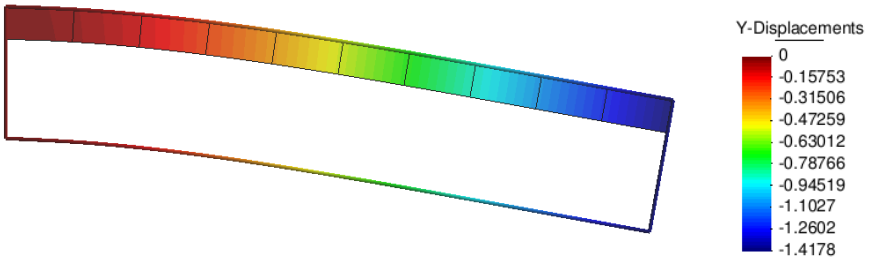

Figure 4.13: Example 4: deformed mesh after the second calculation step

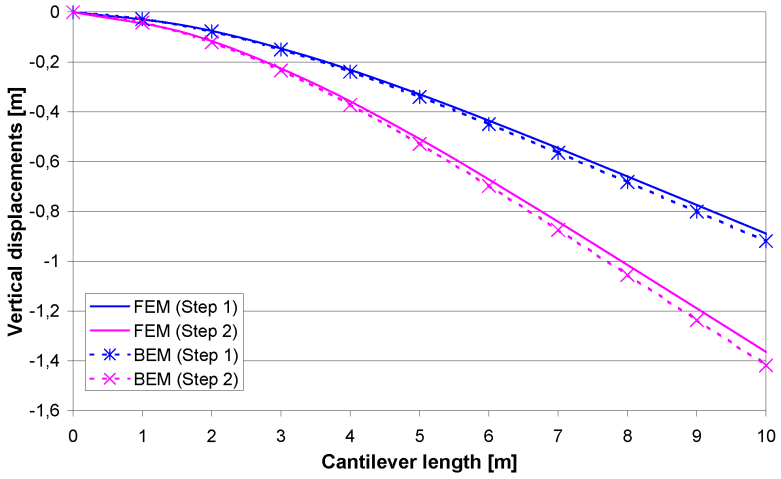

Figure 4.14: Example 4: vertical displacements along the top of the cantilever

Chapter 5

Continuous Anchored Bolts

5.1 General

In conventional tunnel excavation rock bolts, especially in combination with shotcrete lining are the most important support elements (see section 1.2). For different needs a wide variety of bolt types have been developed which are used in mining and civil engineering. The different kinds of bolts can be assigned into two main groups: the continuous anchored bolts (or dowels); and the end-anchored or discrete anchored bolts, see Hoek et al. (1997). In this chapter the modelling of the first of these groups (the continuous anchored bolts) is described. The numerical modelling of the second group (the discrete anchored bolts) will be described in chapter 6.

Technique

Continuous anchored rock bolts generally consist of deformed steel bars which are grouted into the rock. Pre-stressing of the bolt is not possible and the loads in the bolts are generated by movements in the rock mass. In order to be effective, these kind of rock bolts have to be installed before significant movements in the rock mass has taken place, see Hoek et al. (1997). Figure 5.1 shows different types of typical bolts which can be used in tunnelling.

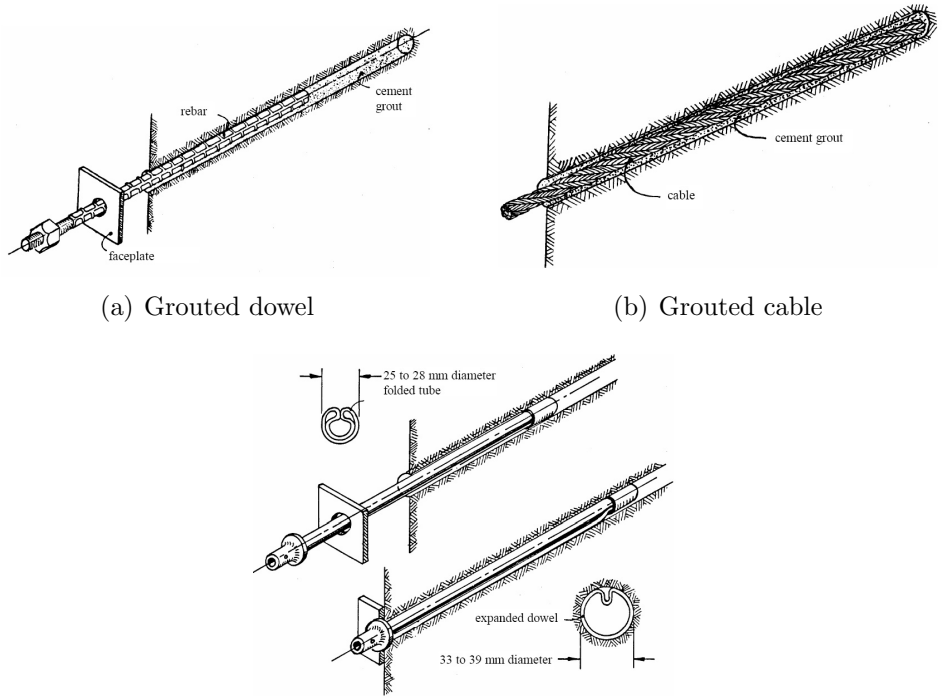

(a) Grouted dowel

(b) Grouted cable

(c) Swellex dowel

Figure 5.1: Different types of continuous anchored bolts, see Hoek et al. (1997)

Numerical Simulation

Fully grouted rock bolts (or rock bolts which are in continuous contact with the ground) could be treated like general inclusions (see chapter 4). However, because of their narrow geometry it is reasonable to introduce some simplifications. A number of special BE-formulations have been developed in the past, for simulating problems containing thin inclusions inside a solid such as piles, reinforcements or rock bolts, see also Riederer et al. (2009).

Most of the approaches use BEM-FEM coupling, where the solid is modelled with boundary elements and the thin inclusions are considered by using finite elements. The coupling is done by enforcing displacement compatibility and traction equilibrium at the interface nodes between inclusion and solid. Such inclusions have been modelled in various degrees of simplification: as simple truss

elements, as beam elements, or as general volume elements. For the simulation of very thin inclusions such as reinforcement or rock bolts the bending stiffness can be neglected and truss elements are used (see for example: Coda 2001, Leite et al. 2003, Leite and Venturini 2005). For simulating the behaviour of inclusions where the bending stiffness is taken into account such as for piles, beam elements are used (see for example: Coda and Venturini 1999, Filho et al. 2005, Padron et al. 2007, Leite and Venturini 2005).

Some papers use pure BEM formulations, where the inclusion is also discretised with boundary elements (for example in: Banerjee 1981, Wang and Gao 1998, Maeso et al. 2005, Aliabadi and Saleh 2002, Ma et al. 2008).

In all these approaches the problem is solved directly and therefore additional unknowns are introduced for the inclusions. Because of this, the size of the system of equations increases with the number of inclusions.

The goal of this work was to efficiently calculate a very high number of thin linear inclusions (rock bolts) with a pure BEM and in combination with nonlinear material behaviour of the rock mass. Because of this a complete new approach has been developed which solves the problem iteratively.

It is assumed that the rock bolts are in continuous contact with the ground and that they are sufficiently thin, so that their bending stiffness can be neglected; they are only able to carry axial stresses. They are modelled by simple *line-cells*.

5.2 BE-approach

In order to simulate the continuous anchored bolts, the general procedure described in section 3.2.2 is adapted for these kind of problem, see also Riederer et al. (2009). Following configurations are used:

- Line-cells are used for the discretisation, see section 5.2.2.
- Axial initial stresses $\boldsymbol{\sigma_{0\,\bar{x}\bar{x}}}$ are applied as loading along the line-cells.
- Internal stress results in axial direction of the bolt $\boldsymbol{\sigma_{\bar{x}\bar{x}}}$ are use for computation, see section 5.2.3.
- The residual-vector is computed as described in section 5.2.4.

5.2.1 Iterative Procedure

First the homogeneous elastic problem is solved:

$$\boldsymbol{A}\,\boldsymbol{\Delta x}_{j=0} = \boldsymbol{b} \tag{5.1}$$

Then the stresses in axial direction of the bolt $\boldsymbol{\Delta\sigma}_{\bar{x}\bar{x}j}$ are calculated at all cell nodes. The total boundary results $\boldsymbol{x}_{j=0}$ and internal results $\boldsymbol{\sigma}_{\bar{x}\bar{x}j=0}$ are initialised:

$$\begin{aligned} \boldsymbol{x}_{j=0} &= \boldsymbol{\Delta x}_{j=0} \\ \boldsymbol{\sigma}_{\bar{x}\bar{x}j=0} &= \boldsymbol{\Delta\sigma}_{\bar{x}\bar{x}j=0} \end{aligned} \tag{5.2}$$

The iteration starts and following steps have to be done:

(i) The index for the iteration step is incremented $j = j + 1$.

(ii) The residual vector $\boldsymbol{\Delta f}_j$ is calculated, see section 5.2.4.

(iii) The convergence is checked by comparing the vector-norm of the residuum $\parallel \boldsymbol{\Delta f}_j \parallel$ with a given tolerance:

$$\parallel \boldsymbol{\Delta f}_j \parallel \leq\ tol \tag{5.3}$$

The tolerance is defined by a percentage of the fist residuum $tol = \| \boldsymbol{\Delta f}_1 \| \epsilon$. If the convergence criterion is fulfilled, the iteration procedure ends here, otherwise it continues with the next step (iv).

(iv) The residual vector is applied to the system of equations as new *right hand side*:

$$\boldsymbol{A}\, \boldsymbol{\Delta x}_j = \boldsymbol{\Delta f}_j \tag{5.4}$$

(v) The stresses in axial bolt direction $\boldsymbol{\Delta \sigma}_{\bar{x}\bar{x}j}$ are calculated at all cell nodes.

(vi) The boundary results and the strain results are updated:

$$\begin{aligned} \boldsymbol{x}_j &= \boldsymbol{x}_{j-1} + \boldsymbol{\Delta x}_j \\ \boldsymbol{\sigma}_{\bar{x}\bar{x}j} &= \boldsymbol{\sigma}_{\bar{x}\bar{x}j-1} + \boldsymbol{\Delta \sigma}_{\bar{x}\bar{x}j} \end{aligned} \tag{5.5}$$

(vii) The iteration procedure continues with step (i).

5.2.2 Line-cells

As described before, the bolts are modelled by line-cells. Line-cells with three nodes and quadratic interpolation functions are used, see figure 5.2. The interpolation functions used for this are the same as these used for the boundary elements in 2D problems (see section 2.4.1):

$$\begin{aligned} \Phi_1 &= \frac{1}{2}\left(-\xi + \xi^2\right) \\ \Phi_2 &= \frac{1}{2}\left(\xi + \xi^2\right) \\ \Phi_3 &= 1 - \xi^2 \end{aligned} \tag{5.6}$$

The line-cells are placed at the position of the bolts centre-line. According to requirement, one bolt can be modelled by a number of connected line-cells. For common problems usually two to four line-cells are sufficiently accurate to model one rock bolt.

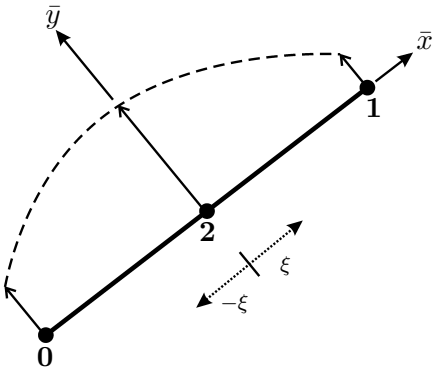

Figure 5.2: Line-cells with three nodes and quadratic interpolation

In order to model these bolts by simple line-cells, some simplifications have to be introduced. It is assumed that the bolts are sufficiently thin, so that their bending stiffness can be neglected and that the cross-section is circular and constant over the length.

Intial axial stresses $\boldsymbol{\sigma_{0\,\bar{x}\bar{x}}}$ are applied as loading along these line-cells to simulate the effect of the bolts inside the rock mass.

5.2.3 Computation of Stresses in Axial Bolt Direction

The internal results needed for the computation of the residuum in the iterative procedure (section 5.2.1) are the stresses in axial bolt direction $\boldsymbol{\Delta\sigma_{\bar{x}\bar{x}_j}}$. These results have to be calculated at all line-cell-nodes. It is possible to compute displacements or stresses directly at the cell-nodes, in spite of the singularities (see section 5.2.5).

Therefor we have two possibilities:

- *Stress based computation*: The stresses are calculated directly by using the integral equation for stresses at internal points (and stress recovery at the boundary). Afterward these stress results are transformed into local coordinate system of the line-cell to obtain the axial stress $\Delta\sigma_{\bar{x}\bar{x}_j}$ at each node.

- *Displacement based computation*: The displacements are calculated by using the integral equation for displacements at internal points (the boundary displacements are already achieved from the BIE). These displacements are transformed into the local coordinate system of the line-cell to obtain the axial displacements $\Delta u_{\bar{x}_j}$ at each node. The axial stresses are calculated from the displacements by using the derivative of the interpolation functions and Hooke's law.

Regarding only the rock bolt oneself, in generally the stress based computation might be the better one, because no derivation of the interpolation function is necessary and thus it is the more accurate method. However, regarding the rock bolt computation together with other methods (like the plasticity or the inclusion calculation) one of both computation methods can be more efficient than the other one. For example when using rock bolts and inclusions (see chapter 4) at the same time and using some equal nodes for both, it might be the best way to use the displacement based computation for the rock bolts, since the displacement results are needed anyway for the inclusion algorithm and thus produce no additional effort.

For this work both methods have been implemented into the program BEFE++, in order to choose the most efficient or most accurate computation for each example. Thus, both methods will be described in the following in more detail.

Stress Based Computation

As described before, for this computation method the stresses are calculated at all cell nodes. Stresses at internal nodes are calculated with the integral equation 2.70, at the boundary nodes the stress recovery method is used. After that, the stresses are transformed into the local coordinate system of the cell. For doing so the transformation matrix $\boldsymbol{T_\sigma}$ for stresses is introduced, see Beer et al. (2008):

$$\boldsymbol{T_\sigma} = \begin{bmatrix} \boldsymbol{T_{\sigma 11}} & \boldsymbol{T_{\sigma 12}} \\ \boldsymbol{T_{\sigma 21}} & \boldsymbol{T_{\sigma 22}} \end{bmatrix} \tag{5.7}$$

$$
\begin{aligned}
\boldsymbol{T_{\sigma 11}} &= \begin{bmatrix} s_{1x}^2 & s_{2x}^2 & s_{3x}^2 \\ s_{1y}^2 & s_{2y}^2 & s_{3y}^2 \\ s_{1z}^2 & s_{2z}^2 & s_{3z}^2 \end{bmatrix} \\
\boldsymbol{T_{\sigma 12}} &= \begin{bmatrix} 2s_{1x}s_{2x} & 2s_{2x}s_{3x} & 2s_{1x}s_{3x} \\ 2s_{1y}s_{2y} & 2s_{2y}s_{3y} & 2s_{1y}s_{3y} \\ 2s_{1z}s_{2z} & 2s_{2z}s_{3z} & 2s_{1z}s_{3z} \end{bmatrix} \\
\boldsymbol{T_{\sigma 21}} &= \begin{bmatrix} s_{1x}s_{1y} & s_{2x}s_{2y} & s_{3x}s_{3y} \\ s_{1y}s_{1z} & s_{2y}s_{2z} & s_{3y}s_{3z} \\ s_{1x}s_{1z} & s_{2x}s_{2z} & s_{3x}s_{3z} \end{bmatrix} \\
\boldsymbol{T_{\sigma 22}} &= \begin{bmatrix} s_{1x}s_{2y} + s_{1y}s_{2x} & s_{2x}s_{3y} + s_{2y}s_{3x} & s_{1x}s_{3y} + s_{1y}s_{3x} \\ s_{1y}s_{2z} + s_{1z}s_{2y} & s_{2y}s_{3z} + s_{2z}s_{3y} & s_{1y}s_{3z} + s_{1z}s_{3y} \\ s_{1x}s_{2z} + s_{1z}s_{2x} & s_{2x}s_{3z} + s_{2z}s_{3x} & s_{1x}s_{3z} + s_{1z}s_{3x} \end{bmatrix}
\end{aligned}
\tag{5.8}
$$

$\boldsymbol{s_1}$, $\boldsymbol{s_2}$, $\boldsymbol{s_3}$ are the unit vectors in the directions of the locals coordinate system of the bolt, see figure 5.3. The stresses in local directions $\bar{\boldsymbol{\sigma}}$ can be written as:

$$
\bar{\boldsymbol{\sigma}} = \boldsymbol{T_\sigma}\boldsymbol{\sigma} \tag{5.9}
$$

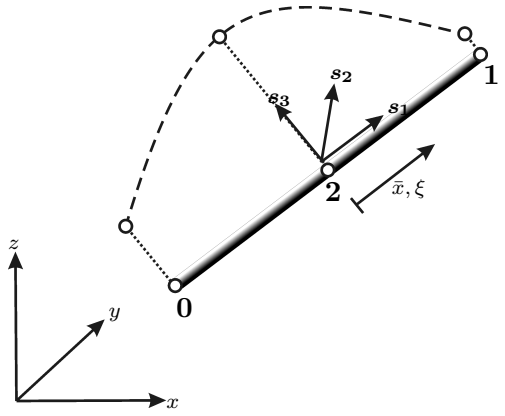

Figure 5.3: Local coordinate system of a bolt in 3D

Here we need only the axial stress $\sigma_{\bar{x}\bar{x}}$, which is the first entry in the vector $\bar{\boldsymbol{\sigma}}$. This can be described by introducing the vector $\boldsymbol{v}^T = [1\ 0\ 0\ 0\ 0\ 0]$; with this

the axial stress is given by:

$$\sigma_{\bar{x}\bar{x}} = \boldsymbol{v}^T \left(\boldsymbol{T}_{\boldsymbol{\sigma}} \boldsymbol{\sigma}\right) \tag{5.10}$$

Displacement Based Computation

After the displacements are computed at all points, they are transformed into the local coordinate systems of the cells:

$$u_{\bar{x}} = \boldsymbol{s_1}^T \boldsymbol{u} = s_{1x} u_x + s_{1y} u_y + s_{1z} u_z \tag{5.11}$$

where $\boldsymbol{s_1}$ is the unit vector in local bolt direction $\bar{x}$, see figure 5.3.

The strains in the cell are computed by using the derivatives of the displacements:

$$\varepsilon_{\bar{x}\bar{x}} = \frac{du_{\bar{x}}}{d\bar{x}} = \frac{du_{\bar{x}}}{d\xi}\frac{d\xi}{d\bar{x}} \tag{5.12}$$

where ξ is the local intrinsic coordinate of the line-cell. Additional, the interpolation over the nodal displacements and the definition of the Jacobian J are introduced:

$$u_{\bar{x}} = \sum_{n=1}^{N^c} \Phi_n u_{\bar{x}_n}; \qquad J = \frac{d\bar{x}}{d\xi} \tag{5.13}$$

For the three node line-cell we have $N^c = 3$, the interpolation functions are specified in equation 5.6. Substituting this into equation 5.12 it occurs:

$$\varepsilon_{\bar{x}\bar{x}} = \sum_{n=1}^{N^c} \frac{d\Phi_n}{d\xi}\frac{u_{\bar{x}_n}}{J} \tag{5.14}$$

The derivations of the interpolation functions (equation 5.6) can be easily obtained:

$$\begin{aligned} \frac{d\Phi_1}{d\xi} &= \xi - \frac{1}{2} \\ \frac{d\Phi_2}{d\xi} &= \xi + \frac{1}{2} \\ \frac{d\Phi_3}{d\xi} &= -2\xi \end{aligned} \tag{5.15}$$

At the end the stresses for the cell-nodes are obtained:

$$\begin{aligned} \sigma_{\bar{x}\bar{x}} &= E^{Rock}\varepsilon_{\bar{x}\bar{x}} - \sigma_{0\ \bar{x}\bar{x}} \\ &= E^{Rock}\sum_{n=1}^{N^c}\frac{d\Phi_n}{d\xi}\frac{u_{\bar{x}_n}}{J} - \sigma_{0\ \bar{x}\bar{x}} \end{aligned} \tag{5.16}$$

5.2.4 Computation of the Residuum

To compute the residuum $\boldsymbol{\Delta f}_j$ in the j-th iteration step, first residual initial stresses $\boldsymbol{\Delta\sigma_{0\ \bar{x}\bar{x}j}}$ in axial bolt direction $\bar{x}$ have to be found. If the residual initial stresses are calculated at all cell nodes, the residual vector $\boldsymbol{\Delta f}_j$ can be computed (see equation 2.43 and equation 2.46):

$$\boldsymbol{\Delta f}_j = \sum_{c=1}^{C}\int_{L_c}\hat{\boldsymbol{E}}\boldsymbol{\Delta\sigma_{0\ \bar{x}\bar{x}j}}d\bar{x} \tag{5.17}$$

where C is the number of line-cells and L^c is the length of the line-cell c.

The residual inital stresses for the iteration step j are calculated by using the axial stress results $\boldsymbol{\Delta\sigma_{\bar{x}\bar{x}j}}$ and the Hooke's law. The relation between axial stress in the bolt $\sigma^{Bolt}_{\bar{x}\bar{x}}$, the axial stress in the rock $\sigma^{Rock}_{\bar{x}\bar{x}}$ and the loading (the axial initial stresses $\sigma_{0\ \bar{x}\bar{x}}$) is shown in figure 5.4; see also:

$$\begin{aligned} \sigma^{Bolt}_{\bar{x}\bar{x}} &= \sigma_{\bar{x}\bar{x}} \\ \sigma^{Rock}_{\bar{x}\bar{x}} &= \sigma_{\bar{x}\bar{x}} + \sigma_{0\ \bar{x}\bar{x}} \end{aligned} \tag{5.18}$$

To achieve this relation, the residual initial stress is obtained in each iteration step j. Again we have two alternative ways for computing the residual stresses: In the first way the *incremental* results $\Delta\sigma_{\bar{x}\bar{x}_j}$ are used for computation and in the second way the *total* results $\sigma_{\bar{x}\bar{x}_j}$ are used. At the end both alternatives lead to the same solution.

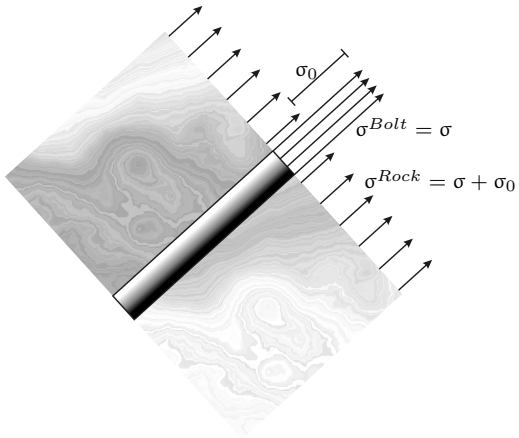

Figure 5.4: Schematic illustration of the stresses in the rock, in the bolt and the initial stresses ($\sigma^{Rock}_{\bar{x}\bar{x}}$, $\sigma^{Bolt}_{\bar{x}\bar{x}}$ and $\sigma_{0\,\bar{x}\bar{x}}$).

- *Incremental calculation:* The residual stress is calculated by the difference of the incremental rock stress and the incremental bolt stress:

$$\Delta\sigma_{0\,\bar{x}\bar{x}_j} = \Delta\sigma^{Rock^*}_{\bar{x}\bar{x}_j} - \Delta\sigma^{Bolt}_{\bar{x}\bar{x}_j} \tag{5.19}$$

  $\Delta\sigma^{Rock^*}_{\bar{x}\bar{x}_j}$ is the expected rock stress, calculated from the bolt stress and the relations of the Young's modulus.

$$\Delta\sigma^{Rock^*}_{\bar{x}\bar{x}_j} = \Delta\sigma_{\bar{x}\bar{x}_j}\frac{E^{Rock}}{E^{Bolt}} \tag{5.20}$$

  where E^{Rock} and E^{Bolt} are the Young's modulus of the rock and the bolt, respectively. At the end one obtains:

$$\Delta\sigma_{0\,\bar{x}\bar{x}_j} = \Delta\sigma_{\bar{x}\bar{x}_j}\left(\frac{E^{Rock}}{E^{Bolt}} - 1\right) \tag{5.21}$$

- *Total calculation:* The residual stress is calculated by the difference of the total calculated rock stress $\sigma^{Rock}_{\bar{x}\bar{x}_j}$ to the total expected rock stress $\sigma^{Rock^*}_{\bar{x}\bar{x}_j}$ (which is computed from the bolt stress):

$$\Delta\sigma_{0\,\bar{x}\bar{x}_j} = \sigma^{Rock^*}_{\bar{x}\bar{x}_j} - \sigma^{Rock}_{\bar{x}\bar{x}_j} \tag{5.22}$$

$\sigma^{Rock*}_{\bar{x}\bar{x}_j}$ is defined analogous to equation 5.20; with this we obtain:

$$\begin{aligned}\Delta\sigma_{0\ \bar{x}\bar{x}_j} =& \sigma^{Bolt}_{\bar{x}\bar{x}_j}\frac{E^{Rock}}{E^{Bolt}} - \sigma^{Rock}_{\bar{x}\bar{x}_j} \\ =& \sigma_{\bar{x}\bar{x}_j}\frac{E^{Rock}}{E^{Bolt}} - \left(\sigma_{\bar{x}\bar{x}_j} - \sigma_{0\ \bar{x}\bar{x}_j}\right)\end{aligned} \tag{5.23}$$

Yielding Bolts

The rock bolt behaviour depends on the behaviour of the steel bar and the connection of the bar to the surrounding rock mass. Here idealized constitutive laws for modelling both of these components are presented. The steel bar is assumed to behave linear elastic up to a defined yield-stress and then perfectly plastic. The yield stress in the bolt $\sigma^{Bolt\,Y}$ has to be defined and with this the residual initial stress can be checked and modified if necessary:

$$\begin{aligned}&\sigma^{Bolt}_{\bar{x}\bar{x}_{j+1}} = \sigma^{Bolt}_{\bar{x}\bar{x}_j} - \sigma_{0\ \bar{x}\bar{x}_j} \\ &\quad \text{if} \quad \sigma^{Bolt}_{\bar{x}\bar{x}_{j+1}} \leq \sigma^{Bolt\,Y} \quad \rightarrow \text{ ok} \\ &\quad \text{if} \quad \sigma^{Bolt}_{\bar{x}\bar{x}_{j+1}} > \sigma^{Bolt\,Y} \quad \rightarrow \Delta\sigma_{0\ \bar{x}\bar{x}_j} = \sigma^{Bolt}_{\bar{x}\bar{x}_j} - \sigma^{Bolt\,Y}\end{aligned} \tag{5.24}$$

If the yield stress in the bolt is reached, the residual initial stress $\sigma_{0\ \bar{x}\bar{x}_j}$ calculated before (in equation 5.19 or equation 5.22) is corrected, see also figure 5.5. In general the yield stress should be compared with the effective stress state (including not only the axial stresses). However, here in this work the yield criterion is strongly simplified (bending moments and shear forces are neglected).

Bond Slip

The connection between steel and rock mass consists of bar-grout interface, the grout itself and grout-rock interface. Several different failure modes can appear (failur of the rock mass, the steel bar, the grout, the bar-grout bond, the grout-rock bond or a combination of these). This problem can be described very detailed and thus also very complex; various publications can be found in

this area, see for example in Hyett et al. (1996), Chen et al. (2004), Benmokrane et al. (1995), Ivanovic and Neilson (2009), Marence (1992).

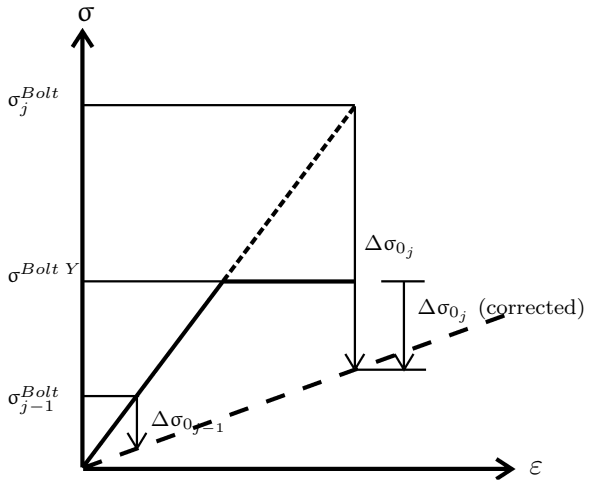

Figure 5.5: Computation of residual stresses by bolt-yielding

However, here a very simple model is used. The bond behaviour is modelled only by the shear stress in the grout which transfers stresses between the bar and the rock mass. Currently only a linear shear behaviour is implemented:

$$f = K\delta = K\left(u^{Rock} - u^{Bolt}\right) \tag{5.25}$$

where K is the bond-stiffness, f are the shear forces in the grout and $\delta = u^{Rock} - u^{Bolt}$ is the *slip* (the relative displacements between rock and bolt). To consider these bond slip effect, the initial stresses $\sigma_{0\,\bar{x}\bar{x}}$ have to be modified; this can be done by the following steps:

(i) Additional to the axial rock stresses and the axial bolt stresses (equation 5.18), the shear forces f are computed by the equilibrium condition, see figure 5.6:

$$f = \tau 2r^{Bolt}\pi = \frac{d\sigma_{\bar{x}\bar{x}}^{Bolt}}{d\bar{x}} r^{Bolt^2}\pi \tag{5.26}$$

r^{Bolt} is the radius of the bolt cross-section. The derivation of the bolt

stresses $\sigma^{Bolt}_{\bar{x}\bar{x}}$ can be done analogous to equation 5.14:

$$\frac{d\sigma^{Bolt}_{\bar{x}\bar{x}}}{d\bar{x}} = \sum_{n=1}^{N^c} \frac{d\Phi_n}{d\xi} \frac{\sigma^{Bolt}_{\bar{x}\bar{x}_n}}{J} \tag{5.27}$$

The derivatives of the interpolation functions Φ_n were shown in equation 5.15

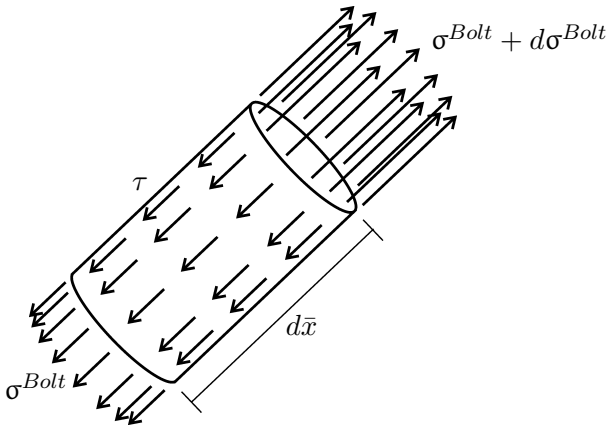

Figure 5.6: Equilibrium on a small part of the bolt

(ii) With equation 5.25 following relation can be obtained:

$$u^{Rock} = u^{Bolt} + \frac{f}{K} \tag{5.28}$$

(iii) In order to compute the residual stresses either in the *incremental* form (equation 5.19) or in *total* form (equation 5.22), the expected rock stress $\Delta\sigma^{Rock^*}_{\bar{x}\bar{x}_j}$ or $\sigma^{Rock^*}_{\bar{x}\bar{x}_j}$ has to be computed. This is done as follows:

$$\sigma^{Rock^*}_{\bar{x}\bar{x}} = E^{Rock}\varepsilon^{Rock}_{\bar{x}\bar{x}} = E^{Rock}\frac{du^{Rock}_{\bar{x}}}{d\bar{x}} \tag{5.29}$$

Substituting equation 5.28 into the above equation we obtain:

$$\sigma^{Rock^*}_{\bar{x}\bar{x}} = E^{Rock}\Bigg(\underbrace{\frac{du^{Bolt}_{\bar{x}}}{d\bar{x}}}_{=\varepsilon^{Bolt}_{\bar{x}\bar{x}}=\frac{\sigma^{Bolt}_{\bar{x}\bar{x}}}{E^{Bolt}}} + \frac{df}{d\bar{x}}\frac{1}{K}\Bigg) \tag{5.30}$$

This can be rewritten in the following form to compute the residual stress in iteration step j with equation 5.22:

$$\sigma_{\bar{x}\bar{x}_j}^{Rock^*} = \sigma_{\bar{x}\bar{x}_j}^{Bolt} \frac{E^{Rock}}{E^{Bolt}} + \frac{df_j}{d\bar{x}} \frac{E^{Rock}}{K} \tag{5.31}$$

And the same can be done for the incremental calculation of the residual stress in equation 5.19:

$$\Delta\sigma_{\bar{x}\bar{x}_j}^{Rock^*} = \Delta\sigma_{\bar{x}\bar{x}_j}^{Bolt} \frac{E^{Rock}}{E^{Bolt}} + \frac{d\Delta f_j}{d\bar{x}} \frac{E^{Rock}}{K} \tag{5.32}$$

5.2.5 Evaluation of the Integral

To solve the BIE (see equation 2.42) and to compute internal displacements or interanl stresses (equation 2.47 or equation 2.70) the body force therms $\boldsymbol{f}$ and $\boldsymbol{f^{\sigma}}$ have to be computed. These terms contain the integration over the cells. For computing rock bolts, the general integrations over the volume-cells V_c are reduced into one-dimensional integrals over the line-cell-length L_c:

$$\begin{aligned} \boldsymbol{\Delta f}_j &= \sum_{c=1}^{C} \int_{V_c} \boldsymbol{E} \boldsymbol{\Delta\sigma_0}_j dV \\ &\rightarrow \sum_{c=1}^{C} \int_{L_c} \hat{\boldsymbol{E}} \Delta\sigma_{0\,\bar{x}\bar{x}_j} d\bar{x} \end{aligned} \tag{5.33}$$

$$\begin{aligned} \boldsymbol{\Delta f^{\sigma}}_j &= \sum_{c=1}^{C} \int_{V_c} \boldsymbol{W^{\sigma}} \boldsymbol{\Delta\sigma_0}_j dV + \boldsymbol{F^{\sigma}} \boldsymbol{\Delta\sigma_0}_j \\ &\rightarrow \sum_{c=1}^{C} \int_{L_c} \hat{\boldsymbol{W}}^{\boldsymbol{\sigma}} \Delta\sigma_{0\,\bar{x}\bar{x}_j} d\bar{x} + \check{\boldsymbol{F}}^{\boldsymbol{\sigma}} \Delta\sigma_{0\,\bar{x}\bar{x}_j} \end{aligned} \tag{5.34}$$

Axial initial stresses $\sigma_{0\,\bar{x}\bar{x}}$ are applied as loading along the line-cells (local direction $\bar{x}$). $\boldsymbol{E}$ and $\boldsymbol{W^{\sigma}}$ are the Kelvin's fundamental solutions and $\boldsymbol{F^{\sigma}}$ is the free term, they are described in chapter 2. In order to reduce the general volume

integral into an one-dimensional integral, Kelvin's fundamental solutions have to be modified ($\hat{\boldsymbol{E}}$, $\hat{\boldsymbol{W}}^{\boldsymbol{\sigma}}$).

For this following assumptions are introduced: the variation of displacements and stresses is assumed to be constant over the cross-section of the inclusion; the inclusions are only able to carry axial stresses; bending is neglected; and the cross-section is assumed to be circular. With these assumptions, the bolt-inclusions degenerate so that they can be represented by line-cells along the centre line, see section 5.2.2.

Modified Fundamental Solutions

The computation of the modified fundamental solution $\hat{\boldsymbol{E}}$ is described by the following points:

(i) First of all the stresses are replaced by the sum over the interpolation functions times the nodal stresses. And all components are expressed in local coordinates $(\bar{x}, \bar{y}, \bar{z})$. This leads to locally expressed fundamental solution $\boldsymbol{E} \rightarrow \bar{\boldsymbol{E}}$, locally expressed initial stressex $\boldsymbol{\sigma_0} \rightarrow \bar{\boldsymbol{\sigma}}_{\mathbf{0}}$ and the local vector $\boldsymbol{f} \rightarrow \bar{\boldsymbol{f}}$:

$$\begin{aligned} \bar{\boldsymbol{f}} &= \sum_c \sum_n \int_{V_c} \bar{\boldsymbol{E}} \Phi_n \, dV \; \bar{\boldsymbol{\sigma}}_{0_n} \\ &= \sum_c \sum_n \int_{L_c} \int_{A_c} \bar{\boldsymbol{E}} \Phi_n \, dA \, d\bar{x} \; \sigma_{0\,\bar{x}\bar{x}_n} \end{aligned} \tag{5.35}$$

The integral over the cell volume V_c is divided into an integral over the cell length L_c and an integral over the cell cross-section area A_c. Since only axial stresses are taken into account the general initial stress $\bar{\boldsymbol{\sigma}}_{\mathbf{0}}$ is replaced by the axial initial stress $\sigma_{0\,\bar{x}\bar{x}}$ and only the first column of the matrix $\bar{\boldsymbol{E}}$ has to be computed:

$$\bar{\boldsymbol{E}} \sigma_{0\,\bar{x}\bar{x}} = \begin{bmatrix} E_{\bar{x}\bar{x}\bar{x}} \\ E_{\bar{y}\bar{x}\bar{x}} \\ E_{\bar{z}\bar{x}\bar{x}} \end{bmatrix} \Delta\sigma_{0\,\bar{x}\bar{x}_j} \tag{5.36}$$

(ii) Since the stresses are assumed to be constant over the cross-section, and the interpolation functions Φ_n are only depending on the cell length, one obtains:

$$\bar{\boldsymbol{f}} = \sum_c \sum_n \int_{L_c} \underbrace{\left(\int_{A_c} \bar{\boldsymbol{E}} \, dA \right)}_{\tilde{\boldsymbol{E}}} \Phi_n d\bar{x} \; \sigma_{0\,\bar{x}\bar{x}_n} \tag{5.37}$$

(iii) $\tilde{\boldsymbol{E}}$ is computed by integrating $\bar{\boldsymbol{E}}$ analytically over the predefined cross-section of the line-cell. After that, the term $\bar{\boldsymbol{f}}$ (which is in the local coordinate system) has to be transformed to the global one by multiplying it with the geometrical transformation matrix $\boldsymbol{T_g}$; it follows:

$$\boldsymbol{f} = \boldsymbol{T_g} \bar{\boldsymbol{f}} = \sum_c \sum_n \int_{L_c} \underbrace{(\boldsymbol{T_g} \tilde{\boldsymbol{E}})}_{\check{\boldsymbol{E}}} \Phi_n d\bar{x} \; \sigma_{0\,\bar{x}\bar{x}_n} \tag{5.38}$$

$\sigma_{0\,\bar{x}\bar{x}_n}$ can be taken out of the transformation, because it is a scalar value. Because of this $\boldsymbol{T_g}$ can be placed inside the integral, to obtain $\check{\boldsymbol{E}} = \boldsymbol{T_g} \tilde{\boldsymbol{E}}$. $\boldsymbol{T_g}$ is defined to be:

$$\boldsymbol{T_g} = [\boldsymbol{s_1} \; \boldsymbol{s_2} \; \boldsymbol{s_3}] = \begin{bmatrix} s_{1x} & s_{2x} & s_{3x} \\ s_{1y} & s_{2y} & s_{3y} \\ s_{1z} & s_{2z} & s_{3z} \end{bmatrix} \tag{5.39}$$

$\boldsymbol{s_1}$, $\boldsymbol{s_2}$, $\boldsymbol{s_3}$ are the unit vectors in the directions of the local coordinate system of the bolt, see figure 5.3.

(iv) With this, the modified fundamental solution $\check{\boldsymbol{E}}$ is obtained, and the general volume integral reduces to a 1D integral over the line-cell length:

$$\boldsymbol{f} = \sum_c \sum_n \int_{L_c} \check{\boldsymbol{E}} \, \Phi_n d\bar{x} \; \sigma_{0\bar{x}\bar{x}_n} \tag{5.40}$$

In a similar way, the body force term $\boldsymbol{f}^{\sigma}$ for the stress integral equation is calculated:

$$\boldsymbol{f}^{\sigma} = \sum_{c} \sum_{n} \int_{L_c} \check{\boldsymbol{W}}^{\sigma} \, \Phi_n d\bar{x} \, \sigma_{0\,\bar{x}\bar{x}_n} + \check{\boldsymbol{F}}^{\sigma} \Delta\sigma_{0\,\bar{x}\bar{x}_n} \tag{5.41}$$

As it was shown, for the calculation of $\check{\boldsymbol{E}}$ also here the modified fundamental solution is calculated starting from Kelvin's fundamental solution $\boldsymbol{W}^{\sigma}$, express it in local coordinate system $\bar{\boldsymbol{W}}^{\sigma}$, compute then $\tilde{\boldsymbol{W}}^{\sigma}$ and finally $\check{\boldsymbol{W}}^{\sigma}$.

$$\begin{aligned} \tilde{\boldsymbol{W}}^{\sigma} &= \int_{A_c} \bar{\boldsymbol{W}}^{\sigma} \, dA \\ \check{\boldsymbol{W}}^{\sigma} &= \boldsymbol{T}_{\boldsymbol{\sigma}} \tilde{\boldsymbol{W}}^{\sigma} \end{aligned} \tag{5.42}$$

The only difference is the transformation matrix for stresses $\boldsymbol{T}_{\boldsymbol{\sigma}}$ which has to be used here instead of geometrical transformation matrix $\boldsymbol{T}_{\boldsymbol{g}}$; $\boldsymbol{T}_{\boldsymbol{\sigma}}$ was defined in equation 5.7.

The free term $\boldsymbol{F}^{\sigma}$ is independent of a coordinate system, thus the modification is done by multiplying it with the transformation matrix for stresses $\boldsymbol{T}_{\boldsymbol{\sigma}}$:

$$\check{\boldsymbol{F}}^{\sigma} = \boldsymbol{T}_{\boldsymbol{\sigma}} \boldsymbol{F}^{\sigma} \tag{5.43}$$

The procedures for calculating $\check{\boldsymbol{E}}$ and $\check{\boldsymbol{W}}^{\sigma}$ are described in detail in Riederer et al. (2009).

Regular Integration

In the regular case, when the source point is not a node of the cell ($P \neq \bar{Q}$), the integrals in equation 5.33 and equation 5.34 can be evaluated numerically by using Gaussian quadrature, see also section 2.4.5.

For this, the line-cells are described in local (intrinsic) coordinates $-1 \leq \xi \leq 1$. The mapping from ξ to $\bar{x}$ involves the Jacobian $J = d\bar{x}/d\xi$. For straight rock bolts the Jacobian is constant over the cell length, i.e. $J = L_c/2$. The integrals

in equation 5.33 and equation 5.34 can be replaced by the sum over the number of Gauss-points M:

$$\begin{aligned} \boldsymbol{f} &= \sum_c \sum_n \int_{L_c} \left(\check{\boldsymbol{E}}\, \Phi_n \right) d\bar{x}\; \sigma_{0\,\bar{x}\bar{x}_n} \\ &= \sum_c \sum_n \sum_{i=1}^{M} \left(\check{\boldsymbol{E}}\, \Phi_n\left(\xi_i\right)\; w_i \right)\; J\sigma_{0\,\bar{x}\bar{x}_n} \end{aligned} \tag{5.44}$$

w_i is the weight corresponding to the i-th Gauss-point with the coordinate ξ_i.

Weakly Singular Integration

When the source point coincides with the cell node ($P = \bar{Q}$) a singularity occurs at the point when $r = 0$ (see figure 5.7), which makes Gaussian quadrature unsuitable, see also section 2.4.5. In this case the integral over the whole cell volume is evaluated analytically:

$$\boldsymbol{f} = \sum_c \sum_n \boldsymbol{T_g} \underbrace{\int_{V_c} \bar{\boldsymbol{E}}\, \Phi_n\, dV}_{\boldsymbol{\Delta \bar{E}}}\; \sigma_{0\,\bar{x}\bar{x}_n} \tag{5.45}$$

When the source point P is one of the cell nodes ($n = 1, 2, 3$), the distance $r = r_{\bar{x}}$ is defined by (see figure 5.7):

$$\begin{aligned} &\text{P at node } n = 0: \qquad r = \frac{L_c}{2} + \bar{x} \\ &\text{P at node } n = 1: \qquad r = \frac{L_c}{2} - \bar{x} \\ &\text{P at node } n = 2: \qquad r = \bar{x} \end{aligned} \tag{5.46}$$

The quadratic interpolation functions $\Phi_n\left(\bar{x}\right)$ in terms of $\bar{x}$ for the line-cell are

given by:

$$\begin{aligned}\Phi_0 &= \frac{2\bar{x}^2 - L_c\bar{x}}{L_c^2}\\ \Phi_1 &= \frac{2\bar{x}^2 + L_c\bar{x}}{L_c^2}\\ \Phi_2 &= \frac{(L_c - 2\bar{x})(L_c + 2\bar{x})}{L_c^2}\end{aligned} \tag{5.47}$$

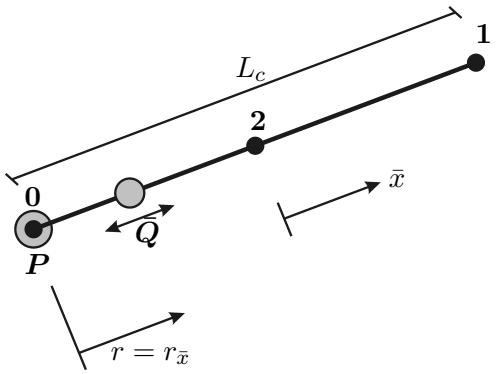

Figure 5.7: Singular integration over the line-cell

Using the interpolation functions equation 5.47 and substituting equation 5.46 to compute the coefficients of $\bar{\boldsymbol{E}}$, the integral $\boldsymbol{\Delta}\bar{\boldsymbol{E}}$ in equation 5.45 can be evaluated analytically. These are weakly singular integrals, they have a singularity of $\mathcal{O}(1/r)$ for 2D or $\mathcal{O}(1/r^2)$ for 3D (see also section 2.5.1). The analytical integration can be done without any difficulties:

$$\begin{aligned}\boldsymbol{\Delta}\bar{\boldsymbol{E}} = \int_{V_c} \bar{\boldsymbol{E}}\,\Phi_n(Q)\;dV &= \int_{V_c} \bar{\boldsymbol{E}}^{\boldsymbol{Rest}}(P,\varphi)\,s(r)\;\Phi_n(Q)\;dV\\ &= \int_{V_c - V_{Ball}} \bar{\boldsymbol{E}}^{\boldsymbol{Rest}}(P,\varphi)\,s(r)\;\Phi_n(Q)\;dV\\ &+ \int_{V_{Ball}} \bar{\boldsymbol{E}}^{\boldsymbol{Rest}}(P,\varphi)\,s(r)\;\Phi_n(Q)\;dV\end{aligned} \tag{5.48}$$

$\bar{\boldsymbol{E}}^{\boldsymbol{Rest}}(P,\varphi)$ is the regular part of $\bar{\boldsymbol{E}}$ without singularity and $s(r)$ contains the singularity ($s(r)=\frac{1}{r}$ for 2D and $s(r)=\frac{1}{r^2}$ for 3D). V_{Ball} is the volume of a circle in 2D or a sphere in 3D centred at the singular point P. The integral over $V_c - V_{Ball}$ in equation 5.48 is regular and the singularity in the other integral (over V_{Ball}) can be easily cancelled out by introducing cylindrical or polar coordinates for 2D or 3D, respectively. For a singularity at node $n=2$ for example, the second integral of equation 5.48 is:

$$\int_{r=0}^{R_c}\int_{\varphi=0}^{2\pi}\left(\frac{\bar{\boldsymbol{E}}^{\boldsymbol{Rest}}(P,\varphi)}{r}\left[\Phi_2(Q)-1\right]\,r\right)d\varphi dr \qquad \text{... 2D} \tag{5.49}$$

$$\int_{\varphi=0}^{2\pi}\int_{\psi=0}^{\frac{\pi}{2}}\int_{r=0}^{R_c}\left(\frac{\bar{\boldsymbol{E}}^{\boldsymbol{Rest}}(P,\varphi)}{r^2}\left[\Phi_2(Q)-1\right]\,r^2\sin\psi\right)dr d\psi d\varphi \qquad \text{... 3D} \tag{5.50}$$

where R_c is the radius of the ball (which is here defined to be the same as the radius of the bolt).

Strongly Singular Integration

The term $\boldsymbol{f}^{\boldsymbol{\sigma}}$ for the stress integral equation has to be evaluated as well. Also here the interpolation functions equation 5.47 are used and equation 5.46 is substituted to compute the coefficients of $\bar{\boldsymbol{W}}^{\boldsymbol{\sigma}}$.

The 2D integral has the order $\mathcal{O}(1/r^2)$ and the 3D integral has the order $\mathcal{O}(1/r^3)$, which are both strong singularities, see section 2.5.2. But, the integrals exist as *Cauchy Principal Value* and thus can be evaluated analytically, see for example Paris and Canas (1997), Gaul et al. (2003), Gakkov (1966), Mikhilin and Prössdorf (1987). The kernel $\bar{\boldsymbol{W}}^{\boldsymbol{\sigma}}$ is subdivided into the singular part $s(r)$ (which is $s(r)=\frac{1}{r^2}$ for 2D and $s(r)=\frac{1}{r^3}$ for 3D) and in the rest, the so called *characteristic* $\bar{\boldsymbol{W}}^{\boldsymbol{Rest}}(P,\bar{\varphi})$.

$$\Delta\bar{\boldsymbol{W}}^{\boldsymbol{\sigma}} = \int_{V_c}\bar{\boldsymbol{W}}^{\boldsymbol{\sigma}}\,\Phi_n(Q)\,dV = \int_{V_c}\bar{\boldsymbol{W}}^{\boldsymbol{Rest}}(P,\varphi)\,s(r)\,\Phi_n(Q)\,dV \tag{5.51}$$

For mathematical describtion the interpolation function $\Phi_n(Q)$ is called here *density*. With this the following equation is obtained:

$$\begin{aligned}\boldsymbol{\Delta\bar{W}^{\sigma}} = &\int\limits_{V_c - V_{Ball}} \boldsymbol{\bar{W}^{Rest}}(P,\varphi)\, s(r)\ \Phi_n(Q)\ dV \\ &+ \int\limits_{V_{Ball}} \boldsymbol{\bar{W}^{Rest}}(P,\varphi)\, s(r)\ [\Phi_n(Q) - \Phi_n(P)]\ dV \\ &+ \Phi_n(P) \int\limits_{V_{Ball}} \boldsymbol{\bar{W}^{Rest}}(P,\varphi)\, s(r)\ dV\end{aligned} \tag{5.52}$$

The singularity arises only for that interpolation function which is equal to 1 at the singular point P ($\Phi_n(P) = 1$). Thus, $\Phi_n(P)$ can be taken outside of the last integral, because it is not a depending on $dV(Q)$. Equation 5.52 can be solved now: the first integral is a regular integral; the second integral exists and is an improper (weak singular) integral if the Hölder condition is satisfied:

$$|\Phi_n(Q) - \Phi_n(P)| \leq A r^{\alpha} \quad \text{with } A > 0 \quad \text{and } 0 < \alpha \leq 1 \tag{5.53}$$

and the last integral in equation 5.52 exists if

$$\int\limits_0^{2\pi} \boldsymbol{\bar{W}^{Rest}}(P,\varphi)\ d\varphi = 0 \tag{5.54}$$

Thus the only singular integral which has to be solved is the second one. It is assumed that the radius of V_{Ball} is the same as the bolt radius (respectively the line-cell radius R_c); wiht this we obtain for example if the singularity is located at node $n = 2$:

$$\int\limits_{r=0}^{R_c} \int\limits_{\varphi=0}^{2\pi} \left(\frac{\boldsymbol{\bar{W}^{Rest}}(P,\varphi)}{r^2}\ [\Phi_2(Q) - 1]\ r \right) d\varphi dr \quad \ldots \text{ 2D} \tag{5.55}$$

$$\int_{\varphi=0}^{2\pi}\int_{\psi=0}^{\frac{\pi}{2}}\int_{r=0}^{R_c}\left(\frac{\bar{\boldsymbol{W}}^{\boldsymbol{Rest}}(P,\varphi)}{r^3}\left[\Phi_2(Q)-1\right]r^2\sin\psi\right)drd\psi d\varphi \quad \ldots \text{ 3D} \qquad (5.56)$$

For 2D cylindrical coordinates (r, φ) and for 3D polar coordinates (r, ψ, φ) have been introduced.

The computation of equation 5.52 as described before is applicable only for points inside the bolt, not for points at the bolt-ends. Here it is assumed that on the ends of the bolt the initial stresses are zero $\sigma_{0\,\bar{x}\bar{x}} = 0$, see figure 5.8. With this assumption the singularity problem at the ends of the bolt is avoided. As well, this assumption seems to be more realistic for real problems, because the bolt stresses at the bolt-ends can not be higher than the rock stresses at this point ($\sigma^{Bolt}_{\bar{x}\bar{x}} = \sigma^{Rock}_{\bar{x}\bar{x}}$) to satisfy the equilibrium condition.

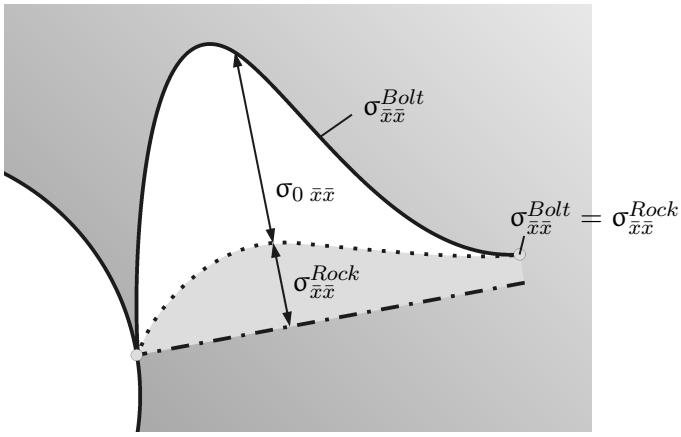

Figure 5.8: Schematic representation of a bolt and it's stress distribution

5.3 Verification Examples

To verify the previously described method to model continuous anchored bolts; some examples have been carried out and compared with the existing finite element program BEFE. Both, 2D (plain strain) and 3D examples have been tested and at the end the effect of yielding bolts and of bond slip effects will be shown.

5.3.1 Example 1: Fully grouted rock bolt in plane strain

In this example a block with a fully grouted bolt in plane strain conditions is presented. The dimensions of the block are $10m \times 10m$, the Young's modulus is $E = 1000MN/m^2$ and the Poisson's ratio is $\nu = 0.3$. The rock bolt has a length of $5m$ and the Young's modulus of the bolt is $E = 10000MN/m^2$, the cross section is $A = 0.05m^2$. The block is fixed at the bottom and on the top of the block is a constant tension $t = 1MN/m^2$ is applied as loading. The results are compared with reference solutions done by the FEM and show very good agreement, see figure 5.9.

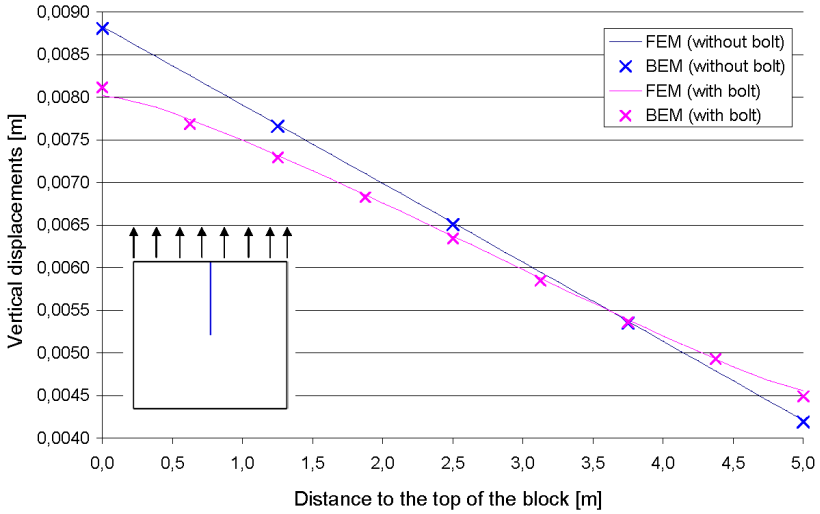

Figure 5.9: Example 1: vertical displacements along the bolt

5.3.2 Example 2: Fully grouted rock bolt in 3D

This example shows a 3D block with a fully grouted bolt. The dimensions of the block are $10m \times 10m \times 10m$, the Young's modulus is $E = 1000MN/m^2$ and the Poisson's ratio is $\nu = 0.3$. The rock bolt has a length of $5m$ a Young's modulus of $E = 10000MN/m^2$ and the cross section is $A = 0.05m^2$. The block is fixed at the bottom and on the top of the block is a constant tension $t = 1MN/m^2$. The results are compared with FE reference solutions and show good agreement, see figure 5.10.

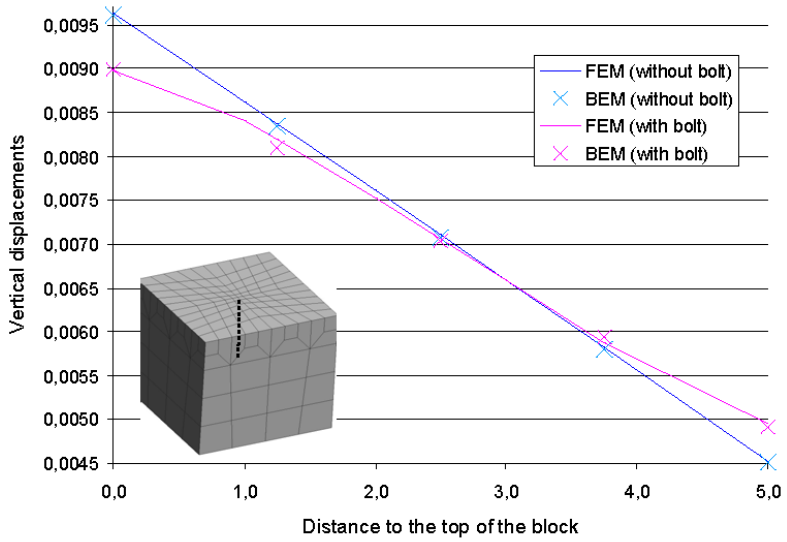

Figure 5.10: Example 2: vertical displacements along the bolt

5.3.3 Example 3: Bond Slip Effects

An other example has been calculated, to show the effect of the bond slip effects. The geometry is the same as presented in example 1, the Young's modulus is $E = 2000MN/m^2$ and the Poisson's ratio is $\nu = 0.3$. The rock bolt has a cross section is $A = 0.002m^2$ and a Young's modulus of $E = 200000MN/m^2$. The block is fixed at the bottom and on the top a constant tension $t = 10MN/m^2$ is applied.

Various calculations with different bond stiffnesses have been carried out (a rigid bond and $K = 2000; 200; 20 MN/m^2$). The relative displacements, the bolt stresses and the frictional forces are presented in figure 5.11.

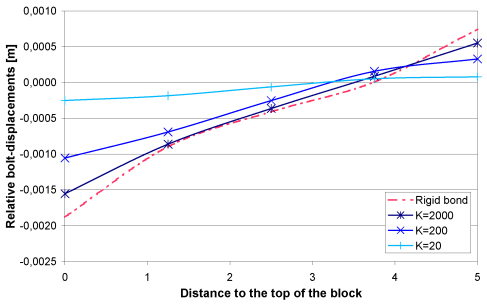

(a) Relative displacements along the bolt

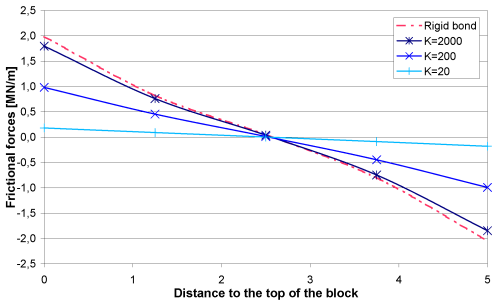

(b) Frictional forces in the bond

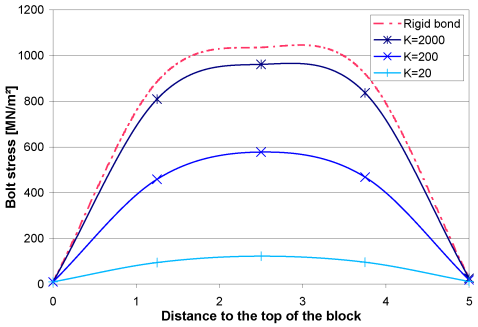

(c) Stresses in the bolt

Figure 5.11: Example 3: effects of variational bond stiffness's

5.3.4 Example 4: Yielding Bolt

Finally, the results of calculations considering yielding bolts are presented. The same configurations as for example 3 are used. Three variational calculations are carried out, one without the yielding of the bolt, one with a bolt yield stress of $\sigma^Y = 900 MN/m^2$ and one with a yield stress of $\sigma^Y = 600 MN/m^2$. The relative displacements and the bolt stresses of all three calculations are shown in figure 5.12.

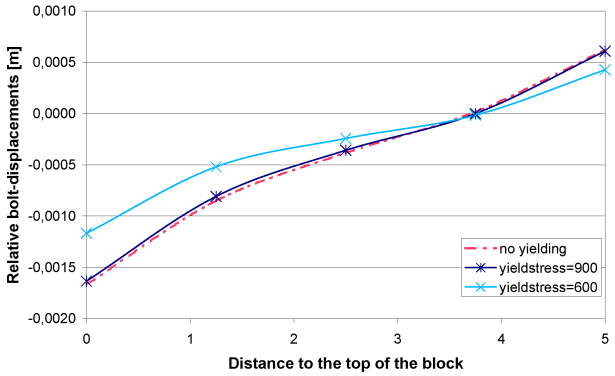

(a) Relative displacements along the bolt

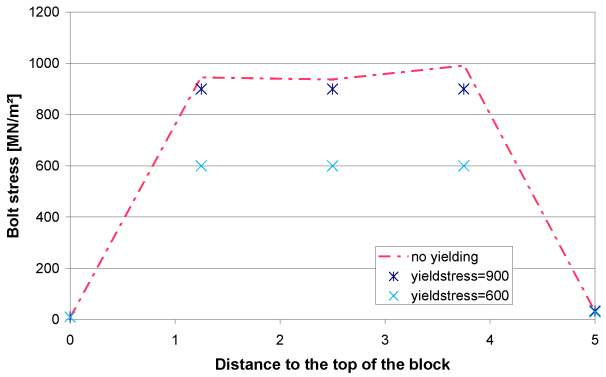

(b) Stresses in the bolt

Figure 5.12: Example 4: effects of variational bolt yield stress

Chapter 6

Discrete Anchored Bolts

6.1 General

Technique

Discrete anchored (or end-anchored) bolts generally consist of plain steel rods with a mechanical anchor at one end and a face plate and nut at the other, see Hoek et al. (1997). They are always tensioned after installation. For short term applications the bolts are generally left ungrouted. For more permanent applications or in rock in which corrosive ground water is present, the space between the bolts and the rock can be filled with cement or resin grout. Figure 6.1 shows different types of typical discrete anchored rock bolts.

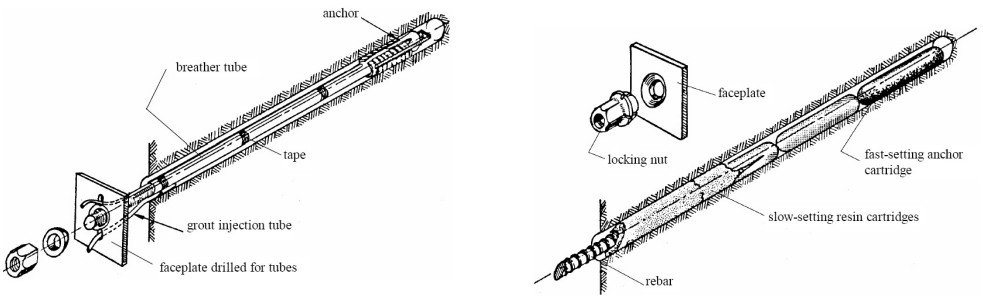

(a) Mechanical anchored rock bolt (b) Resin anchored rock bolt

Figure 6.1: Different types of discrete anchored bolts (see Hoek et al. 1997)

Numerical Simulation

Also for the discrete anchored bolts the system is solved within the iterative procedure.

For simulating this kind of bolts it is assumed that the load transfer between bolt and rock is only at the bonded ends and in between no stresses are assigned to the ground. As in the last section, we assume that the bolts have a constant and circular cross-section and that they carry only axial stresses. They are modelled by a simple *pair of points*.

6.2 BE-approach

To simulate discrete anchored bolts with the BEM, the general procedure described in section 3.2.2 is used. For this the following configurations are specified:

- Instead of cells, just a pair of points is necessary to discretise these kind of bolts, see section 6.2.2.
- Concentrated forces $\boldsymbol{F_{0\,\bar{x}}}$ in axial direction of the bolt are applied to these points.
- Strains in axial bolt direction and bolt forces ($\boldsymbol{\varepsilon_{\bar{x}\bar{x}}}$ and $\boldsymbol{F_{\bar{x}}^{Bolt}}$) are used for computation, see section 6.2.3.
- The residual-vector is computed as described in section 6.2.4.

6.2.1 Iterative Procedure

The procedure starts with an initial homogeneous elastic calculation:

$$\boldsymbol{A}\,\boldsymbol{\Delta x}_{j=0} = \boldsymbol{b} \tag{6.1}$$

After that the strains in axial bolt direction $\boldsymbol{\Delta\varepsilon_{\bar{x}\bar{x}}}_j$ and the bolt forces $\boldsymbol{\Delta F_{\bar{x}}^{Bolt}}_j$ are calculated at all points. The total boundary results, axial strains and the bolt forces are initialised:

$$\begin{aligned} \boldsymbol{x}_{j=0} &= \boldsymbol{\Delta x}_{j=0} \\ \boldsymbol{\varepsilon_{\bar{x}\bar{x}}}_{j=0} &= \boldsymbol{\Delta\varepsilon_{\bar{x}\bar{x}}}_{j=0} \\ \boldsymbol{F_{\bar{x}}^{Bolt}}_{j=0} &= \boldsymbol{\Delta F_{\bar{x}}^{Bolt}}_{j=0} \end{aligned} \tag{6.2}$$

Then the iteration starts and following steps have to be done:

(i) The index for the iteration step is incremented $j = j + 1$.

(ii) The residual vector $\boldsymbol{\Delta f}_j$ is calculated, see section 6.2.4.

(iii) The convergence is checked by comparing the vector-norm of the residuum $\| \boldsymbol{\Delta f}_j \|$ with a given tolerance:

$$\| \boldsymbol{\Delta f}_j \| \leq \ tol \tag{6.3}$$

Where $tol = \| \boldsymbol{\Delta f}_1 \| \epsilon$ is a percentage of the fist residuum. The iteration procedure ends here if the convergence criterion is fulfilled, otherwise it continues with the next step (iv).

(iv) The residual vector is applied to the system of equations as new *right hand side*:

$$\boldsymbol{A}\, \boldsymbol{\Delta x}_j = \boldsymbol{\Delta f}_j \tag{6.4}$$

(v) The axial strain results $\boldsymbol{\Delta \varepsilon}_{\bar{\boldsymbol{x}}\bar{\boldsymbol{x}}j}$ and the bolt forces $\boldsymbol{\Delta F}^{\boldsymbol{Bolt}}_{\bar{\boldsymbol{x}}\ j}$ are calculated at all pair of points.

(vi) The boundary results, the strain results and the bolt forces are updated:

$$\begin{aligned} \boldsymbol{x}_j &= \boldsymbol{x}_{j-1} + \boldsymbol{\Delta x}_j \\ \boldsymbol{\varepsilon}_{\bar{\boldsymbol{x}}\bar{\boldsymbol{x}}j} &= \boldsymbol{\varepsilon}_{\bar{\boldsymbol{x}}\bar{\boldsymbol{x}}j-1} + \boldsymbol{\Delta \varepsilon}_{\bar{\boldsymbol{x}}\bar{\boldsymbol{x}}j} \\ \boldsymbol{F}^{\boldsymbol{Bolt}}_{\bar{\boldsymbol{x}}\ j} &= \boldsymbol{F}^{\boldsymbol{Bolt}}_{\bar{\boldsymbol{x}}\ j-1} + \boldsymbol{\Delta F}^{\boldsymbol{Bolt}}_{\bar{\boldsymbol{x}}\ j} \end{aligned} \tag{6.5}$$

(vii) The iteration procedure continues with step (i).

6.2.2 Pair of Points

Here the bolts are just modelled by a pair of points (see figure 6.2), no cells with interpolation functions are needed for this kind of problem. These two points belonging together and the axial stress or axial strain in between is constant.

The pair of points is placed at the bolts beginning and end. In order to model the anchored end of a bolt in more detail, a number of linked point pairs can be used, see for example figure 6.3.

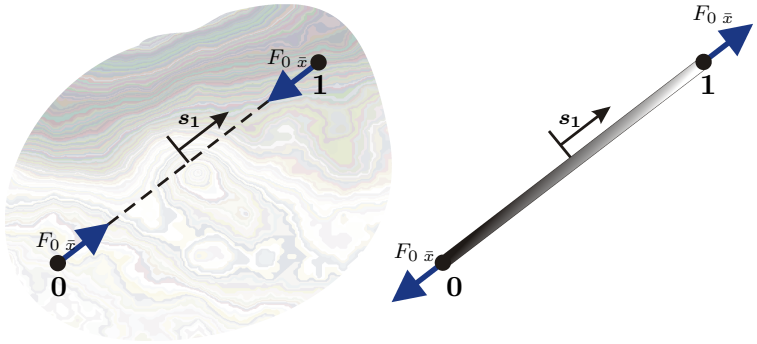

Figure 6.2: Pair of points to model discrete anchored bolts

The simplifications which are introduced for modelling the bolt by pairs of points are: the bolts are sufficiently thin so that their bending stiffness can be neglected; the cross-section is circular and constant over the length. The load transfer between bolt and rock takes place only at the bonded ends and in between no stresses are assigned to the ground. Concentrated forces $\boldsymbol{F_{0\,\bar{x}}}$ in axial direction of the bolt are applied as loading on these points to simulate the effect of the bolts inside the rock mass.

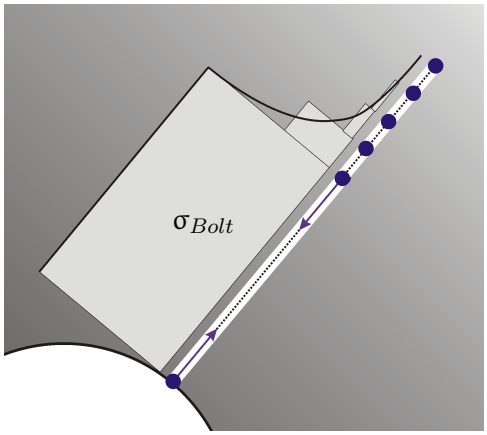

Figure 6.3: Modelling of the bonded end of an anchor

6.2.3 Computation of Bolt Strains and Bolt Forces

Bolt forces $\boldsymbol{F}_{\bar{\boldsymbol{x}}}^{\boldsymbol{Bolt}}$ are needed for the computation of the residuum in the iterative procedure (section 6.2.1). For this first the axial strains in bolt direction $\boldsymbol{\varepsilon}_{\bar{\boldsymbol{x}}\bar{\boldsymbol{x}}}$ are computed. Since the bolts are loaded only at ends and in between no load transfer between bolt and rock is admitted, the strain and the force in the bolt is constant between one pair of points. Because of this, we can directly use the relative displacements between the pair of points to calculate the axial strain in the bolt.

The displacements at the internal points are calculated by using the integral equation for displacements, whereas the boundary displacements are already achieved from the BIE. After the displacements are obtained at all point pairs, they have to be transformed into the local coordinate systems in direction of the bolt:

$$u_{\bar{x}} = \boldsymbol{s_1}^T \boldsymbol{u} = s_{1x}u_x + s_{1y}u_y + s_{1z}u_z \tag{6.6}$$

where $\boldsymbol{s_1}$ is the unit vector in local bolt direction $\bar{x}$, see figure 6.2.

With this the relative displacement ΔL_{pp} between one pair of points is obtained and the constant axial strain between both points is:

$$\varepsilon_{\bar{x}\bar{x}} = \frac{\Delta L_{pp}}{L_{pp}} \tag{6.7}$$

where L_{pp} is the length between the pair of points.

After the strain is known the bolt force $F_{\bar{x}}^{Bolt}$ can be calculated. The relation between axial forces in the bolt $F_{\bar{x}}^{Bolt}$, the axial forces in the rock $F_{\bar{x}}^{Rock}$, the axial strains $\varepsilon_{\bar{x}\bar{x}}$ and the loading $(F_{0\,\bar{x}})$ is:

$$\begin{aligned} F_{\bar{x}}^{Rock} &= \varepsilon_{\bar{x}\bar{x}} A^{Bolt} E^{Rock} \\ F_{\bar{x}}^{Bolt} &= \varepsilon_{\bar{x}\bar{x}} E^{Rock} A^{Bolt} - F_{0\,\bar{x}} \end{aligned} \tag{6.8}$$

where E^{Rock} and E^{Bolt} are the Young's modulus of the rock mass and the bolt, respectively; A^{Bolt} is the cross-section of the bolt; and $F_{0\,\bar{x}}$ is the concentrated

force applied at both points in opposing direction.

6.2.4 Computation of the Residuum

First residual forces in axial bolt direction $\boldsymbol{\Delta F_{0\,\bar{x}j}}$ have to be found. If these residual forces are calculated at all points, the residual vector $\boldsymbol{\Delta f}_j$ can be computed; this means just a multiplication of the fundamental solution with the concentrated force applied at a point p, no integration is needed for this problem, see also equation 2.45:

$$\boldsymbol{\Delta f}_j = \sum_{p=1}^{P} \hat{\boldsymbol{U}} \boldsymbol{\Delta F}_{\boldsymbol{0}\,\bar{\boldsymbol{x}}j}^{\boldsymbol{p}} \tag{6.9}$$

where P is the number of concentrated forces applied at points.

The relations between bolt force, rock force and strain of equation 6.8 is rewritten here:

$$F_{\bar{x}}^{Bolt} = \varepsilon_{\bar{x}\bar{x}} E^{Rock} A^{Bolt} - F_{0\,\bar{x}} \tag{6.10}$$

It can be stated, that at the end when the system is converged, following relation has to be fulfilled:

$$F_{\bar{x}}^{Bolt} = \varepsilon_{\bar{x}\bar{x}} E^{Rock} A^{Bolt} - F_{0\,\bar{x}} = \varepsilon_{\bar{x}\bar{x}} E^{Bolt} A^{Bolt} \tag{6.11}$$

To achieve these relations, the force $F_{0\,\bar{x}}$ is calculated iteratively. In each iteration step j the incremental residual force $\Delta F_{0\,\bar{x}_j}$ has to be computed.

The residual forces $\Delta F_{0\,\bar{x}_j}$ are calculated by the difference of the incremental rock force and the incremental bolt force:

$$\Delta F_{0\,\bar{x}_j} = \Delta F_{\bar{x}_j}^{Rock^*} - \Delta F_{\bar{x}_j}^{Bolt} \tag{6.12}$$

$\Delta F_{\bar{x}_j}^{Rock^*}$ is the expected rock force, calculated from the bolt force and the

relations of the Young's modulus.

$$\Delta F_{\bar{x}_j}^{Rock^*} = \Delta F_{\bar{x}_j}^{Bolt} \frac{E^{Rock}}{E^{Bolt}} \tag{6.13}$$

At the end one obtains:

$$\Delta F_{0\,\bar{x}_j} = \Delta F_{\bar{x}_j}^{Bolt} \left(\frac{E^{Rock}}{E^{Bolt}} - 1 \right) \tag{6.14}$$

where $\Delta F_{\bar{x}_j}^{Bolt}$ is achieved form equation 6.10.

This procedure is used for discrete anchored bolts without a pre-stressing, however in most cases pre-stressed discrete anchored bolts are used in practise. This will be described in the following.

Pre-stressed Bolts

The pre-stressing of the bolt can be defined in two ways:

- A specified pre-stress load is applied to the bolt; however, after setting equilibrium less stress is left over in the bolt because of some deformations due to the loading.
- The finally remaining stress in the bolt is defined; for this a higher pre-stressing has to be applied to achieve finally the specified bolt stress (after setting the equilibrium). In praxis this method is generally used: The bolt is installed and pre-stressing is applied as long as the bolt has the pre-defined stress.

In the first method we start with the initial analysis as described in section 6.2.1, but in addition the specified pre-stress load (which gives the vector $\boldsymbol{\Delta f}_{j=0}$) is applied to this initial system:

$$\boldsymbol{A}\,\boldsymbol{\Delta x}_{j=0} = \boldsymbol{b} + \boldsymbol{\Delta f}_{j=0} \tag{6.15}$$

After the initial analysis has been calculated and the bolt forces are computed and initialised (see equation 6.2) the incremental bolt force has to be corrected

for starting the iterative procedure:

$$\Delta F^{Bolt}_{\bar{x}_{j=0}} = \Delta F^{Bolt}_{\bar{x}_{j=0}} + \Delta F_{0\,\bar{x}_{j=0}} \tag{6.16}$$

$\Delta F_{0\,\bar{x}_{j=0}}$ is the applied pre-stress force. This is the only difference for the calculation considering pre-stressing. After that the procedure and the computation of the residual forces in the next iteration steps $\Delta F_{0\,\bar{x}_j}$ is exactly the same as described above for bolts without pre-stressing (equation 6.14). The residual forces in the further iteration steps are computed from the incremental bolt forces $\Delta F^{Bolt}_{\bar{x}_j}$ (see equation 6.14) and the initial pre-stressing is included in the total bolt forces $F^{Bolt}_{\bar{x}_j}$ from beginning.

In the second method again we start with the initial analysis and apply the specified pre-stress loads in addition, see equation 6.15. After that the axial strains $\boldsymbol{\Delta\varepsilon}_{\bar{\boldsymbol{x}}\bar{\boldsymbol{x}}j=0}$ and bolt forces $\boldsymbol{\Delta F}^{\boldsymbol{Bolt}}_{\bar{\boldsymbol{x}}\,j=0}$ are computed. And the total bolt forces are initialised:

$$F^{Bolt}_{\bar{x}_{j=0}} = \Delta F_{0\,\bar{x}_{j=0}} \tag{6.17}$$

The bolt force is assigned to be exactly this predefined force. During the iteration the bolt forces do not change, the residual forces are computed during the iteration by using the total results:

$$\Delta F_{0\,\bar{x}_j} = F^{Bolt^*}_{\bar{x}_j} - F^{Bolt}_{\bar{x}_{j=0}} \tag{6.18}$$

where $F^{Bolt^*}_{\bar{x}_j}$ is the actual acting bolt force and $F^{Bolt}_{\bar{x}_{j=0}}$ is the predefined bolt force, which should remain finally. The actual bolt force in the j-th iteration step is:

$$F^{Bolt^*}_{\bar{x}_j} = \varepsilon_{\bar{x}\bar{x}_j} E^{Rock} A^{Bolt} - F_{0\,\bar{x}_j} \tag{6.19}$$

Yielding Bolts

The effect of bolt-yielding can be easily considered, in the same way as described in section 5.2.4 for continuous anchored bolts. A linear elastic and perfectly plastic steel behaviour is assumed. The yield stress in the bolt $\sigma^{Bolt\,Y}$ has to

be defined. And with this the residual force can be checked and modified if necessary. If the yield stress in the bolt is reached, the residual force $F_{0\,\bar{x}}$ has to be corrected.

$$\begin{aligned} &\text{if} \quad \frac{F^{Bolt}_{\bar{x}_j}}{A^{Bolt}} \leq \sigma^{Bolt\,Y} \qquad \rightarrow \text{ok} \\ &\text{if} \quad \frac{F^{Bolt}_{\bar{x}_j}}{A^{Bolt}} > \sigma^{Bolt\,Y} \qquad \rightarrow \; \Delta F_{0\,\bar{x}_j} = F^{Bolt}_{\bar{x}_j} - \sigma^{Bolt\,Y} A^{Bolt} \end{aligned} \tag{6.20}$$

6.2.5 Evaluation of the body force terms

To solve the BIE (equation 2.42) and to compute internal displacements or internal stresses (equation 2.47 or equation 2.70) the body force vectors $\boldsymbol{f}$ and $\boldsymbol{f^{\sigma}}$ have to be computed. These terms consist only a product of the fundamental solution and the concentrated force, as described before, no integration has to be carried out.

$$\boldsymbol{\Delta f}_j = \sum_{p=1}^{P} \hat{\boldsymbol{U}} \Delta F^{p}_{0\,\bar{x}_j} \tag{6.21}$$

$$\boldsymbol{\Delta f^{\sigma}}_j = \sum_{p=1}^{P} \hat{\boldsymbol{D}}^{\boldsymbol{\sigma}} \Delta F^{p}_{0\,\bar{x}_j} \tag{6.22}$$

Concentrated forces in axial directions $F_{0\,\bar{x}}$ are applied as loading on the points p. $\boldsymbol{U}$ and $\boldsymbol{D^{\sigma}}$ are the common Kelvin's fundamental solutions described in chapter 2. To compute the global vectors $\boldsymbol{\Delta f}_j$ and $\boldsymbol{\Delta f^{\sigma}}_j$ eigther the concentrated forces $F_{0\,\bar{x}}$ have to be transformed back into the global coordinate system or Kelvin's fundamental solutions have to be transformed. In order to use the scalar value $F_{0\,\bar{x}}$ in local coordinate direction $\bar{x}$, here Kelvin's fundamental solutions are transformed ($\hat{\boldsymbol{U}}$, $\hat{\boldsymbol{D}}^{\boldsymbol{\sigma}}$).

Modified Fundamental Solutions

The computation of the modified fundamental solution $\hat{\boldsymbol{U}}$ is described by the following points:

(i) First of all, all components are expressed in local coordinates $(\bar{x}, \bar{y}, \bar{z})$. This leads to a locally expressed fundamental solution $\boldsymbol{U} \rightarrow \bar{\boldsymbol{U}}$ and the locally expressed vector $\boldsymbol{f} \rightarrow \bar{\boldsymbol{f}}$:

$$\bar{\boldsymbol{f}} = \sum_{p=1}^{P} \bar{\boldsymbol{U}} \Delta F_{0\,\bar{x}_j} \tag{6.23}$$

Since only the axial force $F_{0\,\bar{x}}$ is taken into account, only the first column of the matrix $\bar{\boldsymbol{U}}$ has to be computed and the problem is reduces to:

$$\bar{\boldsymbol{U}} \Delta F_{0\,\bar{x}_j} = \begin{bmatrix} U_{\bar{x}\bar{x}} \\ U_{\bar{y}\bar{x}} \\ U_{\bar{z}\bar{x}} \end{bmatrix} \Delta F_{0\,\bar{x}_j} \tag{6.24}$$

(ii) After that vector $\bar{\boldsymbol{f}}$ has to be transformed to the global coordinate system. This can be done by multiplying it with the geometrical transformation matrix $\boldsymbol{T_g}$ (see equation 5.39); it follows:

$$\boldsymbol{f} = \boldsymbol{T_g} \bar{\boldsymbol{f}} = \sum_{p} \underbrace{(\boldsymbol{T_g} \bar{\boldsymbol{U}})}_{\hat{\boldsymbol{U}}} F_{0\,\bar{x}} \tag{6.25}$$

$F_{0\,\bar{x}}$ can be taken out of the transformation, because it is a scalar value. With this, the modified fundamental solution $\hat{\boldsymbol{U}}$ has been obtained.

In a similar way, the vector $\boldsymbol{f^{\sigma}}$ for the stress integral equation is calculated. First the terms of Kelvin's fundamental solution are expressed in local coordinates $\boldsymbol{D^{\sigma}} \rightarrow \bar{\boldsymbol{D}}^{\boldsymbol{\sigma}}$. Also here only the first column of the matrix $\bar{\boldsymbol{D}}^{\boldsymbol{\sigma}}$ has to be computed, since only axial forces $F_{0\,\bar{x}}$ are taken into account. After that the modified fundamental solution is obtained by multiplying $\bar{\boldsymbol{D}}^{\boldsymbol{\sigma}}$ with the transformation matrix for stresses $\boldsymbol{T_{\sigma}}$ (see equation 5.7).

$$\hat{\boldsymbol{D}}^{\boldsymbol{\sigma}} = \boldsymbol{T_{\sigma}} \bar{\boldsymbol{D}}^{\boldsymbol{\sigma}} \tag{6.26}$$

Singular Term

It is possible to compute displacements directly at the points where the concentrated forces are loaded, in spite of the singularities. However, when the source point coincides with the load point ($P = \bar{Q}$) a singularity occurs which leads to an infinite result. This problem is avoided by replacing the concentrated force at the singular point by a volume force distributed on a small cylinder, see figure 6.4. This cylinder has the same cross-section as the bolt and the length is equal to the radius r_c of the cross-section.

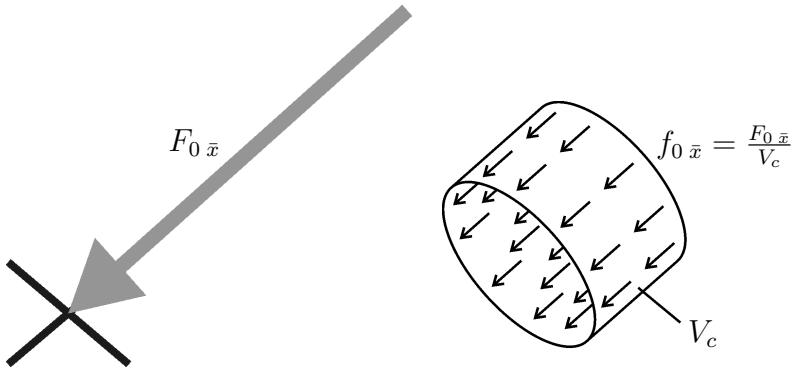

(a) Concentrated point force

(b) Distributed forces on a small volume

Figure 6.4: Replacing the concentrated force by a volume force at the singular point

The volume force is assumed to be constant over the small cylinder, thus following relation is obtained:

$$F_{0\,\bar{x}} \approx V_c f_{0\,\bar{x}} \tag{6.27}$$

where $V_c = r_c^3 \pi$ is the volume of the small cylinder and $f_{0\,\bar{x}}$ is the distributed volume force. With this we obtain:

$$\hat{\boldsymbol{U}} F_{0\,\bar{x}} = \boldsymbol{T_g} \bar{\boldsymbol{U}} F_{0\,\bar{x}} \approx \boldsymbol{T_g} \int_{V_c} \bar{\boldsymbol{U}} \frac{F_{0\,\bar{x}}}{V_c} dV = \underbrace{\boldsymbol{T_g} \frac{1}{V_c} \int_{V_c} \bar{\boldsymbol{U}} dV}_{\hat{\boldsymbol{U}}^{\boldsymbol{sing}}} F_{0\,\bar{x}} \tag{6.28}$$

The integration over the small cylinder V_c is done analytically; with this equation 6.21 can by used directly, where $\hat{\boldsymbol{U}}$ is simply replaced by $\hat{\boldsymbol{U}}^{\boldsymbol{sing}}$ to compute the singular part.

The analytical integration over the small cylinder can be done without any difficulties. The singularity is of order $\mathcal{O}(\ln r)$ for 2D or $\mathcal{O}(1/r)$ for 3D. These singularities can be easily cancelled out by introducing cylindrical or polar coordinates for 2D or 3D, respectively:

$$\int_{V_c} \bar{\boldsymbol{U}} dV = \int_{r=0}^{R_c} \int_{\varphi=0}^{2\pi} \mathcal{O}(\ln r)\, r d\varphi dr \qquad \text{... 2D} \tag{6.29}$$

$$\int_{V_c} \bar{\boldsymbol{U}} dV = \int_{\varphi=0}^{2\pi} \int_{\psi=0}^{\frac{\pi}{2}} \int_{r=0}^{R_c} \mathcal{O}\left(\frac{1}{r}\right) r^2 \sin\psi dr d\psi d\varphi \qquad \text{... 3D} \tag{6.30}$$

Simmilar to the above described procedure also the vector $\boldsymbol{f}^{\boldsymbol{\sigma}}$ for calculating stresses at internal points can be computed (see equation 6.22). As described before also here we have a singularity for the case that the source point coincides with the load point; or in other words: when we want to calculate the stress exactly at the point where the concentrated force is acting.

This singularity is avoided similar as described before for the displacement equation: the concentrated force has to be replaced by a volume force distributed over a very small cylinder at the singular point, see figure 6.4. Again, this cylinder has the same cross-section as the bolt and the length is equal to the radius r_c of the cross-section.

For 2D problems the singularity is of order $\mathcal{O}(1/r)$ and for 3D problems $\mathcal{O}(1/r^2)$, which are both weak singularities, see section 2.5.1.Thus, the analytical integration over the small cylinder can be done without any problems. The singularities are cancelled out by introducing cylindrical coordinates for 2D or

polar coordinates 3D problems:

$$\int_{V_c} \bar{\boldsymbol{D}}^{\boldsymbol{\sigma}} dV = \int_{r=0}^{R_c} \int_{\varphi=0}^{2\pi} \mathcal{O}\left(\frac{1}{r}\right) r d\varphi dr \qquad \text{... 2D} \tag{6.31}$$

$$\int_{V_c} \bar{\boldsymbol{D}}^{\boldsymbol{\sigma}} dV = \int_{\varphi=0}^{2\pi} \int_{\psi=0}^{\frac{\pi}{2}} \int_{r=0}^{R_c} \mathcal{O}\left(\frac{1}{r^2}\right) r^2 \sin\psi dr d\psi d\varphi \qquad \text{... 3D} \tag{6.32}$$

6.3 Verification Examples

The method to compute discrete anchored bolts is verified by two examples. A 2D (plain strain) and a 3D example are shown which include also the pre-stressing of the bolt. The results are compared with those calculated with the finite element program BEFE.

6.3.1 Example 1: Discrete anchored bolt in plane strain (with pre-stressing)

In this example a block in plane strain conditions with a pre-stressed bolt is presented. The dimensions of the block are $10m \times 10m$, the Young's modulus is $E = 1000MN/m^2$ and the Poisson's ratio is $\nu = 0.3$. The bolt has a length of $5m$ the cross section is $A = 0.05m^2$, the Young's modulus of the bolt is $E = 100000MN/m^2$ and variational pre-stress-forces have been tested ($F = 0MN$, $F = 1MN$, $F = 2MN$). The block is fixed at the bottom and on the top of the block is a constant tension $t = 1MN/m^2$. The results are shown in figure 6.5 and compared with FE-solution.

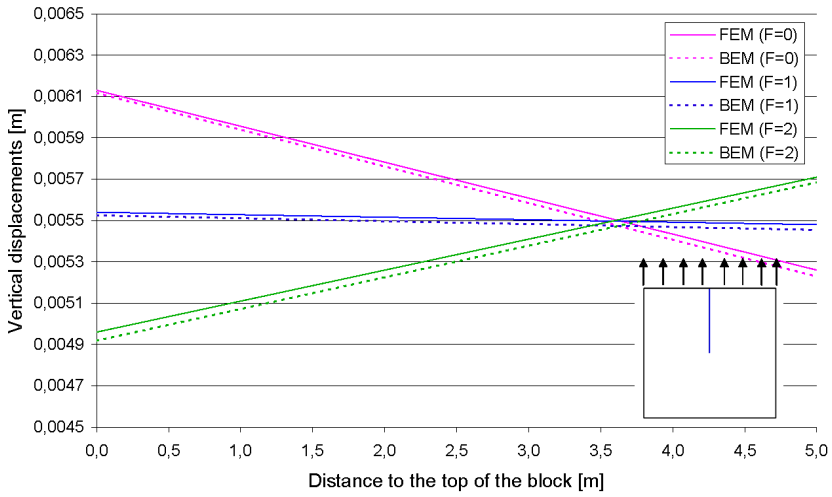

Figure 6.5: Example 1: vertical displacements along the bolt

6.3.2 Example 2: Discrete anchored bolt in 3D

The second example shows a 3D block with a discrete anchored bolt without prestress. The dimensions of the block are 10m x 10m x 10m, the Young's modulus is E=1000MN/m^2 and the Poisson's ratio is ν=0,3. The rock bolt has a length of 5m the cross section is A=0,00786m^2 and variational bolt- Young's modulus have been tested (E=10000MN/m^2, E=50000MN/m^2 and E=100000MN/m^2). The block is fixed at the bottom and on the top of the block is a constant tension t=1 MN/m^2. The results are compared with FE-reference solutions. The results are shown in figure 6.6.

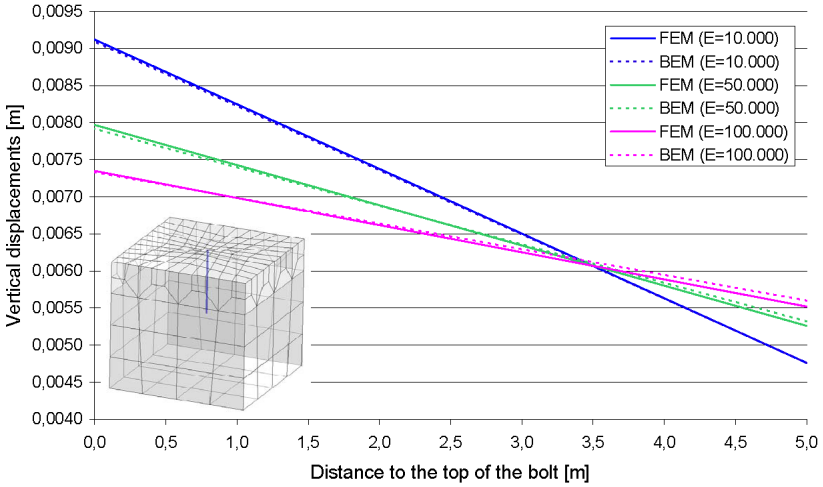

Figure 6.6: Example 2: vertical displacements along the bolt

Chapter 7

Examples

In the previous chapters methods have been presented to simulate geological inhomogeneities, pipe umbrella systems, fully bonded rock bolts and discrete anchored bolts. Very simple examples were shown after each chapter to verify the described methods. In this chapter some bigger examples are presented. First three tunnel examples in plane strain conditions are shown in which different of the above described methods are applied in combination. The results are compared with FE-analyses. Finally a 3D tunnel example including most of the features (rock bolts, pipe umbrella, plasticity, sequential excavation) is presented.

7.1 Plane Strain Examples

7.1.1 Example 1: Tunnel with plasticity and rock bolts

This example is a tunnel with rock bolts and plastic material behaviour. The example is used to investigate the effect of rock bolts in combination with plasticity. The tunnel-radius is $r = 5m$ the material of the ground is: Young's modulus $E = 1000MN/m^2$; Poisson's ratio $\nu = 0.3$; Von Mises yield criterion; yield stress $\sigma_Y = 10MN/m^2$. Six rock bolts with a length of $L = 2.5m$, a cross-section of $A = 0.001257m^2$ and a Young's modulus of $E = 200000MN/m^2$

are introduced. A hydrostatic virgin stress field is assumed $\sigma_v = -9MN/m^2$. The problem has been calculated with elastic and with plastic assumptions. FE reference solutions with the program BEFE have been carried out, both meshes are shown in figure 7.1. The displacement results along the vertical bolt of both calculations (elastic and plastic assumptions) are compared with the FE-reference solution and presented in figure 7.2. The deformed mesh and the contour lines of the total displacements of the plastic analysis are shown in figure 7.3(a) and the contours of the tangential stresses in the rock mass are presented in figure 7.3(b).

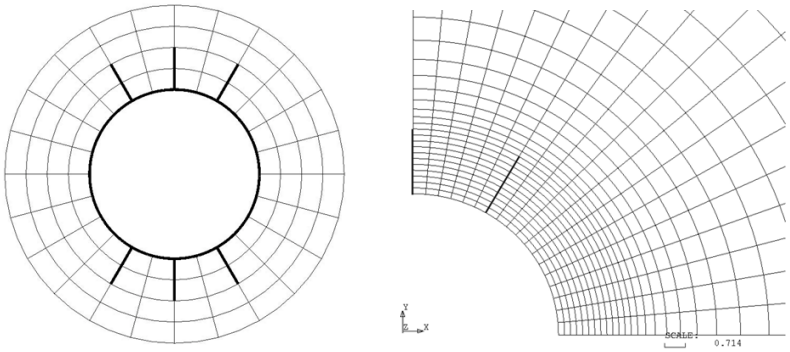

(a) BE-mesh (b) FE-mesh

Figure 7.1: Example 1: mesh discretisation

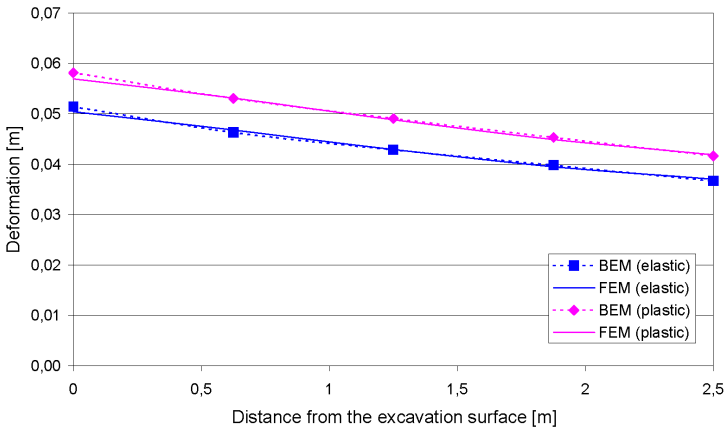

Figure 7.2: Example 1: displacements along the vertical bolt

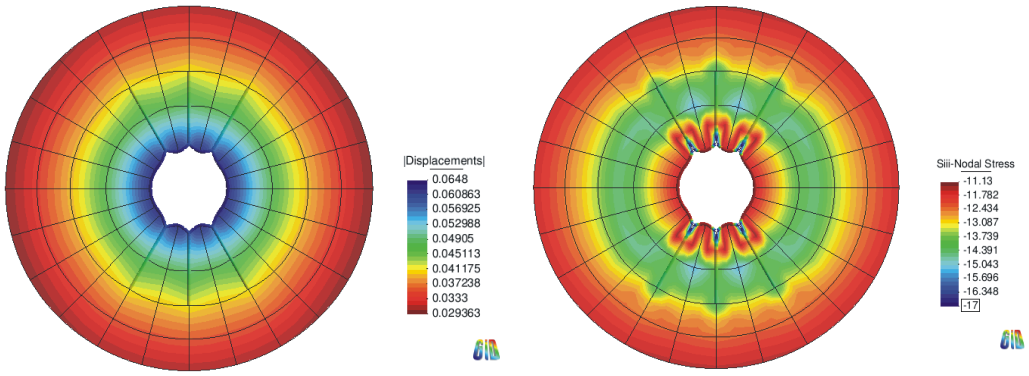

(a) Contours of displacements (b) Contours of tangential stresses

Figure 7.3: Example 1: deformed BE-mesh contour lines

7.1.2 Example 2: Tunnel with inclusion and rock bolts

This example shows a tunnel with rock bolts and soft inclusion zone. The example is used to investigate the effect of rock bolts in combination with an inclusion. The tunnel radius is $r = 5m$, the overburden is $h = 795m$, the soft zone is $2m$ thick and the distance to the tunnel is $1m$. The Rock mass properties are: $E = 10000MN/m^2$, $\nu = 0.333$, $\gamma = 0.02MN/m^3$. The Inclusion properties are: $E = 10MN/m^2$, $\nu = 0.333$, $\gamma = 0.02MN/m^3$. The Bolt properties are: $E = 200000MN/m^2$, $A = 0.001963m^2$.

The results are compared with those calculated by the FE-program PLAXIS. The FE and BE discretisations are presented in figure 7.4, it can be seen that the FE-mesh is much more complex than the BE-mesh. The deformed mesh and the contours of the total displacements are shown in figure 7.5, the displacement results along the bolts are presented in figure 7.6 and the bolt stresses are shown in figure 7.7.

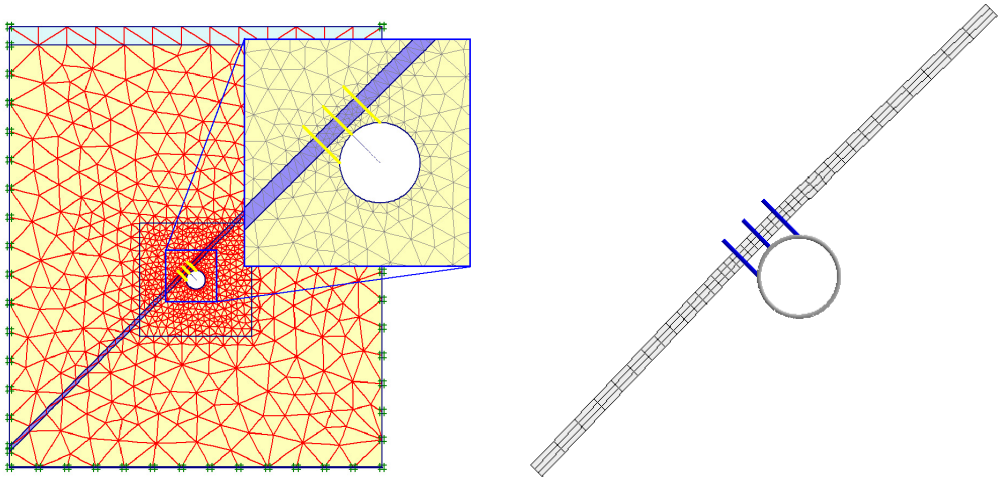

(a) FE-mesh (16886 nodes) (b) BE-mesh (494 nodes)

Figure 7.4: Example 2: mesh discretisation

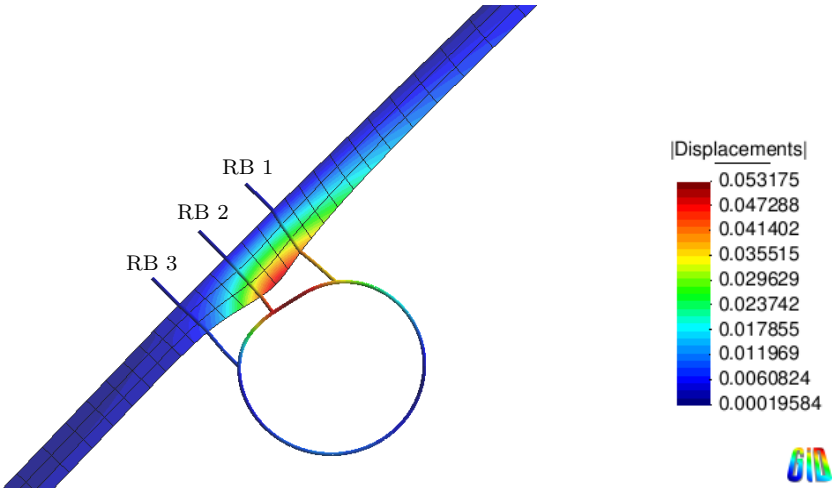

Figure 7.5: Example 2: deformed BE-mesh contours of displacements

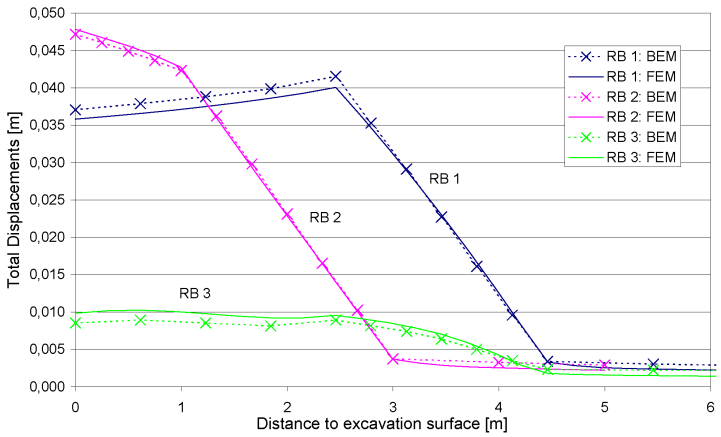

Figure 7.6: Example 2: displacements in axial bolt directions

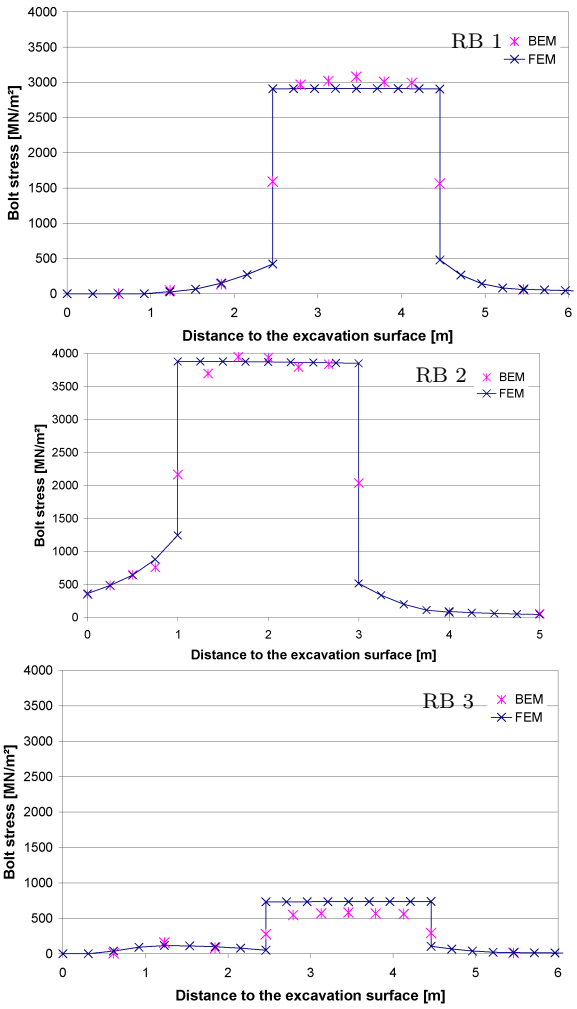

Figure 7.7: Example 2: bolt stresses

7.1.3 Example 3: Tunnel with plasticity, rock bolts and pipe roof

The third example is a tunnel calculated in plane strain conditions, as well. The material parameters of the rock mass are: Young's modulus $E = 313MN/m^2$; Poisson's ratio $\nu = 0.2$; a hyperbolic Mohr-Coulomb yield criterion is used; the cohesion is $c = 0.3MN/m^2$; the friction angle is $\varphi = 26°$; and the tension cut off is by $0.114MN/m^2$.

The overburden is $h = 140m$, the density is $\gamma = 19.6kN/m^3$ and the horizontal earth pressure coefficient is $K_0 = 0.5$; with this the virgin stress state is given by: the vertical virgin stress $\sigma_v = \gamma h = 2.75MN/m^2$ and the horizontal virgin stress $\sigma_h = K_0\sigma_v = 1.375MN/m^2$. The cross section of the excavated tunnel is about $9m$ width and about $6m$ high.

The material of the pipe umbrella zone is computed by homogenising the rock material and the pipe material, the zone is supposed to be $80cm$ thick and the material properties are assumed as follows: Young's modulus $E = 3000MN/m^2$; Poisson's ratio $\nu = 0.3$.

The rock bolts have a cross section area of $A = 0.002827m^2$ (radius $r = 3cm$) and a Young's modulus of $E = 210000MN/m^2$.

Four variational calculations have been carried out:

PL: only plastic material is considered

PL+RB: plastic material and rock bolts are considered

PL+PU: plastic material and pipe umbrella are considered

PL+RB+PU: plastic material, rock bolts and pipe umbrella are considered

The results are compared with those calculated by the FE-program PLAXIS. Figure 7.8 shows the contour lines of the calculation PL+RB+PU, the results of both methods (BEM and FEM) show good agreement. In figure 7.9 the tangential stresses in the rock mass of the BE-calculation are shown. The displacement results in the tunnel roof and the tunnel floor of all four calculations

are summarised in figure 7.10 and compared with those, calculated with the FEM.

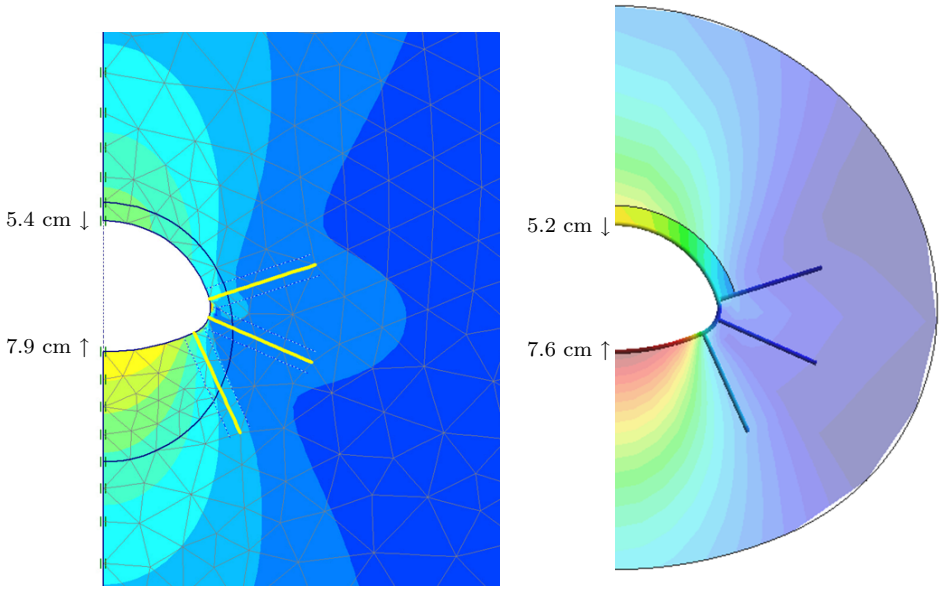

(a) FE-results (b) BE-results

Figure 7.8: Example 3: contours of displacements (PL+RB+PU)

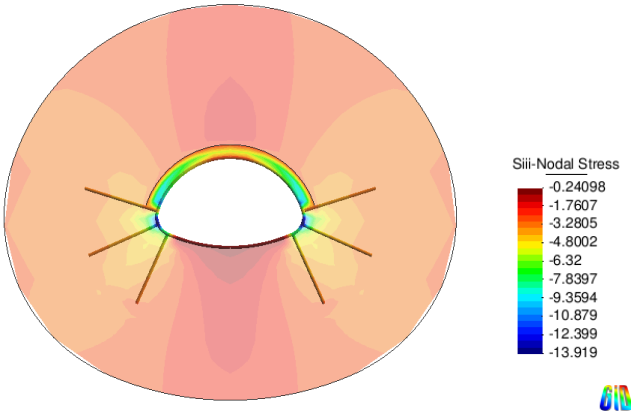

Figure 7.9: Example 3: tangential stresses in the rock mass

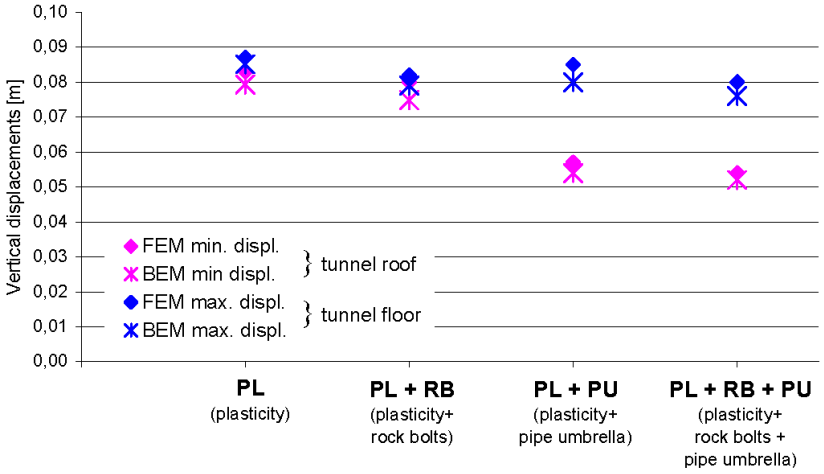

Figure 7.10: Example 3: displacement-results (tunnel roof and tunnel floor)

7.2 Three Dimensional Example

7.2.1 Tunnel with plasticity, rock bolts and pipe roof

Finally a 3D tunnel example is presented. The process of tunnel excavation is calculated sequentially within eight construction stages (i.e. calculation steps). Most of the features (rock bolts, pipe umbrella and plasticity) are involved in this analysis.

The material parameters of the rock mass are: Young's modulus $E = 313MN/m^2$; Poisson's ratio $\nu = 0.28$; a Drucker Prager yield criterion with associated flow rule is used; the cohesion is $c = 0.269MN/m^2$; and the friction angle is $\varphi = 26.1°$. The virgin stress field is assumed to be $\sigma_z = \gamma h = 2.75MN/m^2$ and $\sigma_x = \sigma_y = K_0\sigma_z = 1.375MN/m^2$. This stress field occurs because of following assumptions: the overburden is $h = 140m$, the density is $\gamma = 19.6kN/m^3$ and the horizontal earth pressure coefficient is $K_0 = 0.5$.

To support the excavated tunnel, a pipe umbrella system and rock bolts are installed. The material of the pipe umbrella zone is computed by homogenising

the rock material and the pipe material, the zone is supposed to be $60cm$ thick and the material properties are assumed as follows: Young's modulus $E = 3000MN/m^2$; Poisson's ratio $\nu = 0.3$. The rock bolts have a cross section area of $A = 0.001257m^2$ (radius $r = 2cm$) and a Young's modulus of $E = 200000MN/m^2$.

The cross-section of the tunnel is subdivided into top heading and bench excavation. The geometry and the BE-mesh can be seen in figure 7.11. The shape of the cross-section consists of four circular arcs; the bottom arc has a radius of $9.7m$ and the angles on both sides of the symmetry axis are 23.84°; smaller arcs are on the side walls of the cross-section, they have a radius of $1.2m$ and the angle is 83.54°; and the tunnel roof is made of one arc with the radius $4.8m$ and the angle 72.62° on both sides of the symmetry axis.

The excavation process is simulated for a $50m$ long part of the tunnel; this part is subdivided into 20 segments (per $2.5m$) in longitudinal direction, see figure 7.12. In each construction stage (step) some segments are excavated, and new pipes and rock bolts are installed. The progress of excavation and installation of supports are defined in table 7.1. Where step 0 is only for initialisation: in segments 1 and 2 the whole cross-section is excavated and the rock mass in these segments is linear elastic.

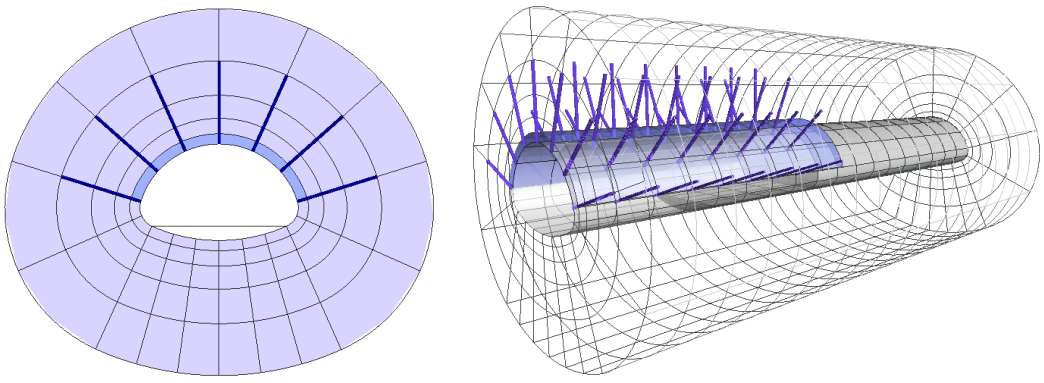

(a) cross section (b) BE-mesh in step 4

Figure 7.11: 3D Example: tunnel geometry and BE-mesh

The deformations along the tunnel roof are presented in figure 7.13. The results are compared with those calculated in plane strain conditions, see figure 7.14 and table 7.2. At the tunnel floor where no supports are installed, the deformations in 2D are bigger because the excavation sequence is not considered. However, on the tunnel roof the deformations in 2D are smaller than in the 3D case, because also the ground supports (pipe umbrella and rock bolts) are installed all at once and not sequentially as in 3D.

Figure 7.15 and figure 7.16 show the deformed meshes and the contours of the total displacements for the steps 1 - 7. For better visualisation the plasticity cells and the pipe umbrella cells are switched off in these figures.

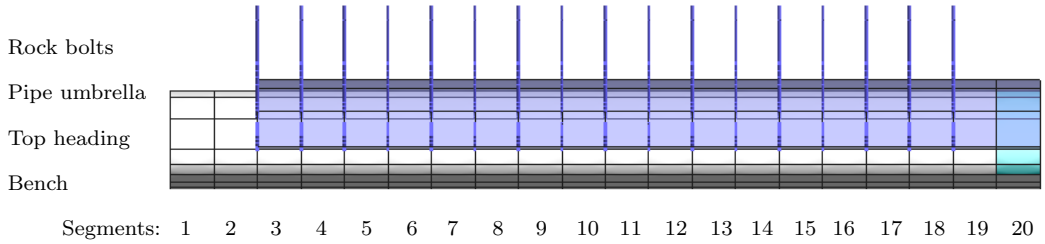

Figure 7.12: 3D Example: longitudinal sections

Step:	Activities in Segments:			
	Excavation: Top Heading	Excavation: Bench	Installation: Pipes	Installation: Rock Bolts
0	1,2	1,2	3	-
1	3,4	-	4,5	3,4
2	5,6	-	6,7	5,6
3	7,8	3,4	8,9	7,8
4	9,10	5,6	10,11	9,10
5	11,12,13	7,8,9	12,13,14	11,12,13
6	14,15,16	10,11,12	15,16,17	14,15,16
7	17,18,19	13,14,15	18,19,20	17,18,19

Table 7.1: 3D Example: activities in segments during construction stages

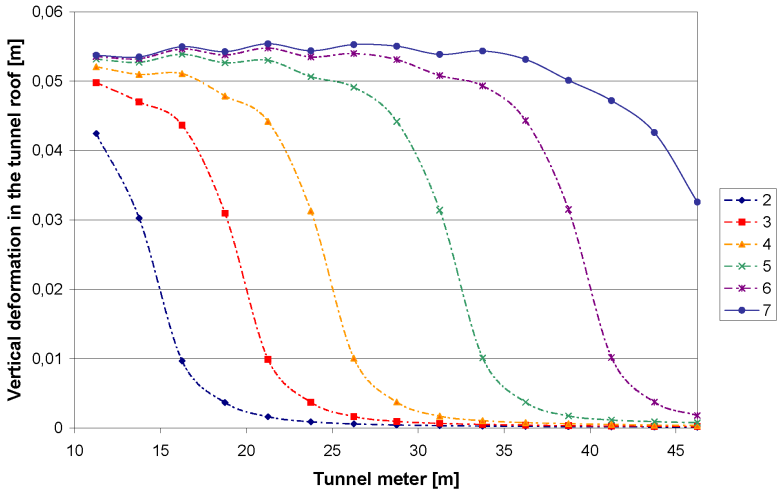

Figure 7.13: 3D Example: deformations along the tunnel roof (steps 2-7)

	2D:	3D:
Tunnel floor	0,085743	0,073734
Tunnle roof	-0,052433	-0,05641

Table 7.2: 3D Example: comparison of vertical displacements

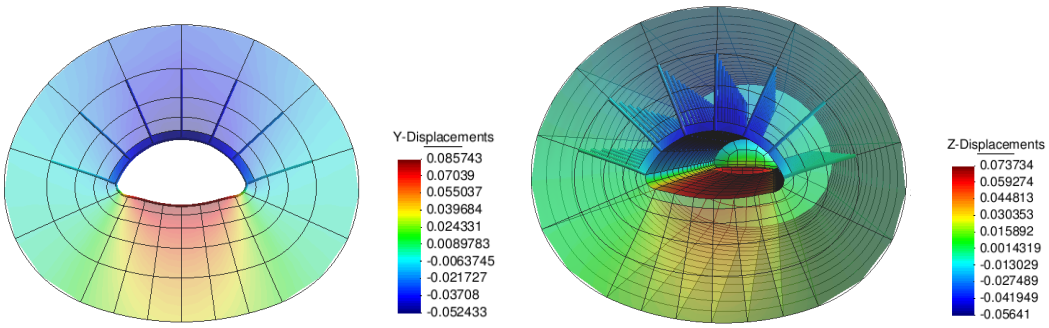

(a) 2D results (b) 3D results

Figure 7.14: 3D Example: comparison of vertical displacements

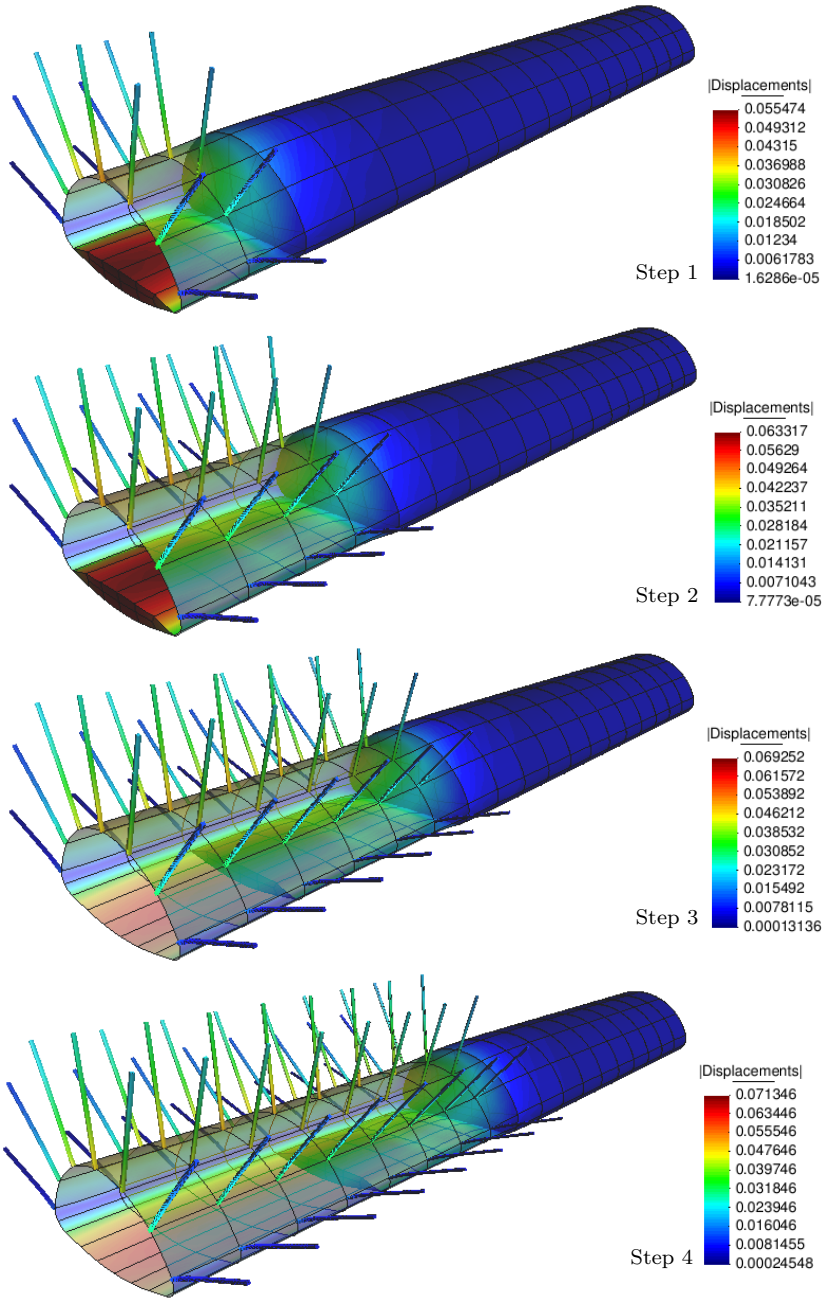

Figure 7.15: 3D Example: deformed mesh and displacement contours (step 1-4)

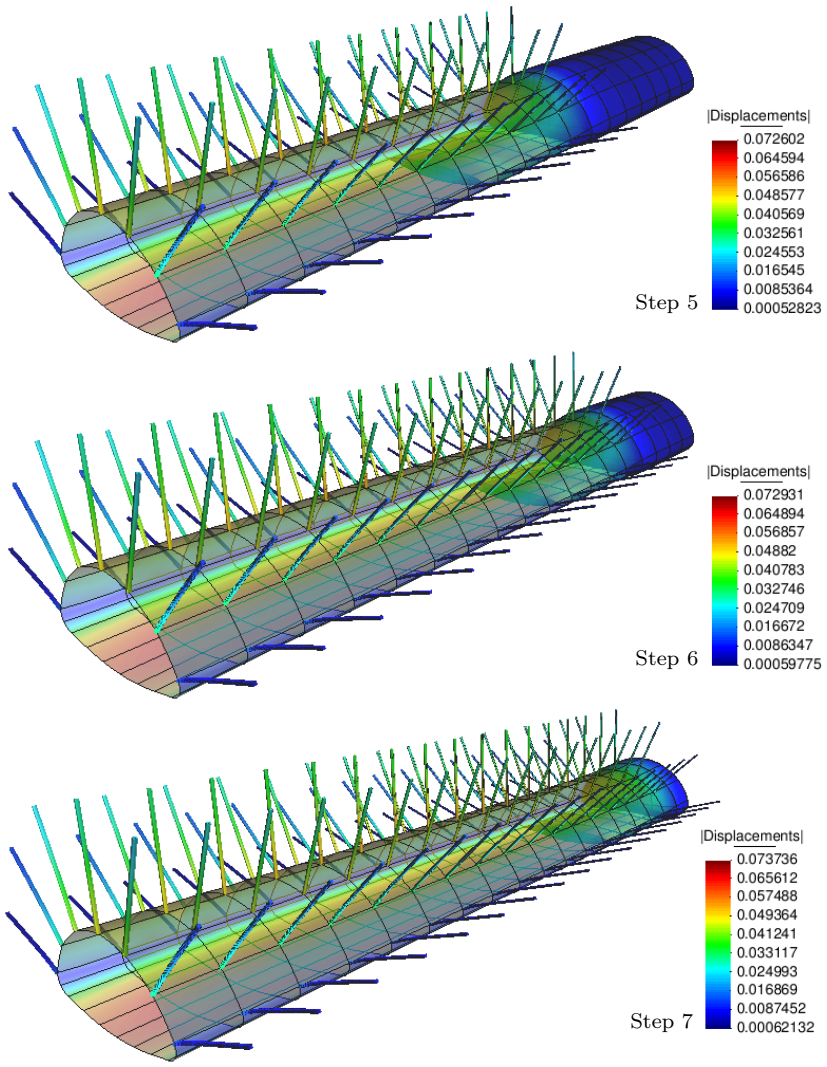

Figure 7.16: 3D Example: deformed mesh and displacement contours (step 5-7)

Chapter 8

Conclusions

The overall aim was the development of a new numerical simulation tool (BEFE++) which is especially capable to simulate conventional tunnelling problems. The ambition was to create a more user-friendly, efficient and accurate program than commonly used programs.

For this the Boundary Element Method (BEM) was chosen. Since the Boundary Element Method (BEM) is the only method which does not require domain discretisation, the mesh is much smaller and simpler. Thus the mesh generation is more user-friendly, the calculation time is shorter and the mesh is less error-prone. The effort to do 3D simulations is significantly reduced. Additional advantages are the better accuracy of stress/strain results and the accurate computability of stress concentration problems.

Since the BEM is not as far developed as other methods a lot of research and developing work had to be done. All necessary features for simulating conventional tunnelling processes (for example: sequential excavation, nonlinear material behaviour, installation of ground supports) had to be developed and implemented into this new program.

The goal of this work was the development and the implementation of approaches to simulate ground support (like rock bolts and pipe roofs) into BEFE++. Novel methods were developed to simulate these *inclusions*. In the previous chapters

the simulation of different kinds of rock bolts, pipe umbrella systems and geological inhomogeneities were presented.

In these methods the inclusions are simulated by applying stresses or forces to the system. An iterative solution procedure was proposed for these calculations. With this, a huge number of inclusions (for example rock bolts) can be calculated efficiently and the iterative procedure can be easily and efficiently combined with a non-linear calculation (for example to simulate plastic material behaviour). It was also shown that these procedures work very well in combination with the coupling algorithm of multiple regions.

In contrast to commonly used methods the mesh generation for such problems is very easy and independent from any domain discretisation. With a relative small effort very accurate results are obtained.

Especially the simulation of rock bolts and anchors has key benefits compared to other methods. Whereas other methods (like the Finite Element Method) needs an extremely fine mesh around the bolts to handle the local stress concentrations, the capability of the BEM to deal with stress concentration problems is utilised and makes the BEM more efficient and more accurate for this kind of problems, see chapter 5 and chapter 6.

At the end of the chapters small examples were presented to verify each method separately. Finally some larger examples were shown in which the different inclusions and also plastic material behaviour were demonstrated to work together.

Bibliography

Aliabadi, M. and Saleh, A. (2002). Fracture mechanics analysis of cracking in plain and reinforced concrete using the boundary element mehtod. *Engeneering Fracture Mechanics*, *69*, 267 – 280.

Banerjee, P. (1981). *The Boundary Element Methods in Engineering*. McGRAW-HILL Book Company Europe.

Beer, G. (2001). *Programming the Boundary Element Method*. JHON WILEY & SONS, LTD.

Beer, G., Smith, I., and Duenser, C. (2008). *The Boundary Element Method with Programming*. Springer WienNewYork.

Beer, G. and Watson, J. (1994). *Introduction to Finite and Boundary Element Methods for Engineers*. JOHN WILEY & SONS.

Benmokrane, B., Chennouf, A., and Mitri, H. (1995). Loboratory evaluation of cement-based grouted rock anchors. *Int. J. Rock Mech. Min. Sci. & Geomech. Abstr.*, *32*, 633 – 642.

Brebbia, C., Telles, C., and Wrobel, L. (1984). *Boundary Element Techniques*. Springer, Heidelberg.

Chen, S.-H., Qiang, S., Chen, S.-F., and Egger, P. (2004). Composite element model of the fully grouted rock bolts. *Rock Mechanics and Rock Engineering*, *37*, 193 – 212.

Cisilino, A. and Aliabadi, M. (1998). A boundary element method for three-dimensional elastoplastic problems. *Engineering Computations*, *15*, 1011 – 1030.

Coda, H. (2001). Dynamic and static non-linear analysis of reinforced media: a bem/fem coupling approach. *Computers and Structures*, *79*, 2751 – 2765.

Coda, H. and Venturini, W. (1999). On the coupling of 3d bem and fem frame model applied to elastodynamic analysis. *International Journal of Solids and Sturctures*, *36*, 4789 – 4804.

Duenser, C. (2001). *Simulation of Sequential Tunnel Excavation with the Boundary Element Method*. PhD thesis, Graz University of Technology, Austria.

Feder, G. and Arwanitakis, M. (1976). Zur gebirgsmechanik ausbruchnaher bereiche tiefliegender hohlraumbauten. *Berg- und Hüttenmännische Monatshefte*, *4*, 102 – 117.

Filho, R., Mendonca, A., and Paiva, J. (2005). Static boundary element analysis of piles submitted to horizontal and vertical loads. *Engineering Analysis with Boundary Elements*, *29*, 195 – 203.

Gakkov, F. (1966). *Boundary Value Problems*. Pergamon Press Ltd.

Galler, R. (2009). The new guidline - natm - the austrian way of conventional tunnelling. In *ITA-AITES World Tunnel Congress 2009 - Safe Tunnelling for the City and for the Environment*.

Gao, X. and Davies, T. (2002). *Boundary Element Programming in Mechanics*. Cambridge University Press.

Gaul, L., Kögl, M., and Wagner, M. (2003). *Boundary Element Methods for Engineers and Scientists*. Springer-Verlag.

Gioda, G. and Swoboda, G. (1999). Developments and applications of the numerical analysis of tunnels in continuous media. *Internaltional journal for numerical and analytical methods in geomechanics*, *23*, 1393–1405.

Guiggiani, M. and Casalini, P. (1987). Direct computuation of cauchy principal value integrals in advanced boundary elements. *Internaltional Journal for Numerical Methods in Engineering*, *24*, 1711 – 1720.

Guiggiani, M. and Gigante, A. (1990). A general algorithm for multidimensional cauchy principal value integrals in the boundary element method. *Journal of Applied Mechanics*, *57*, 906 – 915.

Hagen, C. (2005). *Wechselwirkungen zwischen Bauwerk, Boden und Fluid unter transienter Belastung*. PhD thesis, Technische Universität Hamburg-Harburg.

Hoek, E., Kaiser, P., and Bawden, W. (1997). *Support of Underground Excavations in Hard Rock*. A.A.Balkema Publishers.

Hyett, A., Moosavi, M., and Bawden, W. (1996). Load distribution along fully grouted bolts, with emphasis on cable bolt reinforcement. *International Journal for numerical and analytical Methods in Geomechanics*, *20*, 517 – 544.

Ivanovic, A. and Neilson, R. D. (2009). Modelling of debinding along the fixed anchor length. *International Journal of Rock Mechanics and Mining Sciences*, *46*, 699 – 707.

Jing, L. (2003). A review of techniques, advances and outstanding issues in numerical modelling for rock mechanics and rock engineering. *Rock Mechanics and Mining Sciences*, *40*, 283 – 353.

Jing, L. and Hudson, J. (2002). Numerical methods in rock mechanics. *International Journal of Rock Mechanics and Mining Sciences*, *39*, 409 – 427.

Karakus, M. and Fowell, R. (2004). An insight into the new austrian tunnelling method (natm). In *ROCKMEC 2004 - VIIth Regional Rock Mechanics Symposium*.

Kovari, K. (2003a). History of the sprayed concrete lining method - part i: milestones up to the 1960s. *Tunnelling and Underground Space Technology*, *18*, 57 – 69.

Kovari, K. (2003b). History of the sprayed concrete lining method - part ii: milestones up to the 1960s. *Tunneling and Underground Space Technology*, *18*, 71–83.

Lachat, J. and Watson, J. (1976). Effective numerical treatment of boundary integral equations: A formulation for three dimensional elastostatics. *International Journal for Numerical Methods in Engineering*, *10*, 991–1005.

Leite, L., Coda, H., and Venturini, W. (2003). Two-dimensional solids reinforced by thin bars using the boundary element method. *Engineering Analysis with Boundary Elements*, *27*, 193 – 201.

Leite, L. and Venturini, W. (2005). Boundary element formulation for 2d solids with stiff and soft inclusions. *Engineering Analysis with Boundary Elements*, *29*, 257 – 267.

Ma, F., Chatterjee, J., Henry, D., and Banerjee, P. (2008). Transient heat conduction analysis of 3d solids with fiber inclusions using the boundary element method. *International Journal for Numerical Methods in Engineering*, *73*, 1113 – 1136.

Maeso, O., Aznarez, J., and Garcia, F. (2005). Dynamic impedances of pile and groups of piles in saturated soils. *Computers and Structures*, *83*, 769 – 782.

Marence, M. (1992). *Numerical Model for Rockbolts under Consideration of Rock Joint Movements*. PhD thesis, University of Insbruck.

Mikhilin, S. and Prössdorf, S. (1987). *Singular Integral Operators*. Springer-Verlag.

Padron, L., Anarez, J., and Maeso, O. (2007). Bem-fem coupling model for the dynamic analysis of piles and pille groups. *Engineering Analysis with Boundary Elements*, *31*, 473 – 484.

Pande, G., Beer, G., and Williams, J.-R. (1990). *Numerical Methods in Rock Mechanics*. John Wiley & Soms Ltd.

Paris, F. and Canas, J. (1997). *Boundary Element Method - Fundamentals and Applications*. Oxford University Press.

Pereira, A. (2008). *Coupling BEM/FEM for fluid-soil-structure interaction*. PhD thesis, Graz University of Technology, Austria.

Prazeres, P. G. C. (2009). *Nonlinear Analysis of NATM Tunnel construction with the Boundary Element Method*. PhD thesis, Graz University of Technology, Austria.

Press, W., Teukolsky, S., Vetterling, W., and Flannery, B. (2002). *Numerical Recipes in C++, The Art of Scientific Computing* (Second Edition ed.). Cambridge University Press.

Ribeiro, T. (2006). *Elastoplastic boundary element method with adaptive cell generation*. PhD thesis, Graz University of Technology, Austria.

Ribeiro, T., Beer, G., and Duenser, C. (2008). Efficient elastoplastic analysis with the boundary element method. *Computational Mechanics*, *41*(5), 715–732.

Riederer, K. and Beer, G. (2009). Boundary element analysis of rock bolts and pipe roofs in tunnels. In *Computational Methods in Tunneling*, pages 115–122.

Riederer, K., Duenser, C., and Beer, G. (2009). Simulation of linear inclusions with the BEM. *Engineering Analysis with Boundary Elements*, *33*, 959–965.

Romana, M. (2009). Could the new austrian tunnelling method be used safely in cities? In *ITA-AITES World Tunnel Congress 2009 - Safe Tunnelling for the City and for the Environment, (www.stmr.es/recursos/downloads/AustrianTunnelingMethod.pdf)*.

Schubert, W. (1997). *Grundlagen der New Austrian Tunnelling Method*. Lecture Notes, Institute for Rock Mechanics and Tunnelling, Graz University of Technology, Austria.

Schweiger, H. F. (2008). *Computational Geotechnics*. Lecture Notes WS 08/09, Institute for Soil Mechanics, Graz University of Technology, Austria.

Telles, J. (1983). *The Boundary Element Method Applied to Inelastic Prolems*. Springer-Verlag.

Thoeni, K. (2009). *Error-Controlled Adaptive Analysis of Non-Linear Problems using the Boundary Element Method*. PhD thesis, Graz University of Technology, Austria.

Venturini, W. S. (1983). *Boundary Element Method in Geomechanics*. Springer-Verlag.

Wang, Y. and Gao, X. (1998). Practicable bem analysis of frictional bolts in underground opening. *Journal of Structural Engineering*, *124*, 342 – 346.

Wikipedia. www.wikipedia.com; free encyclopedia.

Zienkiewicz, O., Kelly, D., and Bettess, P. (May 1977). Marriage a la mode - the best of both worlds. *Int. Symp. on Innovative Numerical Analysis in Applied Engineering Science, Versailles, France*.

List of Figures

List of Tables